DELINEATION OF MINERALISATION ZONES USING AEROMAGNETIC AND GAMMA-RAY SPECTROMETRIC DATA IN PARTS OF NORTH CENTRAL, NIGERIA

BY

JIMOH, Nusirat Lawal PhD/SPS/2017/957

DEPARTMENT OF PHYSICS, SCHOOL OF PHYSICAL SCIENCES
FEDERAL UNIVERSITY OF TECHNOLOGY, MINNA

NOVEMBER, 2023

ABSTRACT

Aeromagnetic and Gamma-ray spectrometric data sets were effectively used to provide fundamental information on the structural settings and deduce feasible locations of mineralisation in parts of North-central, Nigeria. Both data sets were analysed to delineate structural lineaments and their trends as well as hydrothermal alteration zones with a view to deducing most favourable areas of mineralisation in the region. A range of mathematical filtering techniques were applied to both data sets. These include such as Reduction-ToEquator (RTE), First Vertical Derivative (FVD), Analytic signal (AS), Horizontal Gradient Magnitude (HGM), Tilt Derivative (TD), Centre for Exploration Targeting (CET) and Ratio grids as well as Ternary measures. The filtering techniques were used to enhance anomalies of selected geologic features thereby transforming them to other grids in readiness for interpretation. Also, the radiometric signatures were interpreted to indicate hydrothermally altered zones related to mineralisation. These filters aided the delineation of structural lineaments as well as probable areas of hydrothermal alteration related to mineralisation. From the aeromagnetic analysis, the directional analysis of the CET lineament map and lineament analysis using the rosette diagram revealed East-west (E-W) and East-Northeast-West-Southwest (ENE-WSW) as the predominant structural trend in the region. In addition, the directions symbolise the orientation of geological structures (lineaments) playing host to different ore mineral deposits in the location. Also, the depths to the geologic features (structural lineaments) were estimated. Depths to the geological structures were calculated utilising Euler deconvolution (ED), Source Parameter Imaging **(**SPI**)** and Power Spectral techniques. The depth estimate to the source bodies (lineaments) playing host to mineral deposits is approximately between 0-300 m. From the radiometric response, an increase in Potassium

(K) content noticed on the Potassium/equivalent Thorium (K/eTh) ratio map was an indicator of hydrothermal alterations in the area. Five

(5) potential zones of mineralisation were delineated. These are “Very poor”, “Poor”, “Moderate”, “Good” and “Very Good” zones. “Very good” to “good” zones are deduced as the most favourable zones of potential mineralisation connected with high structural lineaments. Thus, the coincidence of high structural complexity areas connected with hydrothermal alterations is an indication of prospectivity of high ore deposits.

TABLE OF CONENTS

Contents **Page**

LIST OF TABLES

Table **Page**

LIST OF FIGURES

LIST OF ABBREVIATIONS

ABBREVIATION	**MEANING**
AHP	Analytic Hierarchy Process
APS	Average Power Spectrum
AS	Analytic Signal

ASA	Analytical Signal Amplitude
BW	Butterworth
CED	Central Eastern Desert
CET	Centre for Exploration Target
CMY	Cyan-Magenta-Yellow
ED	Euler Deconvolution
ENE	East North East
ENE-WSW	East-NorthEast-West-SouthWest
ERE	Elemental Ratio Enhancement
eTh	equivalent Thorium
ETM+	Enhanced Thematic Mapper Plus
eU	equivalent Uranium
E-W	East-West
FFT	Fast Fourier Transform
FG	Federal Government
FVD	First Vertical Derivative
GIS	Geographic Information System
GRS	Gamma Ray Spectrometric
HD	Horizontal Derivative

HG	Horizontal Gradient
HM	High Magnetic
HGM	Horizontal Gradient Magnitude
HRAD	High Resolution Aeromagnetic Data
IGRF	International Geomagnetic Reference Field
IM	Intermediate Magnetic
IP	Induced Polarisation
K	Potassium
LM	Low Magnetic
MCDA	Multi Criteria Decision Analysis
NC	North-Central
NE-SW	Northeast-Southwest
NGSA	Nigerian Geological Survey Agency
NNW	North North West
NNW-SSE	NorthNorthWest-SouthSouthEast
NW	Northwest
NW-SE	Northwest-Southeast
PCA	Principal Component
Analysis PM-Map	Prospectivity

Mineral Map ppm	Part Per Million
PS	Power Spectrum
PSA	Power Spectral Analysis
RAPS	Radial Average Power Spectrum
REE	Rare Earth Element
RGB	Red-Green-Blue
R-Maps	Ratio Maps
RTE	Reduced-To-Equator
RTP	Reduced-To-Pole
SED	Source Edge Detection
SI	Structural Index
SPI	Source Parameter Imaging
SR	Shaded Relief
SVD	Second Vertical Derivative
TAD	Tilt Angle Derivative
TD	Tilt Derivative
TD_THD	Tilt-angle Derivative of Total Horizontal Derivative
Th	Thorium

THD	Total Horizontal Derivative
T-Map	Ternary composite
TMI	Total Magnetic Intensity
TMI_RTE	Total Magnetic Intensity Reduced-To-Equator
U	Uranium
UC	Upward Continuation
VD	Vertical derivative
WGS 84	World Geodetic System 84

CHAPTER ONE

1.0 INTRODUCTION

1.1 Background to the Study

Exploration of solid minerals would have been the best avenue to generate economic income, but, much attention is not given to it. Instead, attention shifted totally to mining of crude oil due to the lure of easier profits from crude oil production. For instance, the fact that there are other means of improving and increasing the economic income, yet, the Nigerian economy depends largely on crude oil production as the major source of economic income generation. Though, the Nigerian petroleum sector has played an imperative role in the nation's economy, due to the global downward trend of crude oil price which is neither stable nor sustainable, the need for diversification of revenue stream arises. However, if priority is given to mineral exploration, definitely, improved and increased socio-economic benefits would be established because solid minerals are key element to nations building. Prospecting for minerals would ease the burden on crude oil production which is rarely sufficient for sustainable developmental growth of the nation. Thus, interested foreign investors would negotiate their way into the country to invest in the essential minerals feasible for exploitation and on the other hand, reduce the rising population of unemployed citizens. Mineral exploration has the potential of revealing major geological structures (lineaments) playing host to mineral deposits (Olasunkanmi *et al*., 2018). In this regard, exploring for minerals that are structurally controlled requires the use of appropriate geophysical survey techniques to detect their area of localisation. This is because geologic structures presumed to be lineaments (faults, fractures, folds, joints and shear zones) are very much involved in the movement and localisation of most mineral deposits (Garba, 2000). Since these geological features are essential in prospective exploration targets, most often, they serve as channels for the movement of hydrothermal mineralising fluids, in the process, fluid-rock interaction for minerals

precipitation and localisation are developed (Abubakar, 2012). However, not all geologic structures that exist in a geologically permissive field are mineralised (Gaboury, 2019). The manifestation of hydrothermal alteration haloes in a genetically endowed setting is also an indication that mineralising fluid has traversed through the geologic structures and deposited minerals (Airo, 2007). Thus, hydrothermal fluids that are composed of water, ions of potassium, calcium, sodium, calcium, silica, sulphide and chlorine compounds, carbonates and magnesium travel through the tectonically deformed rocks to precipitate minerals (Cunha *et al*., 2017). Besides, minerals deposits connected to hydrothermal alteration zones are not easily determined except with the application of appropriate geophysical survey tools. The application of airborne geophysical techniques (magnetic, gravity, electromagnetic and radiometric) to lineaments mapping have proven to be effective and efficient in delineating targeting elements that are related to mineralisation zones. (Almasi *et al*., 2017; Cunha *et al*., 2017; Ejepu *et al*., 2018; and Airo, 2002).

In this study, Aeromagnetic and Gamma-ray spectrometric (aeroradiometric) survey techniques (via data sets) were chiefly used for delineation of mineralisation zones through mapping of geologic structures associated with hydrothermal alteration zones. Integration of both techniques (aeromagnetic and gamma-ray spectrometric data) for delineation of geological structures connected to mineralisation zones proves that geological structures play a vital role in mineral prospecting as they highlight orebearing host rocks and act as conduits for mineralising hydrothermal fluids (Austin and Blenkinsop (2008)). Also, Elkhateeb and Abdellatif (2018) confirmed the authenticity of integrating both aeromagnetic and aeroradiometric data sets to determine possible locations of mineralisation via delineation of structures, mapping lithology and hydrothermal alteration zones. However, processing of these geophysical data sets can be used to delineate mineralisation expressions that are not commonly visible during field

geological mapping due to the presence of dense vegetation cover, thick soil cover, large size of outcrops and non-existence of surficial manifestations of mineralisation footprints (Airo, 2007).

These techniques are lengthily utilised globally as a base for geological interpretations because they play a vital role in pin-pointting lineaments (geological features) like faults, fracture and shear zones related to mineralisation since they are helpful when it comes to investigation and localisation of mineralised zones (Yousif *et al*., 2018). Consequently, the basic reason behind this is that different rock types harbour different magnetic responses and as a result several filtering techniques were utilised to enhance the output images of the magnetic responses for improved interpretation. Both are competent techniques predominantly used to recognise geological features that accommodate mineral deposits in most parts of the world (Nafiz and Enver, 2015). Both are also survey techniques that are equally cost-effective, non-invasive, non-destructive in the sense that no energy needs to be put into the ground to obtain any useful information. Besides, they are unique survey practices that could be used predominantly as reconnaissance tools because both allow speedy coverage of large areas when compared with other geophysical survey methods (Graham *et al*., 2013). However, utilisation of aeromagnetic data is not only limited to delineation of structural fabrics of tectonically deformed rocks, but it is also a veritable tool in exploring magnetic mineralogical changes that are linked to syn-mineralisation hydrothermal alteration subsystem (Airo, 2002).

Similarly, airborne gamma-ray spectrometry method is an important technique used all over the world for delineation of mineralised hydrothermal fluids (Telford *et al*., 1990).

Apart from the mineralogical features, recognition of radiometric signatures are as a result of hydrothermal alteration processes, so, gamma-ray spectrometric data (aeroradiometric

data) is equally imperative in delineating potential mineralisation zones. In other words, aeroradiometric data is very helpful in delineating hydrothermal haloes; it gives estimates of apparent surface concentrations of the most common naturally occurring radioactive elements (K, Th and U). The essence of the technique for geological mapping is based on the assumption that absolute concentrations of these radioelements differ measurably and considerably with lithology (Eslam *et al*., 2004). This survey technique uses a gamma-ray spectrometer which measures the radioactivity emanating from the natural decay of elements such as Potassium (K), Thorium (Th) and Uranium (U) from the earth surface. This tool, with shallow depth of penetration, has the special quality of distinguishing these decay elements from one another based on their energy level (Telford *et al*., 1990). Thus, it involves the surface measurement of the most common naturally occurring radioactive elements: K, Th and U which predominantly originates as trace elements in most rock forming minerals (Eslam *et al*., 2004). K is a key mobile element of most rocks, while Th and U are present in a very small amount as immobile elements (Eslam *et al*., 2004). Though, the concentration of the measured radioactive elements (K, Th, and (U) differ among different rock types and could be dependably employed to distinguish different lithological units emanated due to the variation in the mineral composition (Andrson and Nash, 1997); Charbonneau *et al.*, 1997; Jaques *et al.*, 1997; Lo and Pitcher, 1996; Graham, 1993). In comparison with other airborne geophysical methods, application of airborne gammaray spectrometric data is more useful and accurate in the identification of hydrothermal alteration zones (Omar and Mahmoud, 2018). Moreover, it is helpful in deducing several structures that may not be recognised by analysing potential field methods (Omar and Mahmoud, 2018). Furthermore, airborne gamma-ray spectrometry data offers a three-element image of the prospective area in form of Red-Green-Blue (RGB) composition of Potassium (K), equivalent Thorium (eTh) and equivalent Uranium (eU) radioelements which might reflect better structural and hydrothermal alteration

traces than the field observations (Herbert *et al*., 2014). The composite image method is utilised to exhibit simultaneously three parameters of the radioelements concentrations and ratios on a single image. The method offered much in terms of lithologic discrimination based on colour differences and displayed efficiency in describing areas where different litho-facies happen within areas mapped as one continuous lithology (Eslam *et al*., 2004; El-Sadek, 2009).

Hence, aeromagnetic and airborne gamma-ray spectrometric (aeroradiometric) data sets were used as a veritable tool to delineate geologic structures (lineaments) and hydrothermal alteration zones related to mineralisation in this present study. Above all, previous studies have revealed the feasibility of utilising the two datasets in delineating geological structures linked with potential hydrothermal alteration mineral zones (Omar and Mahmoud, 2018; Wemegah *et al.,* 2015). In addition, previous research has shown that airborne gamma-ray spectrometry patterns provide fundamental information used for mineral exploration studies (Wilford *et al*., 1997). It has also been demonstrated in previous study that gamma-ray spectrometry is probably more useful than any other single airborne geophysical technique in supplying information directly interpretable in terms of surface geology (Darnley *et al*., 1989). Interpretation of radioelements distribution for mapping the surface geology is based on the assumption that different rock types are composed of certain amounts of rock-forming minerals which include specific quantities of radioactive elements (Eslam *et al*., 2004).

At the end, both airborne magnetic and gamma-ray spectrometric data sets were analysed and interpreted to delineate different geological structures linked with hydrothermal alteration haloes within the study area. Magnetic filtering techniques, ratio and ternary images were respectively used to sharpen up the edges of shallow seated geologic

structures and different lithologic units based on the spatial differences in the radioelement contents.

1.2 Statement of the Research Problem

Based on previous studies by different researchers (Adewumi and Salako, 2017; Ejepu *et al*., 2018), the region where the study area is situated is naturally endowed with mineral resources that are economically and technically viable for exploitation. The manner of extraction poses great hazards of various degrees not only to the miners but to the environment at large. Yet, comprehensive knowledge on the exact locations and depth to source bodies playing host to different ore deposits are unknown in the area.

Without considering the environmental hazards, the different strategies employed in carrying out exploration activities within the region where the study area is situated causes great menace of various degrees not only to miners but to the environment at large, yet, there are none or limited documented information (database) on the exact locations and depth to the source bodies hosting different ore deposits in the area. This means trial-by-error has been an incessant method of searching for ore deposits in the region. Pessimistically, this practices leads to loss of vegetation and destruction of farmland through excessive digging. Nevertheless, these drawbacks were restrained in this research.

1.3 Justification for the Study

Exploration of various ore minerals will go a long way to lessen the over reliance on crude oil for foreign exchange, though, the Nigerian Petroleum Sector has played an imperative role in the developmental growth of the nation's economy. Due to the global downward trends of crude oil price which is neither stable nor sustainable, the need for diversification

of revenue streams becomes vital. Mineral exploration is an added means of generating higher income, because, prospecting for minerals that are economically viable for exploitation enhances developmental growth of a country's Gross Domestic Product (GDP). Mineral exploration facilitates the detection as well as mapping of areas of mineralisation and therefore makes exploitation much easier. Also, it determines quantity available and makes decision to exploit economically safe and sensible. Thus, mineral exploration is of utmost importance to our country, Nigeria.

Trial-by-error via excessive digging has been a nonstop technique of searching for areas of mineralisation. The practise causes a lot of environmental hazards and waste of money. Yet, there are difficulties in locating mineralised zones. To avoid this drawback, appropriate airborne geophysical survey techniques via application of their respective dataset were adopted. Aeromagnetic and airborne gamma-ray spectrometric data sets were adapted as reconnaissance tools that allow rapid coverage of large area. Integration of the dataset pin-pointed mineralisation signatures that may not be visible due to the existence of dense vegetation cover, thick soil cover and large mass of outcrops if field geological mapping was conducted. Besides, both techniques are non-invasive, nondestructive in the sense that no energy needs to be sent into the ground to obtain any useful information. Hence, the outcomes would be supportive information (database) for prospective research for viable ore deposits in the region, thereby solving the agelong challenges of data dissemination.

1.4 Location and Extent of the Study Area

The study area is located in the North-Central part of Nigeria (Figure 1.1). The area cut across two states (Niger and Kaduna) including parts of the Federal Capital Territory (FCT). The area is bounded by Latitudes $9^{o}\,00'$ N to $10^{o}\,00'$ N and Longitudes $6^{o}\,00'$ E to

7° 30′ E, it covers a total surface area of 18,150 km^2. The study area is marked by two distinct climatic conditions; Rainy season and dry season. The rainy season usually occurs between March and April, lasts till October (NiMet, 2021). Besides, the area receives moderate to high rainfall resulting into high to moderate vegetation cover. Also, the dry season heralded annually by the dry, dusty wind (harmattan) usually begins in November and terminates in March, with an average temperature of 30-38 °C every year (NiMet, 2021), whereas, lower temperatures are recorded in the rainy period because of dense cloud cover. However, the climatic conditions are subjected to changes. The prevailing weather conditions of the area are primarily governed by its undulating topography and the high altitude.

1.5 Aim and Objectives of the Study

The aim of this study is to delineate mineralisation zones within parts of the North Central Nigeria using Aeromagnetic and Gamma-ray Spectrometric data sets. The objectives are:-

1. Production of Total Magnetic Intensity (TMI) map of the study area using Aeromagnetic data set.
2. Delineation of structural lineaments from the First Vertical Derivative (FVD), Analytic Signal (AS) and Lineament maps derived through the application of Aeromagnetic data set.
3. Estimation of depth to source bodies (lineaments) through which mineral deposits are aligned along or connected with using Euler Deconvolution (ED), Source Parameter Imaging (SPI) and Power Spectral Analysis (PSA) techniques.

4. Delineation of hydrothermal alteration zones from produced Ratio and Ternary maps produced from analysis of Aero-gamma ray spectrometric data set.
5. Generation of mineral prospectivity map of the study area by integrating the results obtained from (2) and (4) above.

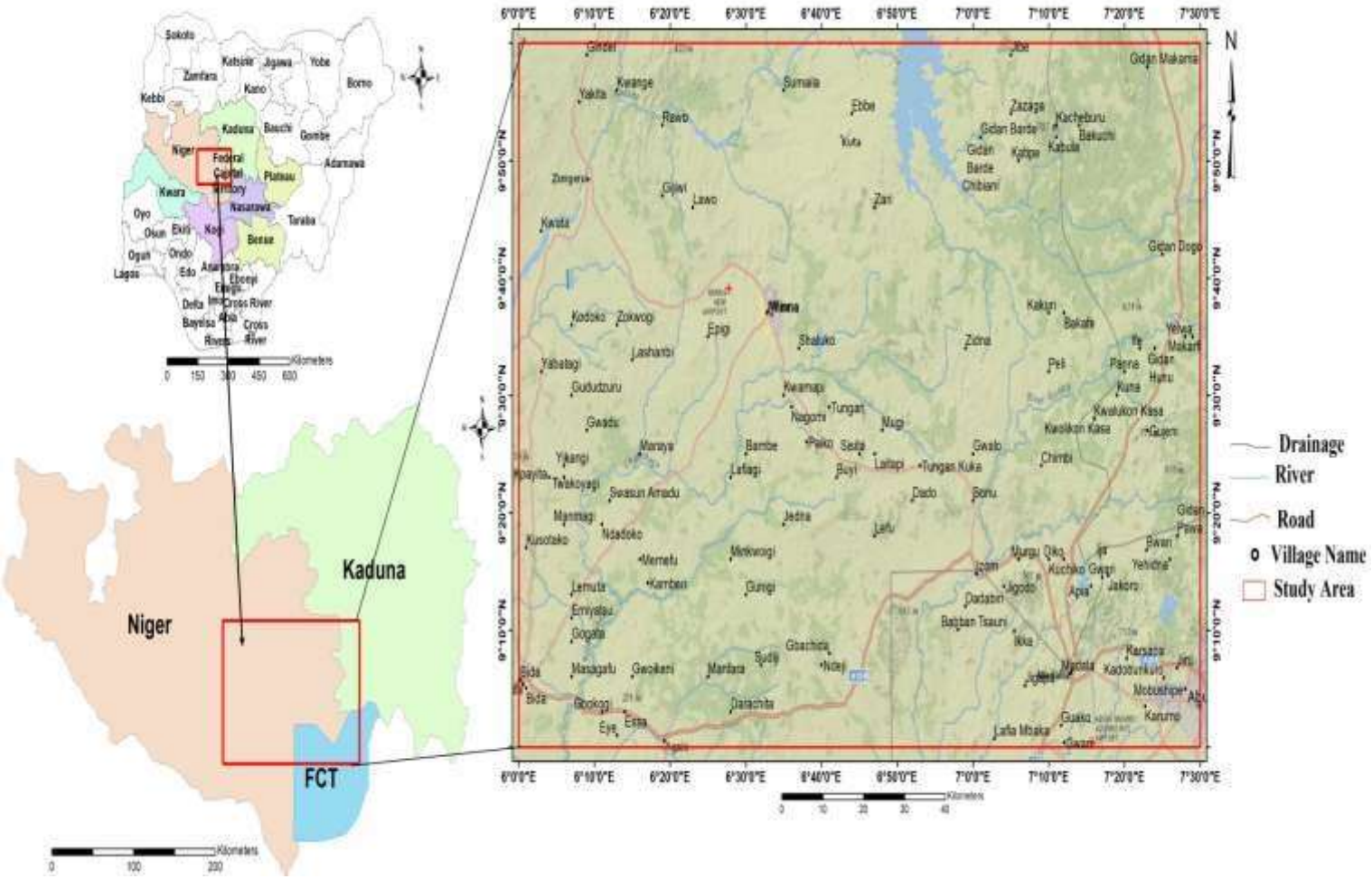

Figure 1.1: Location of the Study Area **CHAPTER TWO**

2.0 LITERATURE REVIEW

2.1 Geological Setting of Nigeria

The landmass of Nigeria is located within the Pan-African mobile belt. The belt is sandwiched between two super-crustal terrains; also referred to as African and Congo Craton (Burke and Dewey, 1972). The process of the geological formation of the country begins in the Archean and Proterozoic eons in the Precambrian (Obaje 2009a). The geology of Nigeria is dominated by crystalline and sedimentary rocks both occurring

approximately in equal proportions (Woakes *et al*., 1987). The regional geology of Nigeria is made up of three major litho-petrological components: the Precambrian Basement Complex, Younger Granites, and sedimentary basins (Kogbe, 1989).

2.2 Geology of the Study Area

Ideally, locating mineral resources entails good knowledge of the general geological makeup of the area. This necessitated a detailed geological outlining of the study area. Obaje (2009a) gave an intense description of the geology of the North-Central (NC) part of Nigeria in which the study area is located. The rocks of NC part of Nigeria are made up of the Basement Complex and the Sedimentary Basin (Bida Basin, Middle Benue Trough and the Northern Anambra Basins). However, 75% of the total landmass of the study area predominately underlain by the Precambrian rocks falls within the Northwestern portion of the Nigeria Basement Complex which is between Archean to early Proterozoic in age (Talabi, 2013), while the remaining 25% is occupied by the Cretaceous Sedimentary rocks belonging to the Bida Basin (Figure 2.1).

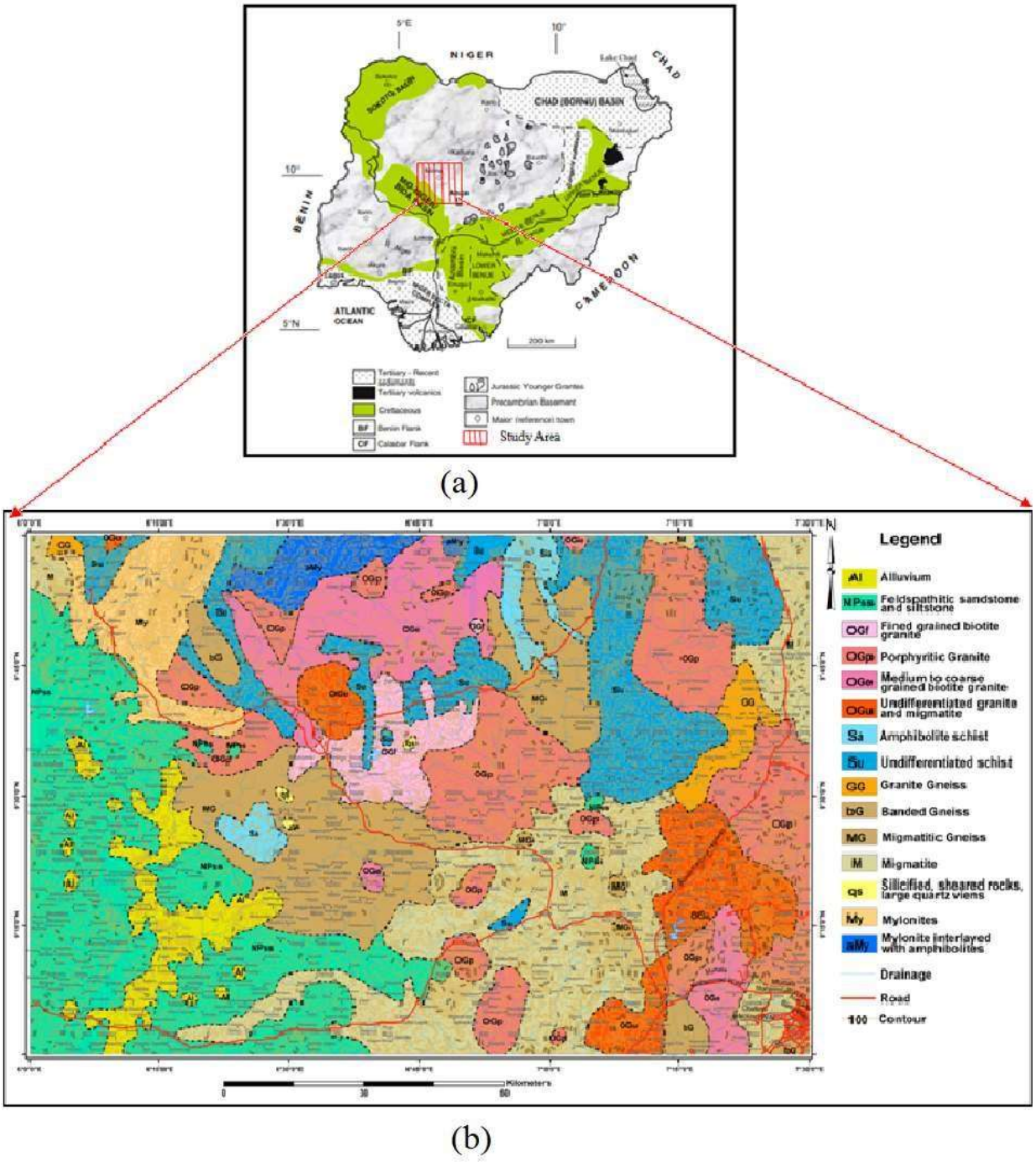

Figure 2.1: (a) Location of the Study Area (in red rectangle) on a Generalized Geological Map of Nigeria (Modified from Obaje, 2009a): (b) Digitised Geological Map of the Study Area extracted from the Geological Map of Nigeria prepared by NGSA (2009).

The sedimentary rock occupies south-western part of the study area, it covers small portion of the Bida Basin (Figure 2.1)

2.2.1 Basement complex

The Nigerian Basement Complex forms a part of the Pan-African mobile belt and lies between the West African and Congo Cratons and south of the Tuareg Shield (Oyawoye, 1972). It is intruded by the Mesozoic calc-alkaline ring complexes (Younger Granites) of the Jos Plateau and is un-conformably overlain by Cretaceous and younger sediments. The noticeable lithologies on the Basement Complex part of the study area are biotite-rich granites, porphyritic granite, amphibolites schist, migmatite, quartz veins and mylonites. Banded gneiss and migmatite with which the host amphibolites schists are closely connected to are considered as the Basement Complex *sensu stricto* (Rahaman, 1988; Dada, 2006). However, it is predominantly distributed within the component units in the Nigerian Basement Complex (Obaje *et al*., 2019). MigmatiteGneiss Complex has a heterogeneous assemblage comprising migmatites, gneisses, plus a sequence of basic and ultra-basic metamorphosed rocks (Obaje *et al*., 2019). Generally, they occur intricately associated with the Older Granites intrusion (mylonites) noticed along the Northwestern part of the geology map (Figure 2.1). But chronologically, the Migmatite-Gneiss complexes are the oldest (older than Schist Belts older and Older Granites). In aerial cover, migmatite-gneisses are most prominent in certain parts of the study area.

According to Dada (2006), the Schist Belts encompasses low-grade, meta-sediment dominated belts trending N-S which are best developed in the western half of Nigeria. These belts are regarded as Upper Proterozoic supracrustal rocks which have been infolded into the migmatite-gneiss complex (Adekoya *et al.,* 2003). The lithological

variations of the schist belts (Zungeru Schist belt) in the area of study contain coarse to fine-grained clastic, pelitic schists, phyllites, banded iron formation, carbonate rocks (marbles), and mafic meta-volcanic (amphibolites). Most belts are confined to an NNE-SSW trending zone of about 300 km wide (Obaje *et al*., 2019). However, part of the study area falls within the Schist Belts (Zungeru Schist belt) of Nigeria. The part of the study area made up of Zungeru schist belt has sequences of conglomerates and acid volcanic. The conglomerates contain fragments basically of quartz grains and feldspars. The Older Granites are believed to be pre-, syn- and post-tectonic rocks that slash both the migmatite-gneiss-quartzite complex and the schist belts (Obaje *et al*., 2019). The rocks that fall into this group vary in composition from tonalites and diorites through granodiorites to true granites and syenites (Obaje *et al*., 2019). Also, Older Granite rocks take place in most location where either rock of the Migmatite-Gneiss Complex or the Schist Belt occurs. The Zungeru Schist belt, to which the study area belongs, is found to have been intruded by large bodies of granitic rocks. The rocks of the Schist belt come about in segregation in the north-western part of the study area. The Schist in the area consists of quartz schist inter-layered with amphibolite (Obaje *et al*., 2019).

2.2.2 Sedimentary basins (rocks)

The sedimentary part of the study area is occupied by the Cretaceous Sedimentary rocks belonging to the Bida Basin (Figure 2.1). Bida Basin is a gently down-warped trough whose genesis may be closely connected with the Santonian orogenic movement of south-eastern Nigeria and the Benue valley (Obaje *et al.,* 2011). The portion that falls within Cretaceous successions was initially formed as a result of series of tectonics and repetitive sedimentation in the Cretaceous time when the South American continent was separated from Africa and the opening of the South Atlantic Ocean (Cyril, 2019a).

Furthermore, the sedimentary part of the study area also contains a North-west trending belt of Upper Cretaceous sedimentary rocks that are mostly siltstones and sandstones deposited which occur as a result of block faulting, basement fragmentation, subsidence, rifting and drifting consequent to the Cretaceous opening of the South Atlantic Ocean (Obaje, 2009b). More so, the alluvium deposits in the sedimentary terrain (Figure 2.1) are composed of sand, silt, clay and gravel

2.3 Geological Structures (Lineaments)

Structural features (lineaments) in the Nigeria Basement complex include fractures, folds and joints. These features originated from various thermo-tectonic deformational episodes mainly of the Eburnean and Pan-African Orogeny (Oluyide, 1988). Thus, the structures are ancient in age, deep seated, and trends towards the E-W direction
(Olasehinde *et al*., 1990). Geological structures play a vital role in mineral exploration. Most time, they act as channels designed to mineralise hydrothermal fluids (Austin and Blenkinsop, 2008). As a result, they have a big role in how mineralised systems are set up. On the other hand, the ground mapping of surface geology may occasionally fail to clearly identify them (Chernicoff *et al*., 2002). When such is the case, airborne geophysical survey techniques are mostly utilised to map the hidden geological structures. Lineaments are linear, continuous features displayed on a map perhaps connected to deformation zones or rock type contacts. The deformation zones are extended mappable rectilinear features of a surface whose parts align in linear or curvilinear shape that may conceivably be the expression of faults, folds, or fractures on the surface of the Earth (O'leary *et al*., 1976). Most often, lineaments act as a reservoir for deposits of vital minerals in the subsurface. Thus, deformation zones are discussed primarily from the geophysical point of view, focusing on their magnetic properties. In this present study, faults, fold, fractures, and joints related to shear zones are the major structural features to

be extracted since mineral deposits associated with hydrothermal occurrences aligned around structures (Adepelumi and Falade, 2017). Meanwhile, the pattern and extent of the alteration determines the type of mineral deposit (Rajesh, 2004). Also, host structures of hydrothermal mineral deposits always reveal the effects of their chemical interactions with the hydrothermal fluids that caused mineral deposition (Pirajno, 1992). Such alteration often forms a halo around the mineralisation, providing an exploration target considerably larger than the deposit itself (Rajesh, 2004). However, (Adepelumi and Falade, 2017) revealed the feasibility of GRS data in the discovery of hydrothermally altered zones. The discovery is based on the fact that ore minerals deposits connected with zones of hydrothermal alteration exhibit certain features that allow their identification (Rajesh, 2004). The colour of rocks is a good key to the identification of the minerals: if iron oxides are noticeable, the colour of the rock is red, brown, orange or yellow; and the presence of clays usually gives pale colour like yellow, violet, green or beige (Rajesh, 2004). Lineaments play a vital role in mineral exploration. They act as conduits for mineralising hydrothermal fluids (Austin and Blenkinsop, 2008). As such, they play a significant role in the formation of mineralised systems; though, sometimes they may not be apparently recognised from the ground mapping of surface geology. When such is the case, geophysical techniques are often used to map the hidden geological structures that might be directly related to mineralisation (Kaufmann, 1988).

2.4 Hydrothermal Alteration

Hydrothermal alteration is a complex process involving the interaction of aqueous hot fluids with rocks leading to textual, mineralogical and chemical changes within the rocks through the fluids circulates under evolving physicochemical situations (Airo, 2002; Pirajno, 1992). Prospecting for hydrothermal alteration zones suggests exploring areas with favourable geologic structural sites within the crustal levels that could provide

conduits for hydrothermal fluids (Sanusi and Amigun, 2020a). The part of the crust where such alteration process happened is regarded as hydrothermal alteration zones. Notably, the style and pattern of hydrothermal alteration depend on the temperature, pressure and composition of the hydrothermal fluids, and by extension the nature and composition of the rock through which the fluids circulates (Airo, 2002). Hydrothermal fluids chemically attack the mineral constituents of the rocks, which tend to re-equilibrate by forming new mineral assemblages that are in equilibrium with the new conditions. Characteristic of hydrothermally ore deposits point toward exploring areas with fractures within the crustal levels. Hydrothermal ore mineral deposits are build ups of precious minerals which formed from hot waters circulating in Earth's crust through fractures (Cordell and Grauch, 1985). Since, lineaments provide excellent pathways for hydrothermal fluids to circulate through. They eventually produce metallic-rich fluids concentrated in a selected volume of rock, which turn into super-saturated and then precipitate ore minerals (Izquierdo *et al*., 2000). However, a lot of alteration minerals are strongly temperature reliant and by delineating alteration mineral assemblages both at the subsurface and in the surface, it is possible to locate zones with high temperatures and permeabilities, which are vital in exploration.

The distribution and type of mineral assemblage in a system is influenced by permeability, rock and water composition, temperature, pressure and duration of activity (Nyandigisi and Katana, 2016). In addition, they provide conduits for hydrothermal fluids to interact with the tectonically deformed crustal rocks (Cunha *et al*., 2017), establish a relationship between K-enrichment zones, and provide haloes around mineralisation targets. However, areas enriched with high percentage of K (%) contents with low concentration of eTh (ppm) are associated with hydrothermal alteration zones linked with different mineral deposits (Ostrovskiy, 1975). Note, K is a major element of most rocks, while Th and U

are present in trace amounts, as mobile and immobile elements respectively (Eslam *et al*., 2004). Since, Th is immobile compare to K and U, it is utilised as a lithological background control that defines ideal K values and concentration of equivalent U (eU) in identification of hydrothermal alteration haloes (Quentin *et al*., 2019). Thus, eTh values are as well needed to conquer the effects of lithology on K and eU concentrations (Saunders *et al*., 1987). This statement makes the ratio maps and Ternary map vital when searching for signatures connected with hydrothermal alteration zones.

In this research work, *F*-parameter proposed by Efimov (1978) as K/eTh, K/eU, eTh/eU, and K×(eTh/eU) maps and Ternary composite (T-Map) image were vital in mapping hydrothermal alteration haloes connected to mineralisation zones in the study area. Meanwhile, lineaments (geologic structures) such as faults, fractures, shear zones, and lithological contacts (where rheological contrast is significant) constitute migration pathways for the deep seated hydrothermal fluids comprising of ore deposits (Yousefi *et al*., 2019; Sanusi and Amigun, 2020b). Under suitable temperature and pressure conditions, the interactions between metamorphic fluid such as water, carbonates, silica, chlorine and sulphide compounds, ions of Potassium, Sodium, Calcium, Iron and Magnesium) and tectonically deformed rocks led to the appearance of hydrothermal alteration targeting element (Sanusi and Amigun, 2020a). All the same, hydrothermal alteration is one of the constituent processes of a syn-mineralisation sub-system (chemical) that promotes the precipitation of minerals that are structurally controlled (Yousefi *et al*., 2019; Nafiz and Enver, 2015). For instance, Potassic ($KAl_3Si_3O_{10}(OH)_2$), Phyllic ($KA_{l2}(AlSi_3O_{10})(OH)_2$) and Prophylitic ($Al_2Si_4O_{10}(OH)_2$) alteration haloes are formed with mineralisation targets especially gold deposits (Sanusi and Amigun, 2020b).

2.4.1 Types of alterations

2.4.2 Potassium silicate alteration (K-silicate) or potassic alteration

K-Silicate is formed as a substitute of plagioclase and mafic silicate minerals, at temperatures within 450–600 Celsius (C) (Nyandigisi and Katana, 2016). K-Silicate alteration is characterised by the formation of new K-feldspar with/or biotite (green colored and Iron- rich (Fe-rich), typically together with minor Sericite, Chlorite, and Quartz. Chlorite displays variability in colours, forms and textures. It differs in colour from light to dark green. Texturally, it appears as small inter-granular patches, forming radial aggregates in vein-lets in association with other alteration minerals (calcite, epidote, pyrite and quartz). While, quartz is colourless though, looks whitish or greyish, and occurs in crystal forms. Thus, it occurs as infilling in both vesicles and veins. KSilicate alteration is vital in porphyry and epithermal systems, where it occurs in the high temperature core zones (Nyandigisi and Katana, 2016). In addition, K-Silicate is connected with sulfides; chalcopyrite and pyrite (Nyandigisi and Katana, 2016). A variation of it involving considerable addition of Sodium (Na) and Calcium (Ca) known as sodic and calcic alteration respectively are characterised by abundant actinolite, albite and epidote (Nyandigisi and Katana, 2016).

2.4.3 Propylitic alteration

Propylitic alteration is characterised by the adding up of water (H_2O) and carbon (II) oxide (CO_2). It contains mainly chlorite and epidote, jointly with less significant quantities of and other vital alteration minerals like albite, calcite, clinozoisite and zoisite (Nyandigisi and Katana, 2016). Epidote is characteristically recognised by its yellow to greenish-yellow colours, and its granular, sugar-like texture and appearance. It is found in fractures if not replacing primary plagioclase and pyroxene (Nyandigisi and Katana, 2016). In most cases, it forms mineral associations with actinolite, calcite, chlorite, pyrite and quartz. Pyrite is characteristically a shiny, brassy, sub-metallic yellow colour, it occurs as nicely

formed cubic crystals. Characteristically, pyrite crystals are deposited in veins and fractures. A large amount of pyrite indicates high activity of Sulphur, good permeability and past or present boiling regimes. Meanwhile, the presence crystallised epidote suggests good permeability and indicates temperatures of feldspars by hydrolysis (H ion metasomatism) in the presence of hydroxide (of more than 250°C (Nyandigisi and Katana, 2016). Propylitic alteration displays mild form of alteration symbolising low to intermediate temperatures (200-350 °C) and low fluid/rock ratios. It typifies the margins of porphyry Copper (Cu) deposits and epithermal valuable metal ores (Nyandigisi and Katana, 2016).

2.4.4 Phyllic (Sericitic) alteration

Phyllic alteration is basically due to the destabilisation OH, K and S, to form quartz, sericite (fine-grained white mica), pyrite, chlorite, and some chalcopyrite (sulphide content). In the process, Fe, K, Mg, Na and Ti are leached out. Sericitic alteration is associated with porphyry Cu deposits, but also with meso-thermal valuable metal ores and volcanogenic massive sulfide deposits in felsic rocks.

2.4.5 Argillic alteration

Argillic alteration pattern is subdivided into intermediate argillic and advanced argillic classes. Intermediate argillic alteration affects plagioclase feldspars mainly, and is characterised by the formation of clay minerals (Kaolinite and Smectite group). It characteristically forms below about 250 °C, and occurs on the fringes of porphyry systems. While, advanced argillic alteration symbolises an intense form of base leaching where rocks have been stripped-off alkali elements by very acidic fluids vigorous in high fluid/rock ratio environments. It is typified by kaolinite and pyrophyllite, depending on the temperature, and alunite jointly with lesser topaz, tourmaline and quartz. Besides, it is often linked with epithermal valuable metal deposits where alteration is connected with

boiling fluids and condensation of volatile rich vapours to form extremely acidic solutions (Nyandigisi and Katana, 2016).

2.4.6 Silicification

Silicification refers specifically to the formation of new amorphous silica minerals or quartz in a rock during alteration. It is usually a by-product of iso-chemical hydrolysis reactions where Silicon (Si) is locally derived. The majority of fractures via which hydrothermal fluids flow are at least partially filled with quartz to form veins. The Si in these settings is derived by leaching of rocks through which the fluids are circulating. Extreme silicification, however, forms as a result of cation metasomatism (Nyandigisi and Katana, 2016). Characteristically, silicification alteration is of the high level epithermal valuable ore deposits.

2.4.7 Carbonatisation

Carbonatisation refers to the formation of carbonate minerals such as calcite, dolomite, magnesite and siderite during alteration of a rock (Nyandigisi and Katana, 2016), promoted by fluids characterised by high partial pressures of CO_2 and neutral to alkaline pH.

2.4.8 Greisenization

Greisens represent an alteration assemblage comprising mainly quartz, muscovite, and topaz, with lesser tourmaline and fluorite, usually forming adjacent to quartz-cassiteritewolframite veins (Nyandigisi and Katana, 2016)

2.5 Airborne Geophysical Survey Techniques

Airborne geophysical survey techniques are widely employed worldwide as a base for geophysical interpretations, these techniques play vital roles in detecting and mapping of

geological features (lineaments) like faults, folds, joints and shear zones (Rani *et al*., 2018) and the identification of hydrothermal alteration zones. These structures are significant in the exploration and localisation of zones mineralisation. This is proofed by the fact that most important mineral deposits are spatially associated with crustal scale structures (Ribeiro and Mantovani, 2016). Globally, demand for mineral commodities has led to the increasing application of geophysical technologies to a wide variety of ore deposits (Dentith and Mudge, 2014). An understanding of the basic geologic characteristics of ore deposits is crucial to evaluating known deposits and delineating prospective areas of mineralisation (Dentith and Mudge, 2014). So, this study, employed magnetic and radiometric techniques to determine the probable location of mineralisation by structure delineation, mapping lithology and hydrothermal alteration connected to probable mineralisation zones.

2.5.1 Magnetic technique

In the prospection of minerals, interpretation of aeromagnetic data is needed to delineate probable rocks, geologic structures playing a host to mineral deposits. Nevertheless, geologic structures (lineaments) such as faults, fractures, folds play a very important role in the task of deposit localization, but their visualisation from the graphical representation of raw data is unpredictable. In this case, some mathematical techniques for signal enhancement were applied to the aeromagnetic data. The results of the match filtering and derivative-based techniques is quite uncertain, therefore it is very important to apply different filters, so that each will leverage to some extent different aspect of the magnetic respond. However, filtering of aeromagnetic data is fundamental prior to interpretation of the data. The essence of the filtering techniques assumed to be edge detectors techniques is to set up data, then produce maps in such a way that magnetic anomalies are interpreted easily in term of their geological sources. One of the basic correction filters is the

Reduction to the Equator. It is meant to determine the asymmetrical shape of anomalies by reproducing the magnetic anomalies.

2.5.2 Radiometric (Gamma-ray Spectrometry) technique

Radiometric survey technique measures the surface distribution of radioelements (Potassium (K), Thorium (Th) and Uranium (U)) occurring naturally. This method typifies the changes in lithological units due to the variations in the concentration level of the radioelements between different rock units (Silva *et al*., 2003; Wemegah *et al*., 2015; Elkhateeb and Abdellatif, 2018). Thus, radiometric technique recognises the presence of the natural radioelements: (K, Th and U) in different rocks. Besides, gamma-ray spectrometry technique is more effective in hydrothermal alteration haloes linked to targeting mineralisation (Airo, 2015). Though, the output effects depend on certain facts that include whether there are measurable variations in the radio-element distributions that can be associated to differences in host rock lithologies and the concentration K content of the rock must have been modified by alteration procedures (Airo, 2015). Radiometry survey entail mapping of surface structures and lithological units as different rock types (igneous, metamorphic, and sedimentary) are discovered based on distinctive radioactive signatures (Kearey *et al*., 2013). This survey technique is barely utilised compared with other geophysical survey techniques because it is merely used for specific target (Kearey *et al*., 2013). Despite the fact that there are numerous naturally occurring radioactive elements, only three radioelements (Potassium

(K), Thorium (Th) and Uranium (U)) are significant in the identification of hydrothermal alteration zones linked with mineral exploration (Kearey *et al*., 2013; Youssef and Elkhodary, 2013). Gamma-ray spectrometry survey provides useful information directly interpretable in terms of hydrothermal alteration zones (Shives *et al*. 2000) than any other single airborne geophysical survey technique (Eslam *et al*., 2004). Thus, it provides a

direct measurement of the surface distribution of the naturally occurring radioactive elements (K, Th and U). These measurements are used for mapping and characterization of different lithologic units arising from the variation in the concentration of these radioactive elements in various rocks (Elkhateeb and Abdellatif, 2018).

On the other hand, the interpretation of radioelements distribution for delineating hydrothermal alteration zones is based on the assumption that different rock types are composed of certain amounts of rock-forming minerals which comprise specific quantities of radioactive elements. Measuring the concentration of each of the radioelements (K, Th, or U) is attained by estimating the intensities of emitted gammaray radiation which can then be used to create maps illustrating the three radioelements with their ratios (Salem *et al*., 2007). Besides, analyses of airborne gamma-ray spectrometric tend to reveal a common correlation among different rock units with their structural trends (Taofeeq, 2020). Airborne gamma-ray spectrometry data proffers a three-element image of the prospective area from the Red-Green-Blue (RGB) composition of K, Th and U and possibly improve the reflection of structures and hydrothermal alteration footprints than the field observations.

Hence, a case study in which airborne gamma-ray spectrometric data sets was analysed and interpreted to delineate hydrothermal alterations associated with mineralisation zones within the study area was executed in this research. The total count image, ratio map display and ternary image techniques were applied to enhance the identification of hydrothermal alterations in the area. The ratio maps are helpful in the sense it makes one get familiar with the zones having high concentrations of K and eTh which is generally considered to be mobile and immobile elements, respectively (Silva et al., 2003).

2.6 Review of Previous Geophysical Work

Utilisation of either aeromagnetic data or gamma-ray spectrometric data or the integration of two data sets is a familiar approach often employed worldwide by the different researcher to delineate geological structures and hydrothermal alteration haloes associated with mineralisation zones. Such studies are summarised as follows:

Shives *et al*. (2000) used gamma ray spectrometric data to delineate Potassium alteration connected with polymetallic volcanic-hosted massive sulfides, magmatic hydrothermal deposits (Au–Co–Cu–Bi–W–As), and porphyry Cu–Au–(Mo). The researchers demonstrated that the Potassium enrichment in the geological settings is characterised by anomalously low eTh/K ratios relative to normal lithological signatures that could be used as an important exploration indicator.

El-Sadek (2009) used an airborne aeromagnetic and gamma ray spectrometry data on Um Salim gold mine situated in Eastern Desert of Egypt. The outcome of the study proved that gold mineralisation is associated to extremely low aero-radio spectrometric levels on the created ratio maps of eTh/K, eU/eTh, and eU/K. Also, the eTh/K and eU/K ratio maps exhibited two anomalies associated with gold occurrences in Um Salim Mine linked to an alteration rim around the major gold mineralisation zone.

Abubakar (2012) executed a research in Kushaka schist belt located within northwestern part of Nigeria with the aim of delineating geologic structures using aeromagnetic, remote sensing and GIS methods. Integration of the three techniques proved that the delineated deep-seated geologic structures associated with mineralisation zones in the area coincide with the exact location where artisanal miners presently exploiting gold deposits. Though, the area is a notable gold mineralisation zones.

Boadi *et al*. (2013) used airborne magnetic and radiometric data to examine Konongo area situated at the North-eastern boundary of the prospective Ashanti Gold Belt in south-eastern Ghana. The purpose of the research is to identify the individual lithology and delineate probable geological structures that host hydrothermal haloes which control gold mineralisation in the area with help of selected filtering techniques. The delineated geological structures (faults, folds, fractures, and lithological boundaries) are assumed to be caused by tectonic structural deformation events that took place in the area. These structural features presumed to be associated with potential hydrothermal gold mineralisation zones within the area trended mainly towards NE-SW and NNWSSE directions. The radiometric datasets retrieving geochemical information on Potassium (K), Thorium (Th) and Uranium (U) concentrations in the study area were used to delineate bedrock lithology formation, alteration as well as contact zones. Finally, integrating both techniques (airborne magnetic and radiometric data) resulted in a better definition of both geological structures and lithological boundaries; it also shows the value of geophysical data in mapping likely geological structures that host hydrothermal gold mineralisation within the study area. The delineated geological structures correlated with the mineral resource map of the study area.

Gaafar (2015) executed a research in Um Naggat area, Central Eastern Desert, Egypt. The aim of the research is to delineate mineralisation zones using geophysical data (aeromagnetic data) and geological techniques. The end products show that the four geological structures delineated trended towards the E-W, ENE, NW and NNW direction. However, it is assumed that the delineated structures are the likely pathways through which mineralised fluids may have travelled. Thus, they played significant roles in mineralisation.

Wemegah *et al*. (2015) utilised airborne magnetic and radiometric data sets to outline geological boundaries, geological structures, hydrothermal alterations associated with gold mineralisation zones in the Kyerano area located within the South-Western Ghana. Application of FVD and TD on the aeromagnetic data set enhanced the edges of geological structures (fold, fractures, and the contact zones) within the area. Analyses of the structures via a rose diagram reveal the direction (NE-SW and NNW-SSE) of the two main tectonic events in the area. The produced Ternary map and Composite map also revealed the lithological units based on subtle differences in the radio-elements concentrations.

Sadiya *et al*. (2016) used remote sensing and GIS methods to extract lineaments in an area situated in the northern part of Nigeria. Band 4 of Landsat 7 ETM+ and PCI Geometric as well as its line extraction algorithm was employed. However, false colour composite of bands 4:7:3 in RGB respectively showed locations of probable hydrothermal alteration zones in purple hue. The satellite imagery makes lineaments extraction easier, time saving and cheaper than the traditional method. Though, limitations encountered with using remote sensing data (satellite image) in mineral prospecting is that, man-made features such as built-up areas, and impermeable surfaces appear as hydrothermal zones due to their high reflectance properties and the materials used in creating them. Comparison between the lineaments with the bands 4:7:3 composite images showed that there is a correlation between locations with prevalence of lineaments. Superimposing recognised minerals locations on the lineaments density map confirm the existence of hydrothermal alteration zones as obtained from the image processing.

Awoyemi *et al*. (2017) examined the likelihood of extension of the Ifewara fault line beyond the Ilesha area by applying enhancement techniques such as ASA, HGM, FVD and Euler Deconvolution to the aeromagnetic data of Ilesha located in the south-western

part of Nigeria. To recapitulate various studies, the Ifewara fault line believed not to have exceeded the south-western part of Nigeria, actually extended to the northern part of Nigeria.

Eze *et al*. (2017) carried out a study in of part of Anambra basin and Southern Benue Trough using aeromagnetic and radiometric data. Their aim was to highlight possible mineralisation zones. AS, First and Second Vertical Derivatives, Horizontal Derivative (HD) and Tilt Derivative (TD) were employed in delineating magnetic lineaments, lithological boundaries, and contact zones within the area. It was observed that the anomalies on the TMI map are characterised by smooth contours and low magnetic relief while the surrounding platform area shows steep gradients and high relief. Thus, lineaments were identified at the central portion of the area. The likely areas with high concentrations of mineral deposits (intrusive areas) correlate with high analytical signal amplitude. Conversely, the researchers concluded that areas with high analytical signal amplitude correspond to high concentration of mineral deposits.

Falade and Adepelumi (2017) used aeromagnetic and radiometric data to execute a research in an area situated in North-eastern part of Nigeria. The aim of the research was to identify the possible zones of Uranium deposition in the area. The aeromagnetic data was processed to accentuate anomalies of interest using RTE, Horizontal Gradient Magnitude (HGM), Analytical Signal Amplitude (ASA), First Vertical Derivative (FVD) filters. Thereafter, 3D Euler deconvolution, spectral analysis and Source Parameter Imaging (SPI) techniques were used for the depths to the basement. Modelling of two profiles taken across the suspected Uranium-rich zones was executed to offer 2D model representations of the basement blocks beneath the zones. The equivalent Uranium (eU) and equivalent Thorium (eTh) distribution maps of the radiometric data were processed to obtain the eU/eTh and eU (eTh/3.5) ratio maps which were used to determine the

concentrations and remobilization of Uranium. Most of the delineated geologic structures trend ENE-WSW, NE-SW, E-W, and NW-SE and depths to the basement is 1.5 km. Thus, the uplifts and depressions on the map of the basement morphology coincide with the basement complex and the sedimentary terrains of the area respectively. Results from the eU/eTh and eU (eTh/3.5) ratio analyses showed that Uranium ores in the area were probably remobilised epigenetically from the granitic rocks and were later deposited into sedimentary rocks.

Muhammed *et al*. (2017) used high resolution airborne magnetic and gamma-ray spectrometric datasets for the detection of hydrothermal alteration zones in Gabal ElRubshi area located at the Central Eastern Desert (CED), Egypt. The results of the airborne magnetic data proved those magnetic signatures linked with the hydrothermal alteration haloes in mafic (ultramafic) rocks are structurally controlled. Besides, airborne gamma-ray spectrometric images prove radioelements measurements for different lithological units. Concurrently, anomalous Th/K ratios along local shear and fracture zones are indicative of mineralisation zones. On the other hand, the variation of U/Th ratios principally reflects the environmental conditions during later deformational phase. In conclusion, the researchers demonstrated the effectiveness of integration of airborne magnetic and gamma-ray spectrometric datasets for delineation of
hydrothermal alteration haloes linked with mineralisation zones.

Ohioma *et al*. (2017) utilised aeroradiometric data set of Isanlu (sheet 225) with aim of delineating hydrothermal alteration zones associated with gold mineralisation zones. The filtering techniques used for the recognition of the concealed hydrothermal alteration zones are the Elemental Ratio Enhancement (ERE) and Shaded Relief (SR), executed by both Geosoft Oasis Montaj Software package and Surfer (Golden) software package. The outcome result via production of the Ternary map shows the delineation of eight

hydrothermally altered zones equivalent to probable sites for gold mineralisation. Besides, the results attained in the research study shows that mapping of hydrothermally altered zones that favours gold mineralisation is feasible even without the actual physical contact and visitation to the study area.

Andrew *et al.* (2018) carried out a research with the main goal of delineating mineralisation zones within the North Central part of Nigeria using aeromagnetic data. The study area under investigation covers a total area of about 27,225 km^2 (bounded by Latitudes $8^o\,30'$ N to $10^o\,00'$ N and Longitudes $7^o\,00'$ E to $8^o\,00'$ E). The research goal was achieved as a result of the concealed lineaments that revealed the potentiality of the area through the utilisation of certain enhancement techniques like FVD, HD, TD and AS. However, the presence of high magnetic susceptibility values within the western part of the study area is an indication of a high mineralisation zone. Also, each of the results of the enhancement maps correlated.

Ahmed (2018) used aeromagnetic, aeroradiometric data and satellite images of the West Safaga located in eastern desert of Egypt with the aim of delineating hydrothermal alteration (anomalous radioactive) zones responsible for mineral deposits. The purpose of the research was achieved via delineation of possible geological structures associated with favourable mineralisation zones areas of mineral deposits. Thus, geologic structures (lineaments) play an imperative role in the task of mineral deposit

localization.

Emmanuel *et al*. (2018) carried out a study in Mambila plateau situated in the North Central part of Nigeria. The purpose of executing the study is to delineate potential mineralisation zones. Thus, aeromagnetic data was used. The result was interpreted qualitatively and quantitatively using two methods: standard Euler deconvolution and

forward and inverse modeling techniques. The maximum depths obtained from each method are approximately 2.3 km, which is an indication for excellent hydrocarbon accumulation in the area. This concurs with the statement of Chinwuko *et al*. (2012) that the minimum thickness of the sediment required is 2.3 km if other factors are satisfactory.

Nwokeabia *et al*. (2018) executed a research in part of Ife-Ilesha Schist Belt situated in Ondo, southwest Nigeria with the aim of delineating zones of mineralisation using aeromagnetic and radiometric dataset. Selected filtering techniques such as RTE, FVD, AS and TD were used to enhance any high intensity magnetic bodies interpreted as linear geological features (lineaments). The main geological structures oriented towards NE-SW and NNE-SSW directions. This corresponds to potential alteration gold mineralisation zones within the area. The lineaments between schist felsic and mafic rocks are alleged to host gold mineralisation in the Ife-Ilesha Belt were also delineated. The radiometric datasets recovering geochemical information on K, Th and U concentrations in the study area were used to delineate bedrock lithology (Granite, schist, gneiss) as well as alteration contact zones. The high resolution airborne magnetic and radiometric data of the study area resulted in better definition of both geological structures and lithological boundaries. At the end, their study demonstrates the economic potential of the Ife-Ilesha Schist Belt within Ondo in southwest part of Nigeria.

Olasunkanmi *et al*. (2018) used High Resolution Aeromagnetic Data (HRAD) to map geologic structures associated with mineral deposits in Igbeti-Moro area, situated within the South-western part of Nigeria. The HRAD was subjected to data enhancement processes and interpreted to set up major geologic features linked with occurrence of marble, gabbro and muscovite mineralisation in the area. The filtering techniques utilised are 2D Fast Fourier transform filters that includes Reduced-To-Equator (RTE),

FVD, Horizontal Gradient (HG), AS, Source Parameter Imaging (SPI) and Average Power Spectrum (APS). The outcome of the research shows that lithological boundaries, geological structures (faults and fractures), contacts and magnetic sources depths were established. However, the delineated lineaments (fractures and faults) represents the geological features associated with emplacement of the quartz-schist and muscovite-schist, which would have formed synchronously with isoclinal fold and hosts marble, gabbro, amphibolites and muscovite mineralogy at shallow depth that ranges from 0-200 m in the area. Conclusively, the geologic features noticed are presumed to be associated with the solid minerals deposits which serve as an additional socialeconomic benefit in the area.

Olomo *et al*. (2018) executed a research in Iperindo which lies within the Ilesha schist belt of the Precambrian Basement Complex located in the Southwestern part of Nigeria, using airborne geophysical and satellite remotely sensing techniques. The combined approach aided the evaluation of the subsurface geology via delineation of geological features associated with mineralisation zone within the study area. The investigation involved the use enhancement filtering techniques like RTE, Upward continuation, different derivatives and 3-D Euler deconvolution as well as radial spectral analysis to locate and estimate the depth to magnetic anomalous bodies in the area. Also, lineaments were extracted from Landsat Thematic Mapper imagery to compliment the effects of the interpreted magnetic anomalies on the produced magnetic anomaly maps. Thus, coincidence of both magnetic and the Landsat extracted lineaments trends implies that lineaments reflect real continuous fault/fractures in depth. However, the processed images shows the major lineaments extracted trended towards the NE-SW direction and they are assumed to be the diagnostic primary structures of potential targets for mineralisation in the area.

Omar and Mahmoud (2018) determined the probable location of gold mineralisation via delineating geological structures, mapping lithology, and hydrothermal alteration zones in a selected part of the Central Eastern Desert of Egypt. The research was executed integrating aeromagnetic and gamma-ray spectrometric data sets. Selected enhancement filtering techniques such as FVD, AS, Centre for Exploration Targeting (CET), and porphyry plus ratio and ternary images were applied on both data sets which provide a high-quality representation of near-surface features that facilitated the interpretation process. The NW-SE was the most significant and considered as the favoured orientation of ore deposits. Composite map consisting of geology, lineaments and hydrothermally altered zones was produced using ArcGIS. Five known locations of gold mineralisation were extracted on the map and three new sites were suggested to be favourable locations for mineralisation emplacement.

Similarly, Elkhateeb and Abdellatif (2018) delineated a probable gold mineralisation zone in part of the central eastern desert of Egypt utilising airborne magnetic and radiometric data sets. Ultimately, the researchers produced different maps of the area pointing out areas of high mineralisation potential. Besides, the filtering techniques
(RTE, FVD, HG and AS) used were helpful in the enhancement and recognition of geologic lineaments (faults, fold, joints, contact, lithologic boundaries including hydrothermal alteration zones) associated with mineralisation zones.

Balogun (2019) evaluated geological settings and structural disposition of Ilorin situated in the North central part of Nigeria using airborne geophysical data sets with a major target of analysing aeromagnetic and aeroradiometric data via application of different enhancement techniques that would facilitate the delineation of geologic signatures, lithological boundaries, hydrothermal alterations as well as estimate the depth to the magnetic sources based on susceptibility contrasts of subsurface rocks in the study area.

In the end, the research concluded that fractures interfering with metamorphic processes could have influenced the crustal deformation pattern of the area.

Cyril (2019a) used high resolution aeromagnetic dataset, sheet 303 for the characterisation of the subsurface litho-structural features within a portion of the Lower Benue Trough in Nigeria. The aim of the research was to delineate probable mineralisation zones in the area. The aeromagnetic data set was subjected to different enhancement methods (RTE, Regional and Residual separation, Upward Continuation, Downward Continuation, and Second Vertical Derivative (SVD), Automatic Gain Control, AS, TD, Radial Average Power Spectrum (RAPS), and ED filters) for both qualitative and quantitative interpretations. The end results from the maps produced proved that the ranges of magnetic intensity values characterised the rocks as shale and Limestone within specific location in the area, and regional trends of these rocks and structure thin-out with measure depth continuation at 0.5 km, 1 km, 2 km, 3 km, 7 km and 10 km. Also, three (3) major faults were delineated NE-SW, NW-SE and ENEWSW directions. The depth to top of magnetic source displayed by RAPS and ED is 0.27 km and 2.64 km for shallower and deeper sources respectively. In conclusion, the study demonstrated the effectiveness of airborne geophysical method for regional mapping of lithologies and structures that may possibly host important minerals as well as aid hydrocarbon accumulation and their likely depths.

Ogungbemi *et al*. (2019) effectively integrated aeromagnetic and gamma-ray spectrometric data sets in a study executed in Agbabu area (Study area) located in Odigbo local government area of Ondo State, South-western, Nigeria. The aim of the study is to delineate lineaments constraining bitumen deposits in the area. Several enhancement techniques applied on magnetic data sets prompted the extraction of concealed lineaments perhaps harbouring bitumen deposits. Also, information concerning depth to the magnetic

basement and lithological boundaries provided more important clues about the potential mineralisation zone. Likewise, the interpretation of the aeroradiometric data sets disclosed geochemical information on K, eTh, and eU and revealed very important clues about bedrock lithology within the area. Thus, the integration of the different data sets was helpful in the identification of the aerial extent of bitumen in the area.

Akinniyi *et al.* (2020) executed a research in Isanlu (sheet 225), located within the North Central part of Nigeria with the aim of delineating interpretable geological structures plus lithological units linked to potential mineralisation zones in the area using gridded aeromagnetic and aeroradiometric data sets (gamma-ray spectrometric data). The acquired aeromagnetic data were reduced to the magnetic equator and then subjected to various filtering procedures such as First Vertical Derivative (FVD), Tilt Derivative (TD) and Analytic Signal (AS) techniques that reveal enhanced magnetic anomalies. Different maps were produced; afterward, a model was created along with a selected profile for improved interpretation of the magnetic anomalies. Similarly, the gridded aeroradiometric data were subjected to both enhancement and statistical operations. The lithological zones were mapped. At long run, several probable hydrothermal alteration zones were delineated within the study area with an obvious interpretable structure trends towards NW-SE direction, which is in general consistent with that of schist belts in Nigeria.

Ohioma (2020) carried out a research in an area bounded by Latitudes $8^{o}\,00'$ N to $8^{o}\,30'$ N and Longitudes $5^{o}\,30'$ E to $6^{o}\,00'$ E using Aeroradiometric data. The aim of the research is to detect Sulphide deposit in the area. The aeroradiometric data was subjected to elemental concentration enhancement using Geosoft Oasis Montaj

Software. From the ratio maps produced, the Red coloured portions indicate high

Uranium and low Potassium formations, while the Blue coloured portions indicate low Uranium and high Potassium formations. However, the regions with very low count rate of Uranium compared to high count rate of Potassium indicate the presence of abundant Potassium while high concentration of Uranium associated with low concentration of Potassium signifies abundant Sulphide deposits. Thus, Sulphide deposits are characterised by an increase in Uranium and a decrease in Potassium. Conclusively, the central part of the area encloses high concentration of Sulphide deposits.

Sanusi and Amigun (2020a) executed a research within the Kushaka schist belt located in the North-central part of Nigeria using airborne magnetic and gamma-ray spectrometry datasets. Their mission is to assess the sub-surface geological structures and hydrothermal alteration haloes that are connected to orogenic gold mineralisation in the area. The geophysical analyses executed to enhance the quality of the aeromagnetic data for better interpretation of the subsurface geology are Reduction-To-Equator
(RTE), Upward Continuation (UC), Total Horizontal Derivative (THD), Analytical Signal, Source Edge Detection (SED) and Tilt-angle Derivative of Total Horizontal Derivative (TD_THD). Also, the analyses executed on the airborne gamma-ray spectrometry data were made on K/eTh, F parameter and deviation of ideal K values (Kd). The end results attained from the different magnetic enhancement methods used in the research proved that major subsurface geologic structures (lineaments) controlling orogenic mineralisation in the area trended towards in the ENE-WSW direction while the minor ones trended towards the E-W and NW-SE directions. The hydrothermally altered zones outlined shows they are structurally controlled and closely connected with orogenic gold mineralisation. However, the lineaments with depth range of 427.96 m and < 607.61 m and aerial extent of 15.5 km by 6.5 km serve as localiser of gold deposits within the Kushaka schist belt situated within North-central part of Nigeria. Taofeeq (2020)

executed a research in the south-western part of Nigeria. The reason behind the research is to delineate mineralisation zones using aeromagnetic and aeroradiometric data sets. Filtering techniques such as First Vertical Derivative (FVD),

Analytic Signal (AS), Power Spectrum (PS) and Centre for Exploration Targeting (CET) methods were used for data analysis and interpretation via mapping of geological structures, lithological units and hydrothermal alteration zones. The end results obtained from aeromagnetic maps demonstrated that most of the geologic structures predominantly trending towards the NE-SW direction are considered to be orientations of mineral deposits in the area. Depth estimation of near-surface structure computed using the AS technique conform/corroborate with the depth estimation obtained from using PS technique. Also, aeroradiometric analysis based on the concentrations of Potassium (K), equivalent Thorium (eTh) and equivalent Uranium (eU) on the radiometric Ternary map (T-map) display lithological units and hydrothermally altered zones within the area. Conclusively, the two airborne geophysical data sets were used to evaluate the spatial relationship between the near-surface structures, hydrothermal alteration zones as well as various lithologies in the zone located between the schist belt and the Migmatite-Gneiss complex units of the south-western basement complex of Nigeria.

Tawey *et al*. (2020) successfully used aeromagnetic data to map prospective mineralisation zones within north-central part of Nigeria. Geological structures playing host to ore solid minerals were delineated on the produced derivative maps. Since, shallow seated structures are the main targets, the Residual Magnetic Intensity (RMI) map of the study area was Reduced- To-Pole (RTP). Afterwards, several enhancement procedures such as First and Second Vertical Derivative (FVD and SVD), Analytic Signal (AS), Tilt Derivative (TD) were executed on the resulted RTP map to clear the picture for interpretation. Also, Euler Deconvolution (ED) was used for direct evaluation of depth to

magnetic structures from the gridded magnetic data. At the end, their results proved that geological and structural maps play a vital role in mineral prospecting as they allow delineation of ore-bearing host rocks and structures related with mineralisation.

Aliyu *et al*. (2021) carried out a research within the North-central part of Nigeria. Their aim was to delineate the lineaments (faults, dykes, folds, and other intrusive bodies) possibly hosting gold deposits using airborne Magnetic and Radiometric data sets. The filtering techniques implemented on the airborne magnetic data sets are Reduce to the Equator (RTE), Analytical signal (AS), First Vertical Derivative (FVD) filters and Centre for Exploration Targeting (CET). Also, enhancing techniques such as Ternary imaging was implemented on the airborne radiometric data in order to delineate hydrothermal alterations linked to gold mineralisation. However, the end results shows that within the North-western part of the study area, the delineated lineaments perhaps hosting the gold deposits trend towards NE-SW direction. Also, towards the E-W direction, there are traces of volcanic activities. Similarly, the delineated radiometric signatures on the Ternary map demonstrate high percentage of Potassium with low concentration of equivalent Thorium (Th). Thus, an indication of hydrothermal alteration zones in the area. Conclusively, gold mineralisation associated with hydrothermal alteration haloes are controlled by geological structures.

Ombiro *et al*. (2021) integrated Induced Polarisation (IP) and resistivity methods (geophysical techniques) with remote sensing and geological methods to delineate geological structures associated with the mineralisation zones in Lolgorien, Kenya. Integration of the three techniques confirmed some of the hidden subsurface mineralisation zones in the area via delineation of geologic structures that acted as conduits for hydrothermal alteration mineral trail. Consequently, the integration assisted in decreasing uncertainty that is frequently associated with mineral exploration in the

area. At long run, it was discovered that the disseminated minerals (gold and sulphide) are hosted in massive quartz veins and auriferous quartz veins hosted in Banded Iron Formations. Thus, the mineralisation was controlled by lineaments which majorly trend in NE-SW and NW-SE directions. Also, the IP and resistivity techniques effects exemplified the depth of the lineaments hosting the minerals as 172 m.

Toafeeq *et al*. (2021) executed a research within Bida Basin, in Nigeria. High-resolution aeromagnetic dataset was analysed using combinations of enhanced mathematical methods: RTE, THD, TD, CET and ED to acquire useful information about lineaments, trends, and depths to metallic sources responsible for prospective mineralisation zones in the area. The outcome on the RTE map shows variations of anomalies of various sizes characterised by positive (high) and negative (low) magnetic anomalies trending majorly in NW-SE and E-W directions. Also, the results in TD, THD and CET maps revealed various striking subsurface structures trending NW-SE, E-W directions, and the estimated depth is within 0.75 and 1.9 km. According to their findings, prospective ore minerals deposits aligned in the orientations of the lineaments.

John *et al*. (2022) integrated aeromagnetic, aeroradiometric and electrical resistivity survey dataset to unravel near surface geological features which are related to Rare Earth Element (REE) enrichment in the Ijero-Aramoko pegmatite site in south-western Nigeria. Selected enhancement filtering techniques were used to delineate shallow structures in the study area. The high concentration content of eTh and eU and high magnetic anomalies at the edge of geologic structures were attributed to REE and gemstone mineralisation in the area. The geophysical characteristics over the REE and gemstone mineralised zones were used to set up a relationship between REE mineralisation and geophysical signatures. The resultant mineral potential map showed a 74% agreement with the known mining pits in the study area (John *et al*., 2022).

In the region where the study is situated, trial-by-error via excessive digging has been a nonstop technique of searching for areas of mineralisation, these practises causes lots of environmental hazards, yet, there are difficulties in locating mineralised zones. To avoid this drawback, appropriate airborne geophysical survey techniques via application of their respective data sets were adopted. Aeromagnetic and airborne gamma-ray spectrometric data sets were adapted as reconnaissance tools that allow rapid coverage of large area within a short period of time, precautionary measures were observed in selecting probable mineralisation signatures concealed due to the existence of extensive outcrops, dense soil, and deep vegetation cover in the area. The information obtained would serve as a supportive database for further prospective research on mineral exploration targets in the region, thereby solving the age-long challenges of data dissemination.

CHAPTER THREE

3.0 MATERIALS AND METHODS

3.1 Materials

The materials used during the course of this study are:-

1. Airborne Magnetic data sets:-
    a. Six (6) Total Magnetic Intensity (TMI) maps designated as sheet 163 (Zungeru), 164 (Minna), 165 (Bishini), 184 (Bida), 185 (Paiko), and 186 (Abuja) covering the study area. Each of the sheets (data) was made available in a digital format (gridded form).
2. Airborne Gamma-ray spectrometric data sets:-
    b. Digital format of high resolution airborne radiometric data (in gridded form) principally Potassium (K), equivalent Thorium

(eTh) and equivalent Uranium (eU).

3. Digitised geology map of the study area,
4. Mineral resource map of the study area,

The software packages utilised are:-

a. ArcView 10.8
b. Geosoft® Oasis Montaj™ version 8.4
c. Matlab
d. RockWorks17.

3.2 Methodology

Description of the steps utilised in achieving the aim and objectives of this study are:-

3.2.1 Data acquisition

The high-resolution airborne magnetic and gamma-ray spectrometric data sets utilised for this study were procured from the Nigerian Geological Survey Agency (NGSA), Abuja. The data set were part of the data amassed during a nationwide airborne geophysical survey exercise organised by the Federal Government (FG) of Nigeria between 2005 and 2009 with the ultimate goal of providing high-quality geosciences data sets useful in promoting mineral exploration and other relevant services in Nigeria.

Under the supervision of the NGSA, the survey exercise was executed by Fugro Airborne Surveys (FUGRO) using light Cessna Caravan fixed-wing aircrafts. Based on the information provided by the NGSA, the aircrafts used had Scintrex Cesium vapour magnetometers, 512-channels gamma-ray spectrometers to measure magnetic and radioelements variations of the earth, respectively and other gadgets mounted on its fixed-wings. The aircrafts were flown in Northwest-Southeast (NW-SE) direction with a nominal terrain clearance of 80 metres with flight line spacing of 500 metres, tie lines in

Northeast-Southwest (NE-SW) direction with tie line spacing of 2 kilometres interval at the rate of 250-290 kilometre per hour (km/h) (NGSA, 2009). The airborne magnetic and gamma-ray spectrometric data sets were recorded and maintained at an interval of 0.1 second and 1.0 second respectively. Also, the projection method used in processing the data sets is the Universal Transverse Mercator (UTM) with the World Geodetic System of 1984 (WGS 84) as Datum.

The Spheroid model used is the Clarke 1880 (modified), 33ºE Central Meridian, a scaling factor of 0.9996, a 500 000 meters X Bias, a 0 (zero) meters Y Bias and 50 meters grid mesh size are the plotting specification (ngsa.gov.ng). All necessary data corrections including the removal of International Geomagnetic Reference Field (IGRF) from the total magnetic data in order to eliminate the regional gradient of the earth's magnetic field due to the continual changes in the magnitude and direction of the earth's magnetic field from one place to another (source: NGSA,2009) were effected on the data sets. Likewise, airborne gamma-ray spectrometric data was amassed based on the measurement of gamma-rays emitted from the decay of naturally occurring radioactive elements: mainly from K, Th and U. At the end of the survey exercise, the airborne geophysical data were provided in the form of digital maps. These maps were initially georeferenced and digitised to create a digital database by digitising the intersection of the flight lines (NGSA, 2009), then interpolated using the inverse distance weighting interpolation technique to acquire maps representing the horizontal variation of Total

Magnetic Intensity (TMI) and concentrations maps of three radioelements: Potassium (K), equivalent Thorium (eTh), and equivalent Uranium (eU).

3.2.2 Processing of airborne geophysical data

The data sets are that of total field and the three commonest, naturally occurring radioelements (six (6) Total Magnetic Intensity (TMI) grid maps and Potassium (K),

equivalent Thorium (eTh), and equivalent Uranium (eU) grid maps). Thus, these data sets were provided in the form of digital maps. The acquired data sets underwent series of corrections. However, processing of the airborne magnetic data involved application of a gridding routine and series of filters that enhanced near surface small-sized geologic features that improved the edge effects that make smaller anomalies more readily visible in the derived derivative. Using Geosoft® Oasis Montaj™ version 8.4 software, the airborne data sets in form of gridded maps were first georeferenced and digitised to create a digital database. Thus, minimum curvature gridding technique embedded in the software packages was used to enhance the structural features.

Airborne radiometric data involved measurements of the surface concentrations of radioelements which are habitually presented as colour images deduced as radiometric signatures.

3.2.3 Airborne magnetic data filtering

Filtering of aeromagnetic data involves the application of different enhancement filters to the data in order to highlight features of interest that will help in the interpretation processes. Besides, it also involves sequential processes of editing and implementation of a gridding routine on the data. In order to demonstrate the effects of the survey, and give detail explanation of the major geological features exposed by the survey in terms of the types of possible geological formations and structures that cause the obvious anomalies, firstly, the six (6) sheets acquired were grid-knitted into a unified sheet (TMI grid map) that represents the aeromagnetic datasets covering the study area using

Geosoft® Oasis Montaj™ version 8.4; a geospatial software package. Note, Geosoft®

Oasis Montaj™ version 8.4 software was used in analysing both airborne geophysical dataset while, ArcGIS version 10.8 was used for geospatial data analysis and map creation.

The gridded unified sheet (in digitised format) was imported into a new database. The data set appeared in a spread sheet in X, Y and Z channel format (Projected coordinate system). The X and Y represent Longitude in meters (Easting) and Latitude in meters (Northing) respectively, while Z represents the Magnetic Intensity values in nano-Tesla (nT). An important point to note is that the correction mentioned above has been applied to the data before procurement. The exciting channels X, Y in metres were modified in to Geographic (Longitude and Latitude as the Northing's and Easting's respectively) coordinate system specified in angular units (degrees). The motive behind the modification is to specify the geographic locations of each of the measured magnetic field on the Earth. Thus, World Geodetic System 84 (WGS 84) was the datum used in obtaining geographic coordinate system. Comprehensive explanation on the subsequent filters applied to the unified TMI grid map are given below.

3.2.3.1 *Butterworth (BW) filter*

The consequence of applying Butterworth filter on the aeromagnetic data sets is to get rid of noise in the gridded data and avoid ringing (Gibb's effect) so as to make certain quality check. Mathematically, BW filter is expressed as:

$$L(k) = \frac{1}{1+\left(k/k_o\right)^n} \qquad (3.1)$$

Where k_o is the Central wave number of the filter, n is the degree of the BW filter function. Butterworth filter, a numerical algorithm embedded in the Geosoft software package has the ability to substantially increase the accuracy and resolution of magnetic data sets was subjected to the Z-values (nT) to get rid of near surface noise and prevent ringing (Gibb's effect) and ensure quality check of the magnetic data sets. There and then, the output effects of Butterworth filter were gridded utilising the geographic coordinate system with a grid cell size of 125 metres by adopting minimum curvature gridding technique. The

minimum curvature gridding technique employed is appropriate for magnetic and radiometric interpretation (John *et al*., 2022). Thus, the chosen grid cell size fulfilled the opinion of Dentith (2011) that grid spacing should be one-fourth of the survey flight line spacing. Initially, the grid size was utilised to shun short-wavelength errors that may appear as lines perpendicular to the survey flight line (Anudu *et al*. 2014). Then, a new grid was produced. Hence, the produced grid was adopted as the real sheet that represents the TMI grid map of the study area. In order to visually enhance the effects of selected geologic sources, get hold of basic information on the edges of near surface magnetic structures and determine the locations and depth to the top of the magnetic bodies, the real TMI grid was further subjected to a number of imaging routines via the application of selected enhancement filters. Butterworth filter was applied to TMI value to increase the signal to noise ratio and to take away all high frequency events which are representative other forms of noise and error in the data and then subjected to further processing.

3.2.3.2 *Reduction-to-equator (RTE)*

RTE filter is mostly used in areas closer to low magnetic latitudes to reposition the observed magnetic anomalies over their sources (Oasis Montaj Tutorial, 2004). Thus, the filter makes the data easier to interpret while not losing any geophysical meaning. Reducing the data to the pole (RTP) does almost the same thing, but at low latitudes, a separate amplitude correction is usually needed to prevent N-S signal in the data from dominating the results (Oasis Montaj^{TM} Tutorial, 2004). As a result, RTE may give a less 'honest' view of the data (Oasis Montaj^{TM} Tutorial, 2004). RTE filter was used in this to get rid of magnetic inclination effect since the study area falls within low magnetic latitudes region (that is areas with geomagnetic inclination less than 15˚). Thus, RTE filter places magnetic anomalies in its exact position.

RTE filter is applied to the aeromagnetic data to eliminate magnetic inclination effect in the area and make magnetic anomalous bodies (structures) appear horizontal over their corresponding sources (Mono *et al*., 2018). RTE has an amplitude component (**sin (I))** and a phase component (**i cos (I) cos (D-θ)).** Mathematically, to reduce magnetic data to equator, the equation below embedded in the software package was used.

$$L\ (\theta) = \frac{\left[Sin(I) - iCos(I).Cos(D-\theta)^2\right] X\left(-Cos^2(D-\theta)\right)}{[Sin^2(I_a) + Cos^2(I_a).Cos^2(D-\theta)] X [Sin^2(I) + Cos^2\ (I).Cos^2(D-\theta)]} \quad (3.2)$$

$$If\ (|I_a|)\ <\ (|I|), I_a\ = I$$

Where I = Geomagnetic inclination (degree)

I_a = Inclination for amplitude correction (never less than I) Default is ± 20 degrees, If $|I_a|$ is specified to be less than |I|, it is set to I. www.geosoft.com

D = Geomagnetic declination (degree azimuth)

Due to proximity of the study area to the magnetic equator, the new TMI grid of the study area was transformed into Total Magnetic Intensity Reduced-To-Equator (TMI_RTE) grid map using the Reduction-To-Equator (RTE) filter. The RTE transformation was executed by considering the conclusion date of the TMI survey and geomagnetic parameters of the area. The essence of transformation was to directly reposition the observed magnetic anomalous bodies over their corresponding causative source bodies since the area of study is located in point of low magnetic latitudes (less than 15˚). Implementing this change, the spatial shift in the shape of the observed magnetic anomalies over their causative source bodies are redefined (Hinze *et al*., 2013). When reducing to the equator, features normal to the declination direction can blow up due to the strong amplitude correction that is applied. In this case, a strong discontinuity occurs in the direction normal to the declination (**D)**. Specifying higher latitude for the amplitude correction alone, this problem can be reduced. However, the transformation was executed by IGRF model embedded in the software package using -6.4° and -1.6° as the respective

inclination and declination average values. Hence, the TMI_RTE grid map was created. A point to note is that subsequent processing is based on the processed TMI_RTE grid map of the study area. In addition, the TMI_RTE grid was upward continued to an optimum plane height of 500 m to eliminate remnants of residual field in the TMI_RTE grid. The upward continuation method ensures the stability of the magnetic anomalies following further processing. During the upward continuation, near-planar signatures which are devoid of near surface magnetic effects and inherent noise were obtained. If a date is entered to calculate the inclination and declination, and if the grid does not have a coordinate system assigned, it will be prompted to define it. The IGRF date and other parameters, once defined, become the values used in other controls that require them. The field strength is only required for apparent susceptibility calculation, but is re-calculated along with the inclination and declination in the other controls, so the values are always synchronized. More often, the edges of magnetic anomalies are equivalent to geological structures like faults, fractures, folds, joints, and shear zones. However, the edge discovery of magnetic sources is probable whenever there is a significant magnetisation difference between two geologic bodies (Bierlein *et al*., 2006). For this reason, selected enhancement filters that visually improve the effects of the near surface features of interest were implemented one after the other on the TMI_RTE grid to map shallow structural framework that are related to mineralisation in the study area.

3.2.3.3 *Edge detection techniques*

Edge detectors techniques are extensively used in geophysical researches, especially in delineating geologic structures like faults, fractures, folds, contacts, dykes and ore bodies (Ibraheem *et al*., 2019). Different edge detector methods were implemented on the aeromagnetic data to improve the delineation process of magnetic anomalies and the definition of the shapes of the causative source bodies regardless of their depths.

Nevertheless, the most common enhancement techniques routinely used in magnetic data are vertical and horizontal derivatives (Arisoy and Dikmen, 2013). These derivatives were employed to highlight the edges of magnetization boundaries (Oruc, 2011). Conversely, the widespread use of the vertical and horizontal derivatives to resolve attenuated anomalies at different ranges is often difficult due to the high amplitude variations in magnetic signals that originate from magnetic sources of different geometries located at different depths with different magnetization properties (Verduzco *et al*., 2004). The magnetic body and its edges produce indistinct features that hinder the study of the magnetic signal behaviour in the structural models and make the task of interpretation complicated (Ardestani and Motavalli, 2007). As a result, a number of edge detection techniques based on derivatives have been introduced to overcome such problems and to deal with complex magnetic anomalies. These techniques have become basic in figuring out the true boundaries of the magnetic source, as they give a comprehensive view of anomalies and delineate the shape of causative sources regardless of their depths (Ferreira *et al*., 2013). Currently, edge detectors constitute an essential step in the process of potential field data interpretation. Thus, detailed explanation on each of the edge detector techniques used in delineating geological structures perhaps hosting mineral deposits from different perspectives in the course of data analysis and interpretation for lineament trend and depth to anomaly evaluation are given below.

3.2.3.4 *First vertical derivative (FVD)*

Derivatives (vertical) are based on the theory that the rates of change of magnetic field are sensitive to rock susceptibilities closer to the surface than at depth (Nwokeabia *et al*., 2018). FVD filter is generally applied to total magnetic field data to enhance the shallowest geological sources in the magnetic data (Eldosouky *et al*., 2017). FVD filter also has the capability of amplifying short-wave lengths anomalous features at the

expense of the longer ones (Ibraheem *et al*., 2019). However, it is often necessary to apply an additional low-pass filter to remove high wave-number noise. As a result, FVD filter was applied to the total magnetic field data to enhance the shallow geologic structures in the study area. Thus, it assisted in the definition of the edges of source bodies in the study area. Mathematically, FVD was derived using Laplace equation. It was also used to describe the magnetic potential field (U) (Nwokeabia *et al*., 2018).

$$If\ \frac{\partial^2 U}{\partial x^2} + \frac{\partial^2 U}{\partial y^2} + \frac{\partial^2 U}{\partial z^2} = 0 \tag{3.3}$$

Where U = Magnetic Potential Field

Assume that, $\partial U = -T$

where T is a function of (x, y and z) therefore,

$$-\frac{\partial T}{\partial x} - \frac{\partial T}{\partial y} - \frac{\partial T}{\partial z} = 0 \tag{3.4}$$

Where T = Total Magnetic Field

$$\frac{\partial T}{\partial z} = -\left(\frac{\partial T}{\partial x} + \frac{\partial T}{\partial y}\right) \tag{3.5}$$

Rewriting equation (2.5) in numerical form,

$$-\frac{\partial T}{\partial x} = \frac{[T(x+\Delta x)] - T(x)}{\Delta x} + 0(\Delta x) \tag{3.6}$$

but, $0(\Delta x) = 0$

therefore,

$$-\frac{\partial T}{\partial x} = \frac{[T(x+\Delta x)] - T(x)}{\Delta x} \tag{3.7}$$

similarly,

$$-\frac{\partial T}{\partial y} = \frac{[T(y+\Delta y)] - T(y)}{\Delta y} \tag{3.8}$$

So,

$$\frac{\partial T}{\partial z} = -\frac{[T(x+\Delta x)] - T(x)}{\Delta x} - \frac{[T(y+\Delta y)] - T(y)}{\Delta y} \tag{3.9}$$

Where Δx = Grid interval in x-direction

Δy = Grid interval in y-direction

Equation (2.9) embedded in Geosoft® Oasis Montaj™ software package was implemented on TMI_RTE grid to create the Derivative maps (Nwokeabia *et al*., 2018). FVD transformation was implemented on the TMI_RTE grid map of the study area. The reason behind the transformation was to enhance the shallowest geological features within the area of study. Thus, FVD has the ability of amplifying high frequency anomalous features (that is, short-wavelengths anomalous features at the expense of longer ones) (Eldosouky *et al*., 2017). In other words, it defines linear feature. Furthermore, the FVD method helped in attenuating broad, more regional anomalies and enhanced local, more delicate magnetic responses because of being sensitive to shallow magnetic source bodies.

3.2.3.5 *Total horizontal derivative (THD)*

THD technique is extensively used to map the boundaries of susceptibility contrasts (Ibraheem *et al*., 2019). It efficiency is as a result of its ability to peak anomaly over the magnetic contacts (Arisoy and Dikmen, 2013). Advantageously, horizontal derivative of magnetic field created by a tabular body tends to have maximum values more than the edges of the anomalous body if the edges are vertical and separated from each other (Ibraheem *et al*., 2019). Thus, it is known for its low sensitivity to noise and essentially requires the computation of the first-order horizontal derivatives of the magnetic field in the x and y-directions (Ibraheem *et al*., 2019). THD is not only less sensitive to the noise, but also more effective in detecting near surface magnetic source bodies (Phillips, 2000). Mathematically, THD is expressed as:

$$\text{THD} = \sqrt{\overline{\quad}^{\,2} + \overline{\quad}^{\,2}} \qquad (3.10)$$

where M = Magnetic field intensity, $\frac{\partial M}{\partial x}$ and $\frac{\partial M}{\partial y}$ are the two orthogonal horizontal derivatives of the magnetic field intensity.

Important point to note, THD algorithm assumes that the nominal (regional) field and source of magnetisations are vertical. Equally, the magnetic contacts are assumed to be vertical and separated, and the magnetic sources are substantially thick (Phillips 1998). The reduction-to-pole (RTP) transformation being the forerunner for THD operations is usually unstable and cannot be easily derived at the point of low magnetic latitude (areas with inclination is less than 15°) (Oyeniyi *et al*., 2016).

THD robustly detects near surface geologic structures (Ibraheem *et al*., 2019). Its effectiveness is as a result of its ability to provide peak anomalies and high amplitude over the edge of the magnetic source (Arisoy and Dikmen, 2013). THD technique is known for its low sensitivity to noise and basically requires the computation of the firstorder horizontal derivatives of the magnetic field in the x and y directions (Ibraheem *et al*., 2019). With these cogent reasons, THD technique was applied to the processed TMI_RTE grid of the study area with the intention to delineate shallow geological structures with the assumption that the regional and induced magnetisations of the magnetic source bodies are horizontal.

3.2.3.6 *Horizontal gradient magnitude (HGM)*

Similarly, HGM is the vector sum of the horizontal derivatives of the magnetic field in a presume direction (Dobrin and Savit, 1988). It enhances lateral changes in the magnetic field while attenuating its regional trend along that direction. Normally, in the locations where magnetic susceptibility difference is highest, the derivative will attain a maximum, this highlights discontinuities perpendicular to the direction of derivation pinpoint the edges of geologic structures (Roest and Pilkington, 1993). However, recognising the maximum horizontal gradient is a straightforward technique for highlighting possible edges of subsurface magnetic source bodies (Roest and Pilkington, 1993). When horizontal gradient maxima are aligned linearly, it is presumed to be the edge of a

magnetic source body. Thus, HGM requires calculating the two first-order horizontal derivatives of the magnetic field, which makes it insensitive to the noise in the magnetic data (Phillips, 2000). If M (x, y) is the total magnetic intensity at location (x, y), the HGM is expressed mathematically as:

$$\text{HGM}(x,y) = \sqrt{\left(\frac{\partial T}{\partial x}\right)^2 + \left(\frac{\partial T}{\partial x}\right)^2} \quad (3.11)$$

$\frac{\partial T}{\partial x}$ and $\frac{\partial T}{\partial x}$ = Horizontal derivatives of the magnetic field intensity

HGM technique was applied to locate the edges of magnetic sources in this study area. Total horizontal gradient technique was used to resolve the structural complexity of basement rocks (Phillips, 1998).

3.2.3.7 *Analytic signal (AS)*

Roest *et al*. (1992) authenticated the application of AS filter on a grid as an edge detection tool. AS also referred to as total gradient operates base on the combination of the horizontal and vertical gradients of the magnetic anomaly, creating a maximum directly over distinctive bodies helpful in detecting lineaments accountable for the observed magnetic anomalies within an area. Its ability to get rid of the complexities of derivatives responses (Dentith and Mudge, 2014) and to estimate amplitudes of geological structures makes it a very helpful method for magnetic data interpretation (Ogungbemi *et al*., 2018). However, AS is applied to determine the magnetic source geometry (Roest *et al*., 1992) because composite analytic signal is specified in terms of the horizontal and vertical derivatives of the total field and the function calculated in the analytic method is the ASA of the potential field (Marson and Klingele, 1993). Also, the amplitude of the analytic signal gets to its maxima when centered over the source limit with bell-shaped anomalies. Thus, the near surface sources become dominant if there is more than one source (Arisoy and Dikmen, 2013). Likewise, Nabighian (1972) recommended the concept of AS and

proposed that in the case of 2-D, the horizontal and vertical derivatives of magnetic fields gratify the Hilbert transform. The amplitude of the AS is the same as the total gradient, that is, independent of the direction of magnetization, and represents the envelope of both the vertical and horizontal derivatives over all possible directions of the earth's field and source magnetization (Luo *et al*., 2011). Analytic Signal **(**AS) is defined as the square root of the squared sum of the vertical derivative and orthogonal derivative of the magnetic field (Jean *et al*., 2018). Mathematically, AS is expressed as:

$$\text{If } \frac{\partial \mathrm{T}}{\partial \mathrm{z}} = \mathrm{H}\left[\frac{\partial \mathrm{T}}{\partial \mathrm{x}}\right] \tag{3.12}$$

where T= Magnetic anomaly data, H = Hilbert transform then,

the AS of a genuine signal f is defined as

$$AS\left(\frac{\partial \mathrm{T}}{\partial \mathrm{x}}\right) = \frac{\partial \mathrm{T}}{\partial \mathrm{x}} - iH\left(\frac{\partial \mathrm{T}}{\partial \mathrm{x}}\right) \tag{3.13}$$

but, $i = -1$ (Luo *et al*., 2011)

The potential field acquired by combining this two quantities into a two-dimensional quantity known as the AS makes equation (3.13) to be rewritten as;

$$AS(x,z) = \frac{\partial \mathrm{T}}{\partial \mathrm{x}} + i\frac{\partial \mathrm{T}}{\partial \mathrm{z}} \tag{3.14}$$

Where $\frac{\partial \mathrm{T}}{\partial \mathrm{x}}$ and $\frac{\partial \mathrm{T}}{\partial \mathrm{x}}$ = Horizontal derivative and vertical derivative of the magnetic field respectively.

$T(x,z)$ = Magnitude of the total magnetic field, z and x = Cartesian coordinates for the vertical direction and the direction perpendicular to strike respectively (Nwokeabia *et al*., 2018). Therefore, the amplitude of the analytic signal is defined as;

$$|\mathrm{AS}\,(\mathrm{z})| = \sqrt{\left(\frac{\partial T}{\partial x}\right)^2 + \left(\frac{\partial T}{\partial z}\right)^2} \tag{3.15}$$

The amplitude of the AS is a symmetric bell-shaped function (Nwokeabia *et al*., 2018).

However, AS can be used in interpretation to give an indication of the edges of the causative body (Nwokeabia *et al*., 2018). Likewise, for the three dimensional case, the analytic signal is given by:-

$$AS(x,y) = \frac{\partial \mathrm{T}}{\partial \mathrm{x}} + \frac{\partial \mathrm{T}}{\partial \mathrm{x}} + i\frac{\partial \mathrm{T}}{\partial \mathrm{z}} \quad (3.16)$$

Therefore, AS amplitude is defined as

$$|\mathrm{AS}\,(\mathrm{x},\mathrm{y})| = \sqrt{\left(\frac{\partial T}{\partial x}\right)^2 + \left(\frac{\partial T}{\partial y}\right)^2 + \left(\frac{\partial T}{\partial z}\right)^2} \quad (3.17)$$

However, the maximum value of the AS determines the edges of a magnetic body (Nwokeabia *et al*., 2018).

In order to get familiar with the source positions of the magnetic anomalies regardless of direction and remnant magnetization of the source effects that are mostly connected with the TMI-RTE, the AS filter was applied to the TMI_RTE grid of the study area with the purpose of revealing the texture with high frequency anomalous features. Nonetheless, its significant characteristic is that, it is independent of the direction of the magnetization of the source (Cyril, 2019a). Besides, significant concentrations of mineral deposits within an area are correlated with high AS amplitudes (Reeves *et al*., 1998). Likewise, AS also known as total gradient is capable of generating a maximum directly over discrete bodies as well as their edges (Omar and Mahmoud, 2018). The generated maximum directly over the causative source bodies and its ability to estimate depth to magnetic bodies makes it an important filter. However, the maximum can be used to detect lineaments responsible for the observed magnetic anomalies within an area. AS image are useful as a type of Reduction-To-Pole, as they are not subjected to the instability that occurs in transformations of magnetic fields from low magnetic latitudes; source positions regardless of any remanence in the sources (Cyril, 2019a). In other words, the amplitude of the AS depends slightly on the direction of magnetization

(Roest *et al*., 1992), and is almost independent when the sources are vertical (Li, 2006).

A very good advantage of the AS filter over other filters is that it is possible to locate the position of the sources in the horizontal and vertical plane.

3.2.3.8 *Tilt angle derivative (TAD)*

TAD is an algorithm used for positioning magnetic sources on magnetic profile data (Miller and Singh, 1994). TAD is the arctangent of the ratio of the vertical derivative (VD) of the potential field to its total horizontal derivative (Ibraheem *et al*. 2019). The tilt angle amplitudes are limited to values between $-\pi/2$ and $\pi/2$ radians (-90° and 90°) (Ibraheem *et al*. 2019). So, the technique delimitates the amplitude variations into a certain range, it also acts like an automatic-gain-control filter which makes it reacts evenly well to near surface sources and deep seated sources (Ibraheem *et al*. 2019). In the presence of noise, TAD technique operates as an effective signal discriminator for both shallow and intermediate sources but becomes blurred for sources at considerable depths, where it can not reveal deep-level geologic boundaries (Arisoy and Dikmen, 2013). Even though, its efficiency reduces with depth. The amplitude of the tilt angle is positive over the magnetic sources, crosses through zero at or near the edge of the source, and is negative outside the source (Arisoy and Dikmen, 2013). Thus, TAD technique produces relatively sharp anomalies and generates better definition of edges over the body (Verduzco *et al*., 2004).

Instead of inputting TMI_RTE grid into TAD filter, the transformed THD grid obtained by implementing THD filter on the TMI_RTE grid was inputted into TAD enhancement filter. Thus, TD_THD grid was created. The essence of executing this procedure is to merge the advantages of TD and THD derivatives for improved images of shallow geologic structures. Likewise, HGM technique was applied to delineate the edges of magnetic sources in the studied area. HGM was utilised to resolve the structural

complexity of basement rocks. In order to get familiar with the source positions of the magnetic anomalies regardless of direction and remnant magnetization of the source effects that are mostly connected with the TMI-RTE, the TAD filter was applied to the TMI_RTE grid of the study area with the purpose of revealing the texture with high frequency anomalous features. In other words, Tilt filter delineates relatively shspe anomalous bodies with better definition of edges of lineaments

Since, TAD is defined as the arctangent of the ratio of the vertical derivative (VD) of the field to its total horizontal derivative (THD), mathematically, it is expressed as:

$$TAD = tan^{-1}\left(\frac{VD}{THD}\right) \quad (3.18)$$

Where VD = $\frac{\partial T}{\partial z}$ = Vertical Derivative and

THD = $\sqrt{\left(\frac{\partial T}{\partial x}\right)^2 + \left(\frac{\partial T}{\partial y}\right)^2}$ = Total Horizontal Derivative.

Meanwhile, VD can either be positive or negative and THD is always positive (Nwokeabia *et al*., 2018). Therefore, equation (3.18) is rewritten as

$$TAD = tan^{-1} = \left|\frac{\frac{\partial T}{\partial z}}{\sqrt{\left(\frac{\partial T}{\partial x}\right)^2 + \left(\frac{\partial T}{\partial y}\right)^2}}\right| \quad (3.19)$$

The TAD, being an automatic gain control for normalising both strongly and weakly magnetised bodies, provides an essential help for a reliable subsurface structural mapping in the study area. The TAD technique, being an automatic gain control for normalising both feeble and strongly magnetised bodies, was employed to provide a vital aid for a reliable subsurface structural mapping in the study area. TAD is a normalized edge detector technique used to determine lineaments (faults, fractures, folds and joints), contacts and edges or boundaries of magnetic source bodies (Cyril,

2019b). In this case, it was applied to processed TMI_RTE data of the study area to enhance both weak and strong magnetic anomalies by placing anomalies directly over their source bodies especially at shallow depths via the theory that the zero contours are the edges of the sources. Note its amplitude is rated in three ways: zero at or near the edge of the source body, negative outside the source and positive over the source body (Ibraheem *et al*., 2018). Besides, its application on the TMI_RTE grid helped in delineating relatively sharp anomalies with better definition of edges of lineaments. Thus, the major benefit of this technique is its abilities to normalise a magnetic field image as well as to distinguish between noise and signal. The enhanced amplitudes of the tilt derivative can be carried through to its total horizontal derivative (or local wavenumber) in which the edge anomalies prominent and invariant to geomagnetic inclination, thus making this derivative effective for mapping geologic edges.

3.2.3.9 *Tilt derivative of total horizontal derivative (TD_ THD)*

TDR_ THD is obtained by taking the ratio of arctangent of the vertical derivative (VD) of the modulus of the total horizontal derivative (THD) in the x and y directions Sanusi and Amigun (2020a). Due to the properties of the arctangent function, the TD_THD values range between $-\pi/2$ and $\pi/2$ radians. The focal characteristics of the TDR_THD are to provide peak amplitudes over the edges of magnetic sources and then normalize signals from both near surface sources and deep seated sources.

Mathematically, TD_THD is expressed as (Ferreira *et al*., 2011):

$$\text{TD\_THD} = \theta = \tan^{-1}\left(\frac{\frac{\partial THD}{\partial Z}}{\sqrt{\left(\frac{\partial THD}{\partial x}\right)^2 + \left(\frac{\partial THD}{\partial y}\right)^2}}\right) \quad (3.20)$$

The TD-THD proposed by (Ferreira *et al*. 2011) merges the advantages of tilt-angle and total horizontal derivatives for an improved imaging of magnetic edges. However, this

approach was employed in this study by using the already obtained THD grid as the input grid for TD enhancement filter.

Instead of inputting TMI_RTE grid into TD filter, the transformed THD grid obtained by implementing THD filter on the TMI_RTE grid was inputted into TD enhancement filter. Thus, TD_THD grid was created. The essence of executing this procedure is to merge the advantages of TD and THD derivatives for improved images of shallow geologic structures. Likewise, HGM technique was applied to delineate the edges of magnetic sources in the study area. HGM was utilised to resolve the structural complexity of basement rocks.

3.2.4 Centre for exploration targeting (CET) grid analysis method

The CET grid plugin is often employed for lineament extraction, grid texture analysis as well as structural complexity analysis of magnetic dataset (Holden *et al*., 2008; Core *et al*., 2009). If applied on a grid, it automatically delineates lineaments as a skeletal line segment, revealing the location and direction of prospective mineralisation zones by means of different statistical steps (Omar and Mahmoud 2018): Texture analysis, Phase symmetry and Amplitude thresholding. Texture analysis highlights the locations of complex texture often associated with discontinuities in magnetic data, Phase symmetry makes use of the output effects of the texture analysis to detect any laterally continuous line-line regions of discontinuity (Holden *et al*., 2011), while Amplitude thresholding uses the output effects of phase symmetry in to delineates structures and reduces the regions containing discontinuities into line like structures (Holden *et al*., 2011). It highlights the locations of complex texture often associated with discontinuities in magnetic data (Holden *et al*., 2011). At each location in the grid, standard deviation is calculated to give an estimate of the local variation in the data. For this to be achieved, a mathematical

expression was utilised. For a window containing N cells, whose mean value is μ, the standard deviation (σ) of the cell values x_i is given as:-

$$\sigma = \sqrt{\frac{1}{N} \sum_{i-1}^{N} (x_i - \mu)^2} \tag{3.21}$$

In the cause of interpretation of the output, values that approaches zero indicate very little variation, while values above one indicate high variation. Often, the edges of magnetic anomalies correspond to lineament (faults, fractures, shear zones, and crustal discontinuities). However, edge detection of magnetic sources is probable whenever there is a vital magnetisation contrast between two geologic bodies (Bierlein *et al*., 2006). So, the above mentioned enhancement techniques were employed to delineate subsurface structural framework related to mineralisation in the study area.

In order to automatically outline lineaments and identify promising areas of ore deposits by delineating areas of convergence and divergence of structural features using some statistical steps embedded in the Geosoft software package, CET technique was executed on the TMI_RTE grid map of the study area. The steps followed in achieving the purpose of implementing this technique on the processed data are:-

1. Texture Analysis: It highlights the locations of complex texture associated with discontinuities in magnetic data.
2. Phase Symmetry: It utilises the output effects of (1) above to detect any laterally continuous line-line regions of discontinuity.
3. Amplitude Thresholding: Uses the output effects of (2) above to delineate lineaments as well as reduce the regions containing discontinuities into linelike structures.

Conversely, to recognize the tectonic trends having an effect on the area of study, the outlined lineaments displayed from the results of CET technique was imported into Rock Works version 17 software package. The results were presented in the form of rosette diagrams.

3.3 Depth Estimator

Generally, processing algorithms used for the analysis of magnetic data either locate boundaries or estimate the depth to magnetic source bodies. However, quantitative analysis for estimation of depth of geological structures was executed by adopting Source Parameter Imaging (SPI), Power Spectrum Analysis (PSA) and Euler deconvolution (ED) techniques. At the end, the effects were evaluated to know if the results corroborate each other, since the three techniques serves as both boundary finder and depth estimator (Reid *et al*. 1990).

3.3.1 Source parameter imaging (SPI)

The SPI function is a rapid and strong technique use for calculating the depth of magnetic sources. Its accuracy has been proven to be +/- 20 % in tests on genuine data sets with drill whole control (Al-Banna and Daham, 2019). SPI has the benefit of creating more complete set of coherent solution points and it is a straightforward technique to make use of. SPI is a technique used for automatic computation of source depth from the gridded magnetic data (Thurston and Smith, 1997). The output results are independent of the magnetic inclination and declination and are automatically saved in a database. The SPI plugin embedded in the Geosoft® Oasis Montaj™ software packages was applied on the anomaly grid to automatically calculate the depth of lineaments probably hosting deposits of vital minerals in the study area. SPI is one of the techniques used for the determination of depth to the magnetic basement covered with lots of sediments. The outcome is

independent of the magnetic inclination and declination values. SPI is obtained from the computed vertical and total horizontal gradients; it also uses the relationship between local wave number (k) of the observed field and the source depth calculated for any point within a grid through vertical and horizontal gradients. Analysis of an anomalous magnetic response involves detecting the parameters that characterize the source of the anomaly. The depth to the top of the geologic structure is a parameter that is commonly sought, and the SPI technique is easier way of determining this depth estimate. SPI assumes a step-type source model.

For a step, the following formula holds:-

$$Depth = \frac{1}{Kmax} \tag{3.22}$$

where Kmax is Peak value of the local wave-number (K) over the step source (Thurston and Smith, 1997). Also, the SPI algorithm embedded in the geosoft software package estimated the depth from the local wave-number of the analytical signal.

Mathematically, it is expressed as:-

$$A_1(X,Z) = \frac{\partial T}{\partial x}(X,Z) - j\frac{\partial T}{\partial z}(X,Z) \tag{3.23}$$

where T(x,z) is the magnitude of the anomalous total magnetic field, j is the imaginary number, x and z are Cartesian coordinates for the vertical direction and the horizontal direction perpendicular to strike, respectively. According to Nabighian (1972), vertical and horizontal derivatives include imaginary and real parts of the 2D analytical signal and are connected by:-

$$\frac{\partial T(X,Z)}{\partial x} \Leftrightarrow \frac{\partial T(X,Z)}{\partial z} \tag{3.24}$$

where $\Leftrightarrow$ denotes a Hilberts transformation pair. Also, Thurston and Smith (1997) defined the local wave-number K as:-

$$K = \frac{\partial}{\partial x} tan^{-1} \left[\frac{\partial T}{\partial z} \Big/ \frac{\partial T}{\partial x} \right] \quad (3.25)$$

One good thing about SPI is that no shifting data window is involved and the computation time is comparatively short. Besides, errors due to noise are reduced by careful filtering of the data before depths are calculated. However, SPI algorithm is based on the extension of complex analytical signal (AS) to estimate magnetic depths. Sometimes, this technique is referred to as the local wave-number technique because it bases it estimation of magnetic source depths on a profile or grid (Thurston and Smith, 1997).

Source parameter imaging (SPI) is one of the techniques utilised for the determination of depth to the magnetic structures beneath the Earth surface. This technique sources its parameters from gridded data and uses an extension of complex analytical signal to estimate the magnetic source depth (Adepelumi and Falade, 2017). The technique often referred to as the local wave-number technique is a profile (gridbased technique) that estimates the magnetic source depth susceptibility contrast and dip of some source geometries (Thurston and Smith, 1997). Afterwards, TMI_RTE was subjected to SPI algorithm to determine depth to the magnetic sources. It automatically calculates the source depths from gridded magnetic data where the depth solutions are saved in a database. SPI picks its parameters from gridded data and utilises an extension of complex analytical signal to estimate the magnetic source depth which is displayed as an image. However, to carry out SPI transformation, $\partial x, \partial y \; and \; \partial z$ were processed.

Then, the output grids were used as input grids into the SPI processing tool embedded in the geosoft software package. Initially, SPI algorithm was utilised on gridded

TMI_RTE for the purpose of estimating the direction at each grid point. The vertical gradient is calculated in the frequency domain, and the horizontal derivatives are

calculated in the direction perpendicular to the strike using the least-squares method (Al-Badani and Al-Wathaf, 2018). Careful filtering of data was ensured so as to have good estimates of the local wave number and hence the depth. Thereafter, SPI grid map was produced. The first order derivative was adhered to, as the SPI technique is sensitive to noise at higher derivative order. So, the data was carefully filtered to ensure improve estimate of the local wave-number. The technique at times referred to as the local wave-number method is a profile or grid-based technique that estimates the magnetic source depth, dip, and susceptibility contrast of some source geometries (Nwosu, 2014). At the end, the resulted depth was displayed as an image. Thus, the depth estimation is independent of the magnetic inclination, declination and any remanent magnetization (Thurston and Smith, 1997).

3.3.2 Power spectrum analysis (PSA)

PSA is an algorithm widely utilized for the processing and interpretation of potential field data. Meanwhile, the technique is adapted for depth estimates using aeromagnetic profiles. PSA technique uses the fast Fourier transform to convert field intensity to the frequency domain and then calculates the logarithmic energy spectrum (Spector and Grant, 1970). The technique also filters the spectrum to correct for the finite horizontal dimensions of magnetic sources, and smooth the spectrum to clarify its decay characteristics (Spector and Grant, 1970). In order words, PSA technique is based on the principle that a magnetic field measured at the surface is considered to be the integral of magnetic signatures from all depths (Tsepav, 2018). Thus, the spectral depths are usually calculated from measurement made on the widths and slopes of individual anomalies of the data profiles. The Fourier integral transform of a function that differs continuously along a profile of observation, such as magnetic field intensity, transforms the function

from the space to the frequency domain. Mathematically, the two dimensional Fourier transform pair may be written as (Spector and Grant, 1970):-

$$G(u,v) = \iint_{-\infty}^{\infty} g(x,y)\, e^{i(u_x - v_y)} dxdy \tag{3.26}$$

$$G(u,v) = \frac{1}{4\pi^2} \iint_{-\infty}^{\infty} g(x,y)\, e^{i(u_x - v_y)} dudv \tag{3.27}$$

where u and v are the angular frequencies in x and y directions respectively.

$$E(u,v) = exp(-4\pi hr) \tag{3.28}$$

The exp (-4πhr) term is the leading factor in the power spectrum. The average spectrum of the partial waves falling in this frequency range is computed and the resulting values comprise the radial spectrum of the anomalous field. If h is replace with D and r with *f*, The equation becomes

$$\log E = -4\pi D f \tag{3.29}$$

where D is the required depth of anomaly, and *f* is the frequency.

If the linear graph of log E against *f* provides slope (m) as

$$slope\ (m) = -4\pi D \tag{3.30}$$

Then, equation (3.30) is rewritten as

$$D = -\frac{m}{4\pi} \tag{3.31}$$

Hence, equation (3.31) is used for the estimation of the depth to magnetic sources (Spector and Grant, 1970). In this case, equation (3.31) is used for the estimation of the depth of geological structures hosting different ore mineral deposits.

In order to complement the depth information by the SPI technique, power spectral analysis was applied on the upward continued TMI_RTE grid of the study area. The upward continued TMI_RTE grid was divided into 14 overlapping blocks containing 35 data points. The geospatial software package (Oasis Montaj) was used to transform the

TMI_RTE data into the radial energy spectrum for each block. The essence of doing this is to make sure that essential parts of each anomaly were not cut off in the blocks as each block is made to contain more than one maximum, as suggested by Hahn *et al*.,
(1976). For this to be achieved, the blocks were made to overlap each other using Microsoft Excel software package. The Excel software package has the Fourier mathematical algorithm embedded in it used to calculate the Fast Fourier Transform (FFT) magnitude and FFT frequency. The energy spectrum is calculated from the complex Fourier amplitude spectrum, and the logarithm of the energy is plotted against radial frequency or wave number as suggested by Spector and Grant (1970). At length, the average source depth is obtained from the slope of the linear portion of the energy decay-curve. Thus, the depths to magnetic sources of ensembles obtained by manually fitting a straight line to each linear interval of the logarithmic energy decay-curve yielded negative slopes. Significant changes in the leading gradient indicate the presence of sources at more than one characteristic depth. However, each linear interval were analysed independently. Smoothing was performed to the signals to filter as well as determine a linear curvature (trend) on the decay-curve by getting rid of high frequency noise. Also, the problems of aliasing effect and Gibb's phenomenon which are normally encountered in the course of performing PSA were taken care of by applying small sampling intervals to reduce frequencies greater than Nyquist frequency as suggested by Spector and Grant (1970).

3.3.3 Euler Deconvolution (ED)

ED is an efficient filtering technique used for direct evaluation of depth to magnetic source/structures from the gridded magnetic data (Emmanuel *et al*., 2018). The effect of ED is mostly on potential data, it generates mathematical solutions, yet with no recourse to whichever geological constraints (Sanusi and Amigun, 2020b). Normally, ED is

employed in TMI data interpretation because it only needs a minute or no involvement of prior knowledge about the magnetic source geometry within a survey area (Sanusi and Amigun, 2020b). Essentially, it needs no information about the magnetisation vector. ED technique is an equal technique based on the Euler's homogeneity equation built up by (Reid *et al*., 1990; Ravat, 1996).) following it application on gridded magnetic data. The outcome of ED technique does not only estimate the depth to magnetic source, but also delineate the horizontal boundaries (Olomo *et al*., 2018). Besides, the technique is based on the concept that anomalous magnetic fields of localized structures are homogeneous function of the source coordinate which also gratifies Euler's homogeneity equation. ED determines apparent depth to the magnetic source body through derived Euler's homogeneity equation (Thompson, 1982). This technique transmits s the magnetic field and its gradient components to the location of the source of an anomaly, with the degree of homogeneity expressed as a "*Structural Index* (SI)". Thus, it entails picking a suitable SI value and utilizing least-squares inversion to generate as well as to solve equation. The SI is an exponential factor equivalent to the rate at which the field falls off with distance, for a source of a given geometry (Emmanuel *et al*., 2018). It value depends on the type of source body of interest and the type of potential field data (either magnetic or gravity). More often than not the SI is fixed for different materials. The ED method used in this study is based on solving Euler's homogeneity equation expressed mathematically as:

Any three-dimensional function f (x, y, z) is supposed to be homogeneous of degree *n* if the function obeys this expression:

$$f(tx, ty, tz) = t^n f(x, y, z) \tag{3.32}$$

From equation (3.32), Euler's homogeneity relationship for magnetic data (Thompson, 1982) is expressed as:

$$(x - x_o)\frac{\delta T}{\delta x} + (y - y_o)\frac{\delta T}{\delta y}(z - z_o)\frac{\delta T}{\delta z} = N(B - T) \tag{3.33}$$

where (x_o, y_o, z_o) = Position of the magnetic source whose total field (T) is detected at (x, y, z,)

B = Regional magnetic field

N = is the measure of the fall-off rate of the magnetic field. It may be interpreted as the structural index (SI).

It is important to note that N in equation (3.33) is equivalent to *n* in equation (3.32). This shows that simple magnetic model conform to Euler's equation (Thompson, 1982). The degree of homogeneity, N, can also be interpreted as a SI, which is a measure of the rate of change with distance of a potential field. For magnetic data, an important benefit of Euler's equation is that it is insensitive to magnetic inclination, declination since both are part of the constant in the anomaly function of a model.

Furthermore, ED process is applied at each solution. The technique involves setting an appropriate SI value and using least-squares inversion to solve the equation for an optimum (x_o, y_o, z_o) and B. Also, a square window size must be specified which consists of the number of cells in the gridded dataset to use in the inversion at each chosen solution location. The window is centred on each of the solution locations. All points in the window are utilized to solve Euler's equation for solution depth, inversely weighted by distance from the middle of the window. The window should be sufficient to include each solution anomaly of interest in the total field magnetic grid, but preferably not bulky enough to include any adjacent anomalies. The essence of executing ED is to produce one or more maps that exhibit the locations and depths of the sources of potential field anomalies. The source type and structural index are very vital because this aid the determination of sources of interest before commencement of the procedure. ED is a statistical procedure and the resulting solution positions have connected uncertainties. The X and Y position error is a mixture of the separate X and Y uncertainties. Both the

depth uncertainty and location uncertainty are reported as a percentage of the depth below the sensor, which has an appropriate normalizing effect. Therefore, It is required to do away with solutions with high uncertainties, because the system generates a solution for all window positions whether any vital source is present or not. Low SI values are connected with bodies which give rise to low gradients, so solutions with low SI values have elevated uncertainties. The general level of uncertainty depends on the data quality. Selection criteria must therefore be established by examination of the database solutions. Point to note is that the choice of selection criteria is based on two requirements: Position uncertainties must be kept low, and sufficient solutions ought to be retained to delineate the structures required (Jean *et al*., 2018).

The ED was used in this study for the purpose of depth estimation. The technique detects magnetic source position and depth in whichever geologic setting (Reid *et al*., 1990). However, the ED procedure needs four Geosoft format grids as input data: total magnetic field, FVD grid, first horizontal derivative in the X direction and the first horizontal derivative in the Y direction. Process grids menu option was used to calculate the derivative grids from the TMI-RTE grid. The menu option computes the X and Y derivatives in the space domain using a simple nine-point convolution filter. The Z derivative filter does not have such a simple spatial representation, so it is implemented in the frequency domain via a Fast Fourier Transform (FFT) procedure. Upward continuation was necessary because the data need to be smoothed to reduce shortwavelength noise before calculating the derivatives. Though, it was time consuming when choosing an appropriate distance. Note that the mentioned procedure was executed via Geosoft® Oasis Montaj™ version 8.4, software. Then, a new grid file name was specified for the upward continued grid. Further processing of ED was based on the new processed grid. Following gridding procedure and data preparation, X, Y, and Z-

derivative grids were computed. After generating X, Y, and Z-derivative grids, the derivatives grids were displayed for comparison with the TMI-RTE grid. Though, this is optional. The Structural Index (SI) is an exponential factor corresponding to the rate at which the field falls off with distance, for a source body of a given geometry. Being the most important parameter for regional interpretation of depth estimate, the SI parameter depends on the type of source body of interest and the type of potential field data used. Since, the correct SI with the best clustering solution is presumed to symbolise the geologic model of an area, in this case, SI=1 was chosen because it matches well with the fault model, and gave better clustering solutions. Also, the software package (Geosoft Oasis Montaj™) permits the sampling window size to be varied from 3 to 20 %, depending on the wavelength and size of the sampled anomalies. 15 % maximum depth tolerance was chosen in this work. This parameter determines which solutions are accepted. Thus, it recognizes solutions with error estimate lesser than the specified tolerance. However, a smaller tolerance will result in less but more dependable solutions. Other specified parameter are Window size as (>=20), the Maximum distance to accept, Flying height and Survey elevation. The Window size parameter determines the grid cells used to calculate the Euler solutions. All points in the window are applied to solve Euler's equation for a source position. ED toils better when the search window is large enough to contain the entire anomaly being analyzed, but not so large that it takes multiple anomalies. In view of the fact that a typical survey includes anomalies of different sizes, it is wise to run ED a few times with different window sizes. The Maximum distance to accept parameter states the maximum distance offset from the centre of the search window to the point of the source solution. The deconvolution result is most accurate when the source is centred within the search window, so, source solutions positioned far from the centre of the search window may be rejected. Generally, solutions located outside the boundary of the search window may be rejected as erroneous while the Flying height and

survey elevation parameters determine the mode in which the results are displayed. Since, the main objective of ED processing is to create maps that show the locations and depths of the sources of potential field anomalies. For this reason, 1.0 was assigned as a value of structural index (SI) to locate the probable mineral deposits since it is principally better at delineating the geologic structures likely playing host to ore deposits. A partly cover moving window of 10 km by 10 km, a tolerance of 15% and a proportioned symbol base of 250 were used in executing the procedure. Afterwards, ED map was created to visualize the results after calculating Euler solutions.

3.4 Gamma-Ray Spectrometric Data Filtering

The acquired airborne gamma-ray spectrometric (radiometric) data contain Potassium (K), equivalent Thorium (eTh) and equivalent Uranium (eU) grid maps. Each of the grid maps demonstrates the apparent surface distribution of the radioelements (K, Th and U). The aero- radiometric data was corrected for background radiation ensuing from cosmic rays and variations rooted by changes in the aircraft altitude relative to the ground and Compton-scattered gamma-rays in K and U energy windows. To augment the aeromagnetic interpretation, the airborne radiometric data was statistically analyzed to emphasize the overall variations in radioelement concentrations, since radiometric data are naturally displayed as images (Joshua *et al*., 2021), and vital in the recognition of hydrothermal alteration zones (Youssef and Elkhodary 2013; Kearey *et al*., 2013). The radiometric data was interpolated by minimum curvature gridding technique, arranged in three different grids as radioelements (K, eTh and eU) and displayed as pseudocoloured images to reveal the surface concentration of each of the radioelements. Note, in radiometric, estimates of Th and U concentration are often reported as equivalent Thorium (eTh) and equivalent Uranium (eU), because these estimates are usually based on the assumption of equilibrium conditions.

3.4.1 Total count image

An image was produced after micro-levelling the whole data set to get rid of any apparent residual errors by combining the three radio contents utilising the Grid and Image tool embedded in the Geosoft® Oasis Montaj™ software package. Measuring the concentration level of each of the radioelements was achieved by estimating the intensities of emitted gamma-ray radiation which was used to produce maps showing the three radioelements with their ratios (Salem *et al*., 2007)

3.4.2 Ratio maps

To identify radiometric signatures associated with mineralisation, ratio maps were developed to outline the hydrothermal alteration zones, since an increase in the concentration level of K (%) and a decrease in concentration level of eTh (ppm) or U (ppm) is an indicator for altered zones in various ore deposits (Ostrovskiy, 1975). Not in all cases for U (ppm). The production of the ratio maps followed the *F*-parameter expression developed by (Efimov, 1978) in form K/eTh, K/eU, and K× (eU/eTh) or vice-versa. Hence, *F*-parameter expression was adopted to assess the potential of the gamma-ray spectrometric technique characterization of areas of change connected with hydrothermal occurrences in the area under investigation. The ratio maps with diverse geological meanings were generated from significant arithmetical combination by shuffling between the enhanced gridded images of K (%), eTh (ppm) or eU (ppm)
(Taufiq *et al*., 2020)

3.4.3 Ternary image

A histogram equalisation to provide a better colour variation was employed to enhance the contrast of the individual histograms of K, Th and U before combining to create the ternary image. Ternary image in a Cyan-Magenta-Yellow (CMY) colour model was

produced by assigning Cyan, Magenta and Yellow to K (%) grid, eTh (ppm) grid and eU (ppm) grid respectively. The essence of the ternary image is to provide a simultaneous display of the three radio parameters on one image, and to allow the interpretation of three channels using preservative colours. Since, different radiometric signatures are recognised based on distinctive radioelement signals. Thus, the ternary image serves as the typical radiometric response in the ratios of the radioelements (K,

Th and U). Besides, it was also utilized to delineate the lithological units. Geosoft® Oasis Montaj™ version 8.4 was used to generate the ternary colour image. Primarily, the reasons behind the production of the ratio and ternary maps is to identify hydrothermal alteration assemblages lithological units, and interpret the radiometric signatures linked with the rocks vital to zones of mineralisation within the study area.

3.5 Analytic Hierarchy Process (AHP)

AHP is one of the most extensively used decision-making tools capable of resolving complex decisive problems (Thomas, 1983). The good thing about APH is its ability to integrate multiple techniques (data), bring out benefits from all the combined techniques, and attain the desired target in an enhanced way (Omkarprasad and Sushil, 2006). Systematic developments in the globe of geospatial skills and its equivalent increase in spatial correctness have led to the explosion of executing zones of mineralisation using this tool. AHP is a straightforward, effectual, and consistent method (Machiwal *et al*., 2011). In this case, AHP was used in location of mineralisation zones within the area of study. The Multi Criteria Decision Analysis (MCDA) embedded in the ARC GIS software was utilised for the integration. The points where structural complexity coincides with alteration assemblages indicate a high likelihood for ore mineralisation. Besides, superimpose GIS method was executed via the integrated ore (mineral) indicators to develop the prospecting zones of mineralisation. The analysis was executed utilising the

spatial analysis with Weighted superimpose tools, considering the comparative values derived from the AHP computations via a template by Goepel (2018). To create the probable mineralisation map of the locale, selected parameters were taken into account and their comparative weights were determined by the AHP technique. An algorithm in ArcGIS environments was used for the implementation of the model. Implementation of AHP gives the needed flexibility and objectivity in delineating potential zones of mineralisation. The final map product is a direct reflection of both the number of criteria choices and the weights assigned to different grids. The mixing Geographic Information System (GIS) based AHP-MCDA technique was employed to create prospectivity map of the study area using airborne geophysical data without executing field survey in the process. Seven (7) criterions (decisive factor) resulted from geology, lineament density (structural features), hydrothermal change assemblages from the K/eTh ratio map, FVD, AS, TD, SPI were considered. The weights of each the decisive factor were decided by the AHP-MCDA technique in a GIS setting. Thereafter, a prospectivity mineral map was created. The prospectivity map would serve a vital source of information that can help in locating mineralised zones in the region.

3.5.1 Criteria weight assignment

Execution of AHP with the help of MCDA is an incredibly technique utilised in allotting weights to different significant decisive factors. Saaty's scale (Saaty, 1987) of 1-9 of comparative rating was accepted for relative comparison. Thorough researches were further made to constrain the data acquired to allot important weights to the different parameters. Every one of the parameters was evaluated on Saaty's scale, and relative percentage values (weights) were given as a result of utilising a template prepared by (Goepel, 2018). The template is a free-web based AHP choice supporting tool for composite decision-making processes. A pair-wise comparison medium is created to

calculate consistency ratio, Eigen vector, and normalised weight. The consistency index and consistency ratio are expressed mathematically as:

$$CI = \frac{\lambda_{max} - n}{n-1} \quad (3.34)$$

$$CR = \frac{CI}{RI} \quad (3.35)$$

CI = Consistency Index, CR = Consistency Ratio, RI = Random Index (with value of 7%), $\lambda_{max} = E$igenvalue, and n = number of influencing criteria (Saaty, 2006).

Given that, Saaty's pair-wise comparisons are constant with the value (< 0.10) (Jude *et al*., 2022: Saaty, 2006).

$$PZM = \sum_{i=1}^{m} \sum_{j=1}^{n} M_i \times R_j \quad (3.36)$$

Where = Potential Zones of Mineralisation

Implementation of The Multi Criteria Decision Analysis using GIS gives the essential objectivity in outlining potential zones of mineralisation. On the other hand, there are a number of levels of subjectivity in choosing suitable thematic criteria considered to have different levels of traces of edges of lineaments perhaps playing host to different ore deposits. This subjectivity comes from selecting and allotting different weights to different criteria. Nevertheless, the use of AHP before employing the MCDA-based GIS tool permits a technically accurate and satisfactory weight assignment by making sure that the CR of all the resulting weighs of the assigned criteria is not more than 10% (Saaty, 2006). However, the AHP calculator permitted the pair wise comparison for weight assignment of the chosen criteria. Due to its flexibility, Analytic Hierarchy Process (AHP) module was used for the integration of extracted lineaments and hydrothermally altered zones. AHP facilitate the extraction conclusion from all the joint data and help to attain the required goal in an improved manner.

CHAPTER FOUR

4.0 RESULTS AND DISCUSSION

4.1 Total Magnetic Intensity (TMI) Map of Study Area

The initial point of the interpretation is the production of TMI anomaly map (Figure 4.1) of the study area. The TMI grid map (Figure 4.1) is a pictorial representation of concealed magnetic features assumed to be geological attributes displayed in different colour

aggregate. As the name implies, the TMI is the magnetic field that is observed in a precise location. It is a combination of the Earth's magnetic field and the field produced by magnetic bodies that are beneath the Earth surface. Distinctively, the TMI map (Figure 4.1) is zoned into two parts denoted as zone 'S' and zone 'B' with anomalies of various magnetic features. Normally, the magnetic susceptibility of sedimentary terrain is negative (low) when compared to the basement terrain which is always positive (high) (Al-Kadasi, 2014). However, reverse is the case in the TMI map

(Figure 4.1) of the study area. The map (Figure 4.1) demonstrates extremely high

(especially in zone 'S') and low magnetic anomalies of various wavelengths with varied magnetic intensity values ranging from a minimum value of -413.4 nT to a maximum value of 256.5 nT, after the removal of 33,000 *nT* from the total magnetic field intensity values for ease of processing. Effectively, this is as a result of the variations in the shapes, sizes, depths, and magnetic susceptibilities of the underlying rocks. Perhaps, the variations in the magnetic intensity values could be from the complexity in the geologic setting in terms of tectonic history indicating differences in mineral composition of the rocks in the study area.

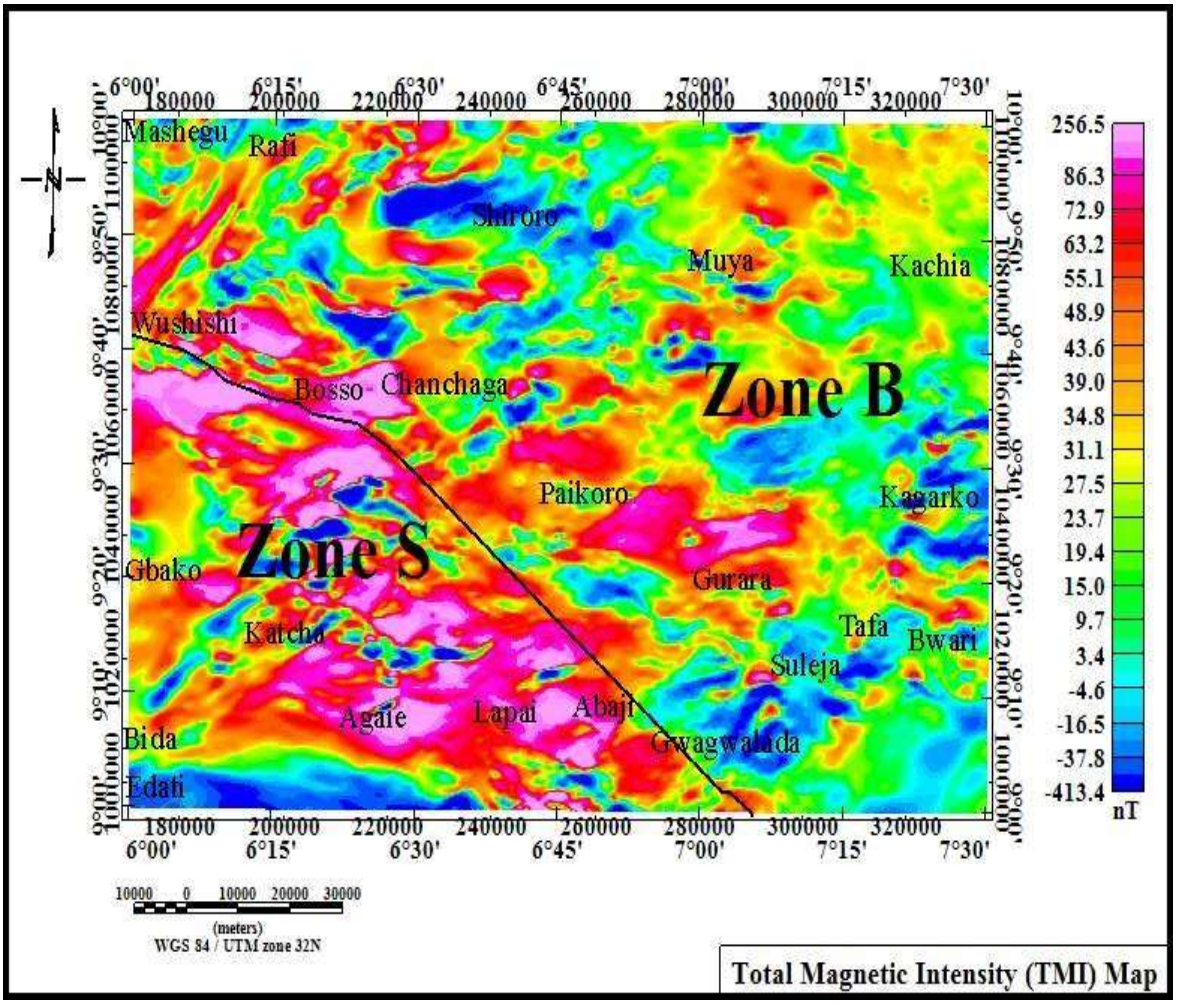

Figure 4.1: Total Magnetic Intensity (TMI) Anomaly Map of the Study Area. Colour Bar at the Right Side Signifies the Intensities of the Magnetic Anomalies Measured in Nanotesla (nT). 33,000nT was stripped out of the Total Magnetic field Intensity value.

Besides, zone "S" is more magnetically perturbed than the zone B because of the presence of high magnetic rocks beneath the sediments. It correlates well with the sedimentary part of the study area belonging to the Bida basin (Figure 2.1). it can also be seen from

Figure 4.1 that most prominent magnetic anomalies trends towards the EW direction, while others trend in the NE-SW and NW-SE directions.

4.2 Total Magnetic Intensity-Reduced to Equator (TMI-RTE) Map of the Study Area

The TMI-RTE map (Figure 4.2) of study area is a transformed form of TMI map (Figure 4.1) of study area. In view of the fact that study area is situated at low magnetic latitude (less than 15˚), Figure 4.2 (TMI-RTE map) is a reduced to equator map
corrected for effect of latitude prior to further processing. Displayed on the map (Figure 4.2) are the magnetic anomalies that have been improvingly accentuated and accurately positioned. Remarkably, it is an indication that the magnetic anomalies have been symmetrically centred over their corresponding source bodies. Thus, the magnetic anomalies have shifted vertically either upward or downward to their exact position. Besides, The TMI-RTE map (Figure 4.2) exhibits difference in the magnetic intensities demonstrating variations in lithology within the study area, characterised by short wavelength and elongated anomalies orienting majorly towards E-W, NE–SW and NWSE directions. The amplitude of the magnetic anomalies depends on the magnetisation of rocks, which are equated as the magnetic susceptibility of the rocks at precise geological locations. Also, The TMI-RTE map (Figure 4.2) shows that the magnetic field intensity ranges from a minimum value of -420.6 nT to a maximum value of 218.9 nT. The highest positive and lowest negative magnetic intensity values are emphasised with pink and blue colours, respectively.

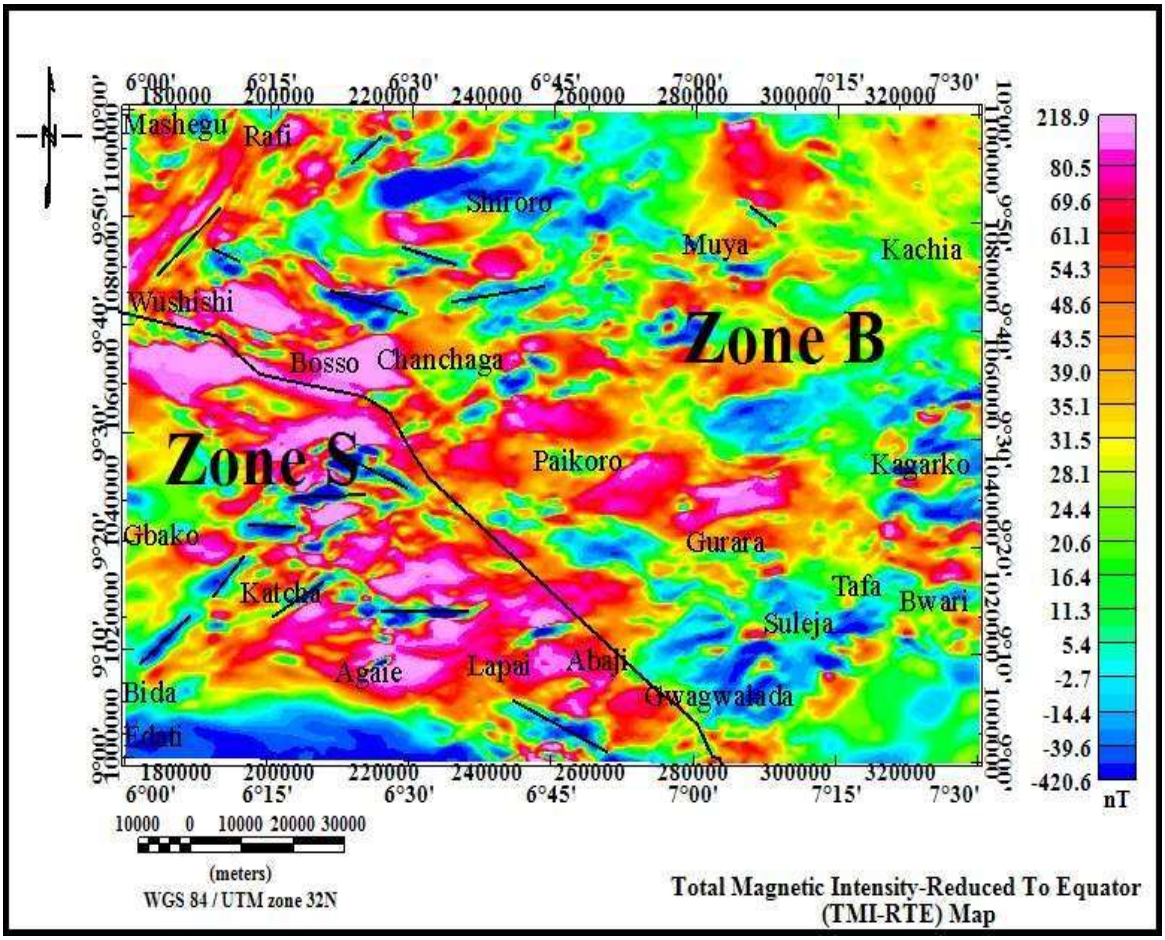

Figure 4.2: Total Magnetic Intensity-Reduced To Equator (TMI-RTE) Anomaly Map of the Study Area. Colour Bar at the Right Side Signifies the Intensities of the Magnetic Anomalies Measured in Nanotesla (nT).

Since the study area is situated at low magnetic latitude, areas with high magnetic field values have rocks with low magnetic susceptibility and vice versa. Furthermore, TMI_RTE map (Figure 4.2) was compared with the geology map (Figure 2.1) to

highlight the imprints of geological attributes in the area. Just like the TMI map (Figure 4.1), the distribution of the magnetic anomalies distinctly zoned the TMI-RTE map (Figure 4.2) into two parts: zone ‘S’ and zone ‘B’. Zone ‘S’ corroborates with the Cretaceous Sedimentary terrain made up of Feldspathitic sandstone and siltstone with traces of Alluvium deposits while zone ‘B’ corroborate with the Basement Complex terrain made up of different assemblage of rocks that includes Migmatite, Granite gneiss, Biotite granite, and Amphibolite schist. Invariably, the relatively high magnetic anomalies in zone ‘S’ may be either due to the composition and presence of magnetic minerals in rocks or the nature of the remanence in the area. Also, some intercalations of magnetic lows (negative anomalies) with shorter wavelengths (marked with back lines) observed between magnetic highs (positive anomalies) in the map suggest the presence of relatively smaller magnetic rock bodies with the low magnetic anomaly signature.

4.2.1 First vertical derivative (FVD) map

The research area's FVD map (Figure 4.3) revealed enhanced short wavelength (high frequency) anomalies attributed to shallow-seated features assumed to be geological structures (lineaments). The map (Figure 4.3) demonstrates deformation with an increase in the visibility of shallow structural features presumed to be lineaments (faults/fractures (in red and blue lines) and contact zones (in black lines)). The highlighted lineaments provide lithological information that is not visible on the research area's TMI-RTE map (Figure 4.2).

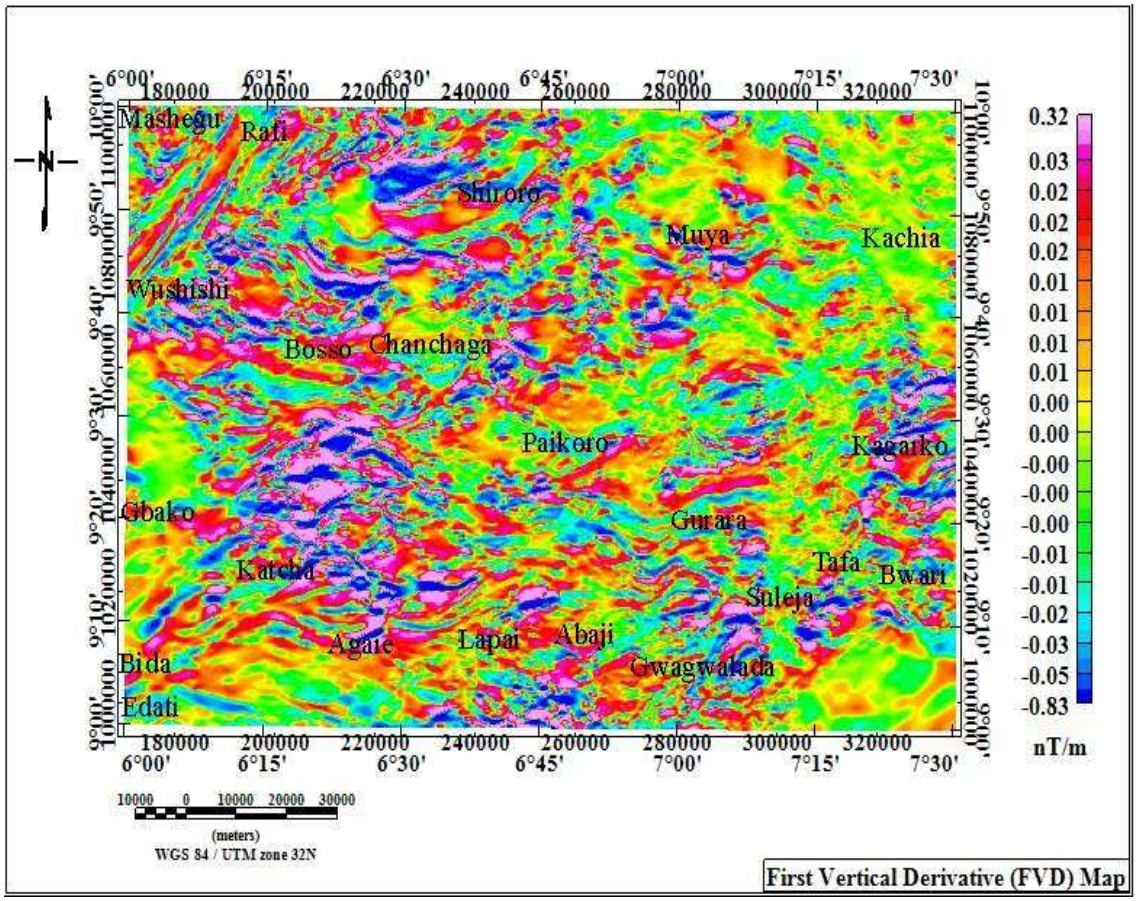

Figure 4.3: First Vertical Derivative (FVD) Map of Study Area in Gray Scale with Mapped Lineaments. Colour Bar at the Right Side Signifies the Intensities of the Magnetic Anomalies Measured in Nanotesla per Metre (nT/m)

In other word, the map (Figure 4.3) showed clearer images of near surface geologic features that are not obvious on TMI_RTE map (Figure 4.2). The study area is occupied largely by these high-frequency anomalies, signifying shallow depth to causative source bodies except in southwest, southeast, and northeast part of the area (contact zones) with

deeper source bodies which indicate the presence of Sedimentary covers. The displayed short, long linear and curvilinear features (red, blue and black lines) distinguishes the edges of magnetic source bodies signifying the locations of the faults, fractures, folds or contacts. The short and long linear features (blue and red lines), which are continuous trend in the E–W, NE–SW and NW–SE directions, could

symbolise lithological boundaries and are interpreted as lineaments (fault/fracture lines). Also, the curvilinear features (black lines) are concentrated within the lithological boundaries of magnetic source bodies, these features are interpreted as folds or contacts. Thus, a glance at the map (Figure 4.3) shows that the E-W trend is the most pronounced directions of the lineaments in the area. Mineral deposits are usually concentrated along or aligned with such geologic structures (lineaments) within the Earth crust. Lineament serve as a channel for the mineralising fluids that are composed of different compounds like ions, iron, carbonates, chlorine and sulphide via the tectonically deformed rocks to precipitate and restrict valuable metal (Almasi *et al*., 2017; Cunha *et al*., 2017).

4.2.2 Analytical signal (AS) map

AS map (Figure 4.4) accentuate the difference in the magnetisation of the magnetic source bodies in the study area and emphasises discontinuities as well as anomaly texture. Thus, indicates that the geologic structures are playing host to ore deposits. On the AS map (Figure 4.4), clusters of Analytic Signal Amplitude (ASA) peaks (pink colour) are noticed in almost every part of the map.

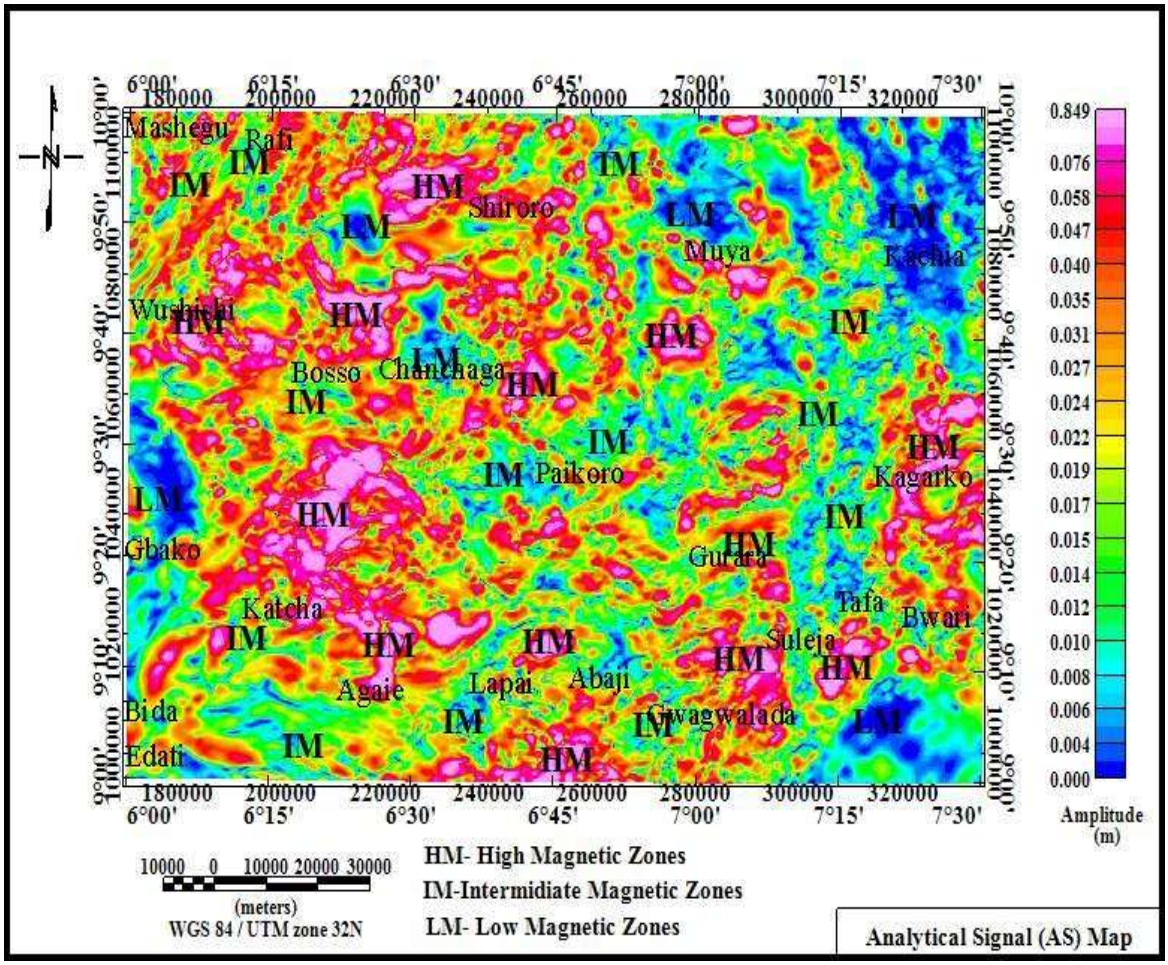

Figure 4.4: Analytical Signal (AS) Map of the Study Area. Colour Bar at the Right Side Signifies the Amplitude of the Magnetic Anomalies Measured in Metres (m).

.

The occurrence of these ASA peaks could be as a result of tectonic deformation and different grades of rocks. The production of AS map of (Figure 4.4) makes it feasible to limit the contacts of the geological bodies of strong magnetisation. In short, the limits of

the invasive bodies are well highlighted; also the edges of similar magnetic responses are discernible on the map (Figure 4.4) and are thought to delineate lithological boundaries that produce the responses. The edges have enabled the characterisation of the whole area into three major lithology zones. The three different lithological mappable zones exhibited on (Figure 4.4) are High Magnetic (HM) anomalous zones with gradient maxima (> 0.076 m), Intermediate Magnetic (IM) anomalous zone with gradients ranging from 0.012 to 0.076 m and Low Magnetic (LM) anomalous zones with gradients ranging from 0.000 to 0.012 m. Majority of HM anomalous bodies with maxima values trends towards the NE–SW direction particularly along south-western part and north-western flank of the map. It is also obvious on the map that there are lots of HM segments with high anomalous values trending towards the E-W, NE-SW and N-S direction. HM anomalous zones are assumed to be connected to rock bodies such as

Porphyritic Granite, Medium to coarse grained Biotite granite, Amphibolite Schist, Migmatite and Granite Gneiss in the area as these bodies have high ferromagnesian low quantity of felsic minerals (Ahmed, 2018; Balogun, 2019). However, rocks connected with these zones have more than 60% quartz; therefore they are recognised as metavolcanic, meta-sediments, and granites (Ahmed, 2018; Telford *et al*., 1990). Thus, the three different magnetic anomalous zones are based on the magnetisation contrast, produced by varying mineral composition, and depth of the magnetic sources (Cyril, 2019a). Besides, alternations of low and high magnetic anomalies which appear to be structurally controlled are well-pronounced on the map (Figure 4.5). This could possibly coincide with localisation of mineralised zones. In other word, the map demonstrates networks of magnetic discontinuities that might symbolise fracture zones that could be targets for mineral prospection.

4.2.3 Horizontal gradient magnitude (HGM) map

Just as AS map (Figure 4.4) displays peaks over the magnetic source edges, so does HGM map (Figure 4.5), analytic signal, however, is independent of the direction of the magnetization of the source. The obvious magnetic gradient expressions particularly the high magnetic (HM) zones on the map (Figure 4.5) except in some parts are characteristic of near surface, composite magnetic bodies. Thus, random distribution of these magnetic gradients (HM zones) in the map signifies magnetic susceptibility overlaps in rocks. The low magnetic gradient expressions prominent (low magnetic (LM) zones) especially in the northeast part, southeast and southwest flank correspond to lithological contacts. These contact zones helps in the migration and precipitation of ore mineral deposits. The HGM map (Figure 4.5) shows more structural complexities of lithological contacts of various geological bodies than the ones revealed on AS map (Figure 4.4). The various geological bodies displayed on the HGM map (Figure 4.5) are presumed to be displaced in the down dip direction for dipping contact sources (Philips 2000). Visual inspection on geologic structures has been decoded based on (Figure 4.4) and (Figure 4.5). All zones of magnetic minima as well as displacements

(discontinuities) of magnetic anomalies were interpreted as linear structures. The map (Figure 4.5) also shows prominent NE-SW, NW-SE and E-W trending structures. This map (Figure 4.5) shows a good similarity with the AS map (Figure 4.4).

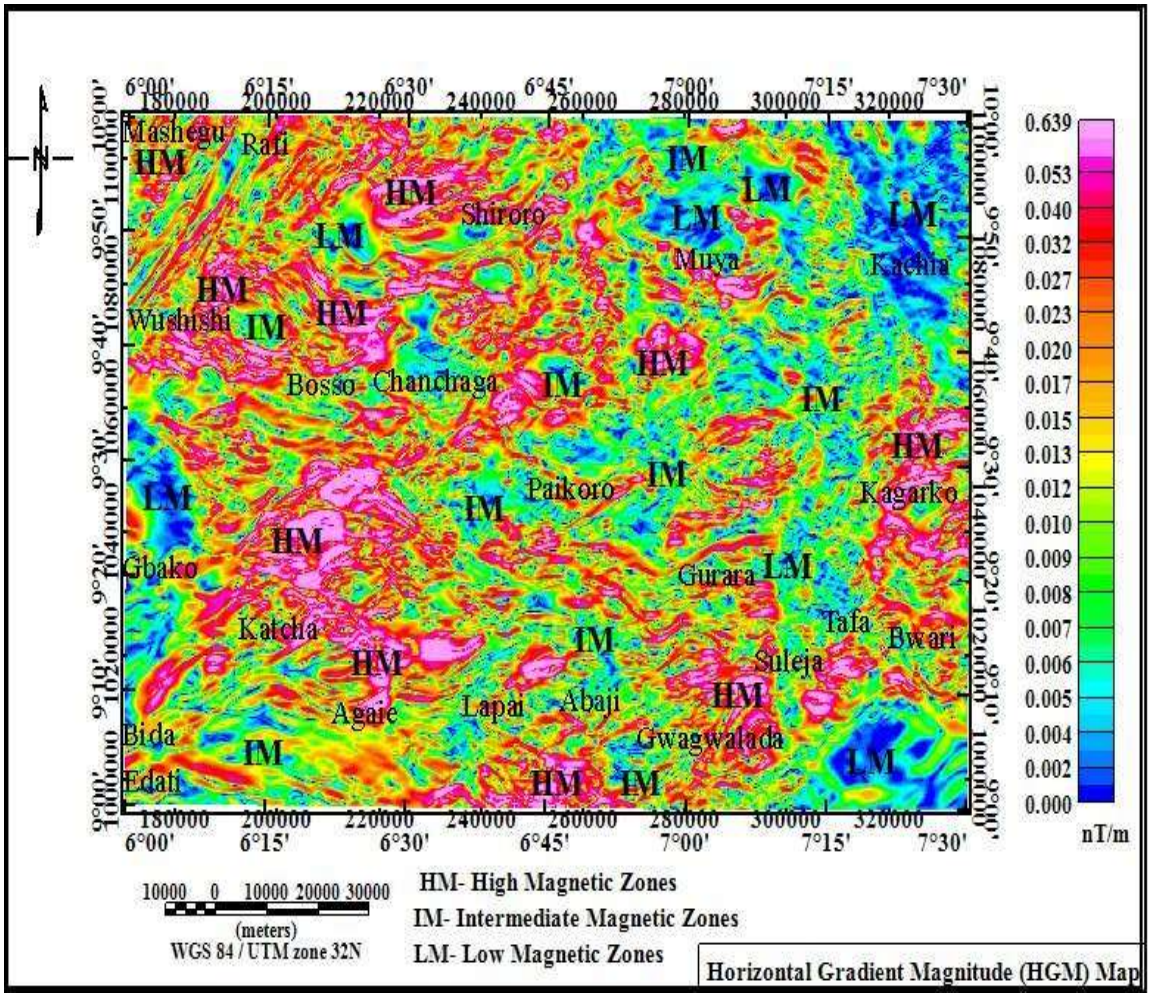

Figure 4.5: Horizontal Gradient Magnitude (HGM) Map of the Study Area. Colour Bar at the Right Side Signifies the Intensities of the Magnetic Anomalies Measured in Nanotesla per Metre (nT/m).

4.2.4 Tilt-angle derivative (TD) map

TD map (Figure 4.6) demonstrates more structural dispositions better expressed as lineaments. Figure 4.6 (TD map) displays different geologic features (lineaments) viewed to be exceedingly faulted and deformed. The deformations could be as an effect of the obvious deformation and remobilisation that occurred in the area. Thus, Figure 4.6 exhibit amplified lineaments. The change between the high (positive) and low (negative) magnetic anomalies are deformational events that occurred in the area assumed to be concentrated with mineral deposits. Figure 4.6 displays amplified lineaments. Changes between high (positive) and low (negative) magnetic anomalies are deformational events that occurred in a region presumed to be mineral-rich. It was discovered that the zero contours can estimate the location of abrupt changes in magnetic susceptibility values. The zero contour lines in this map (Figure 4.6) were coloured yellow. In addition, horizontal locations of geologic features with extended edges are portrayed on the map (Figure 4.6). The thin black lines seen on the map (Figure 4.6) represent the magnetic source contact boundary. As indicated by the colour scale bar, magnetic anomalies (contours) appear as light-yellow colour anomalies (0.064 Rad/m) separating the red (positive value) and green (negative value) hues. Consequently, pale yellow anomalies estimate the position of sudden changes in magnetic susceptibility values, while blue anomalies are assumed to be lineaments and pink anomalies are undamaged (undeformed) magnetic sources. The majority of the lineaments trended in an E-W, ENE-SWS and NE-SW direction, thus indicating the presence of ore mineral deposits. In conclusion, the map (Figure 4.6) is an effective tool for accurate lineament mapping. In addition, the TD map (Figure 4.6) demonstrates the accumulative characteristics of a brittle tectonic, perhaps showing the existence of an ancient tectonic legacy absorbed in lineaments and sheared by recent tectonic activity.

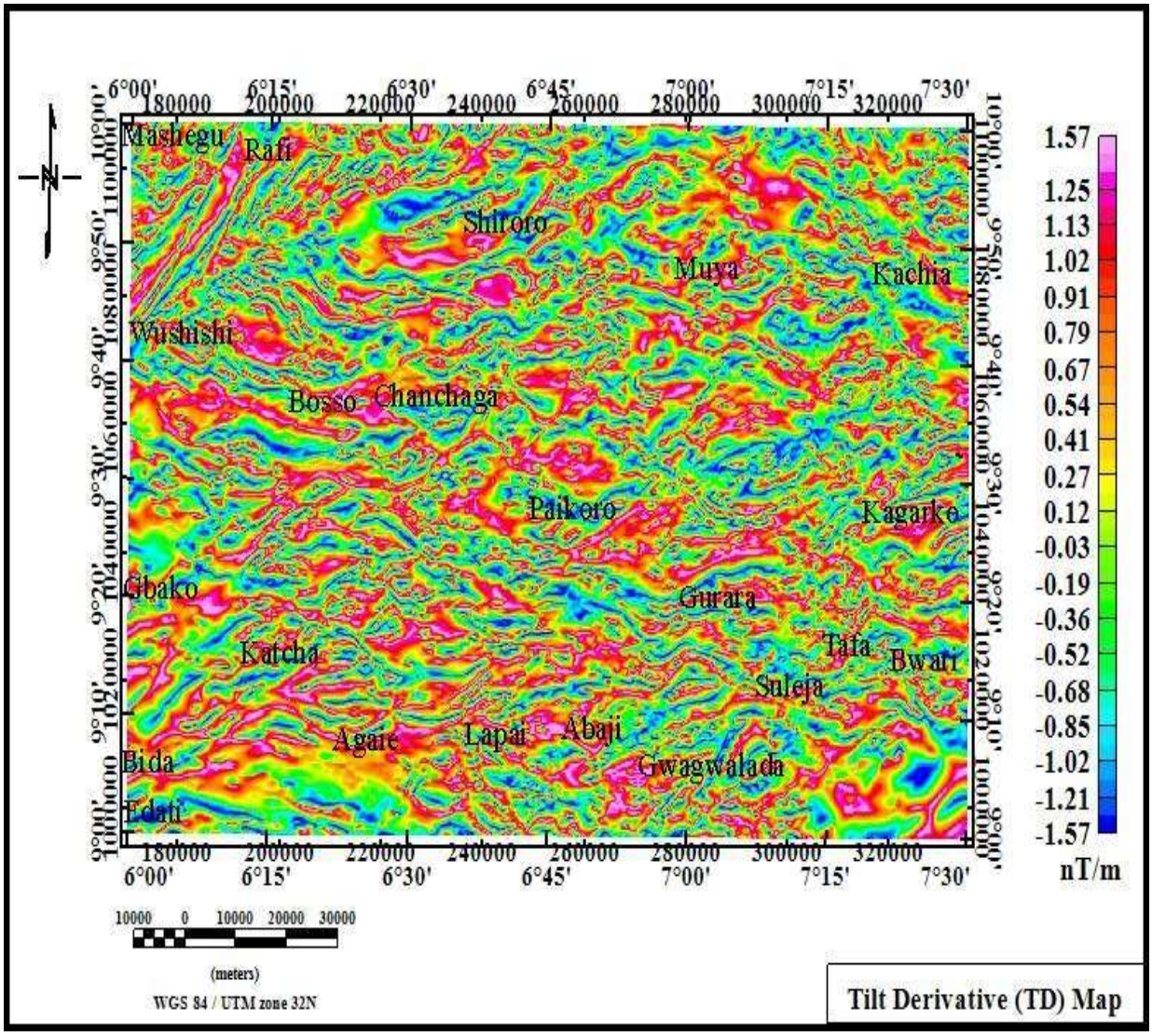

Figure 4.6: Tilt Derivative (TD) Map of the Study Area. Colour Bar at the Right Side Signifies the Intensities of the Magnetic Anomalies Measured in Nanotesla per Metre (nT/m).

4.2.5 Centre for exploration targeting (CET) map

Figure 4.7a is a vectorisation lineament map of the study area. Figure 4.7a displays uneven scheme of the geological lineament control and lithologic deformations in the study area. Lineation usually follows regional geology that is useful for mapping structural trends (Dobrin and Savit (1988)). The researchers also stated that well-defined boundaries between zones containing significantly different degrees of magnetic relief frequently indicate the presence of lineaments. The lineaments extracted depict level of tectonic deformation in the area. The orientations of lineaments disclose the results of the profound heterogeneity of the Earth's crust which symbolises geologic features affecting both Basement Complex and the overlying sediments (Balogun, 2019). The evaluation of the lineaments and direct geological observation on the produced lineament map (Figure 4.7a) suggests that magnetic lineaments represent brittle deformation zones. Thus, the displayed linear features are evidence to prove that the different concealed ore minerals in the study area are structurally controlled. The orientation of the lineament extracted from the CET map (Figure 4.7a) were exhibited in a rosette diagram (Figure 4.7b) to analyse the spatial distribution of lineaments, and to add to the understanding of the directions of the structural control of the study area. The

rosette diagram (Figure 4.7b) showed that E-W trends, ENE-WSW and NE-SW structural trends are the most prominent ones with minor traces of N-S trends. These structural trends noticed in the rosette diagram (Figure 4.7b) showed the tectonic trends that occurred in the area. Thus, it symbolises the orientation of the aligned ore deposits in the study area. On the whole, these trends agreed with previous work executed in the north central of Nigeria by Akinniyi *et al*., (2020).

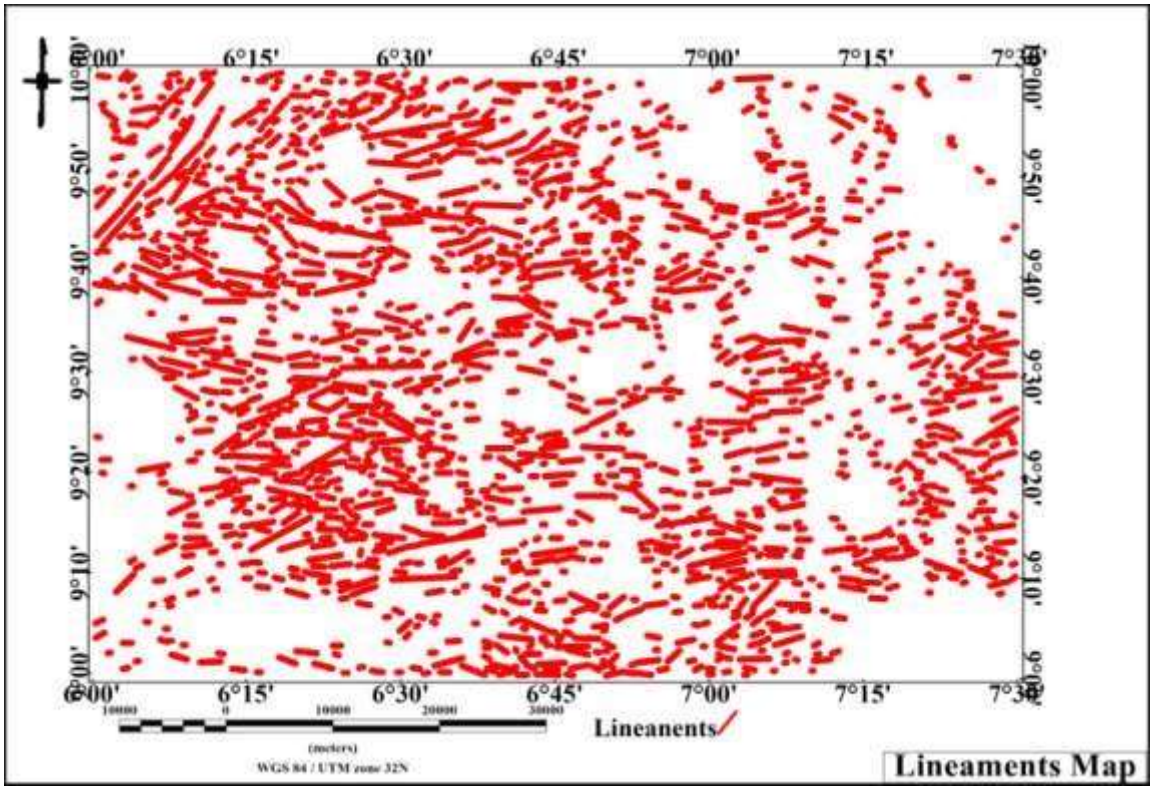

Figure 4.7a: Lineament map of the study area

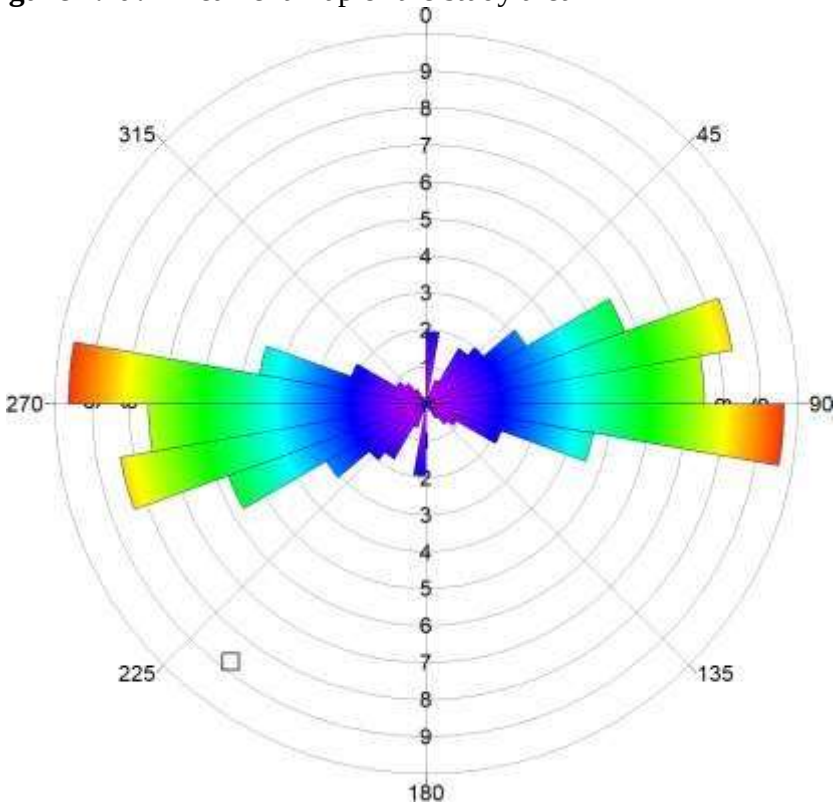

Figure 4.7b: Rosette diagram of lineaments derived from Lineament Map The E-W trends are the oldest and the deepest, they are the earliest structural orientations formed. Whereas, NE-SW trends are the youngest and shallowest, they confirm to the foliation

trends of the Schist Belts of Nigeria (Akinniyi *et al*., 2020). Besides, the diagram (Figure 4.7b) revealed a compilation of the orientations of the linear features that agreed with FVD and TD map and demonstrates that the E-W and NE-SW are the prevalent structural trend of the area.

4.2.6 Euler deconvolution (ED) map

The depths to geologic bodies where probable mineral deposits are concentrated along or aligned within the study area are shown in Figure 4.8. Figure 4.8 displays the linear clustering circles that are thought to be the effect of lineaments with depth values ranging between 0 m and 150 m. The non-uniformity of the depths of the lineaments suggests that all the outlines of the circles do not have the same source, and the orientation of the solutions trends towards E-W and NE-SW directions. Obviously, lineaments are perfectly distinguished on Euler's solutions map (Figure 4.8). Nevertheless, the obvious assemblages of solutions indicate that the locations of the source bodies are well determined. The solutions showed excellent conformity with the produced derivative maps of the study area. The bead-like shape and different colourations displayed on ED map (Figure 4.8) are the reflections of the spatial locations and depth levels of the delineated geological structures. As a result, near surface seated structures, brittle–ductile transition zone that have been previously suspected during the cause of interpretation are well accentuated on the map (Figure 4.8). Visible enough, the clustering length is every 30 m from the colour legend bar located on the right side of the map. Thus, the estimated depths of the lineaments ranges from 0 to 150 m. Displayed on the map (Figure 4.8) are prominent E-W and NE-SW trending structures. A critical visual examination of the faulting pattern demonstrated by

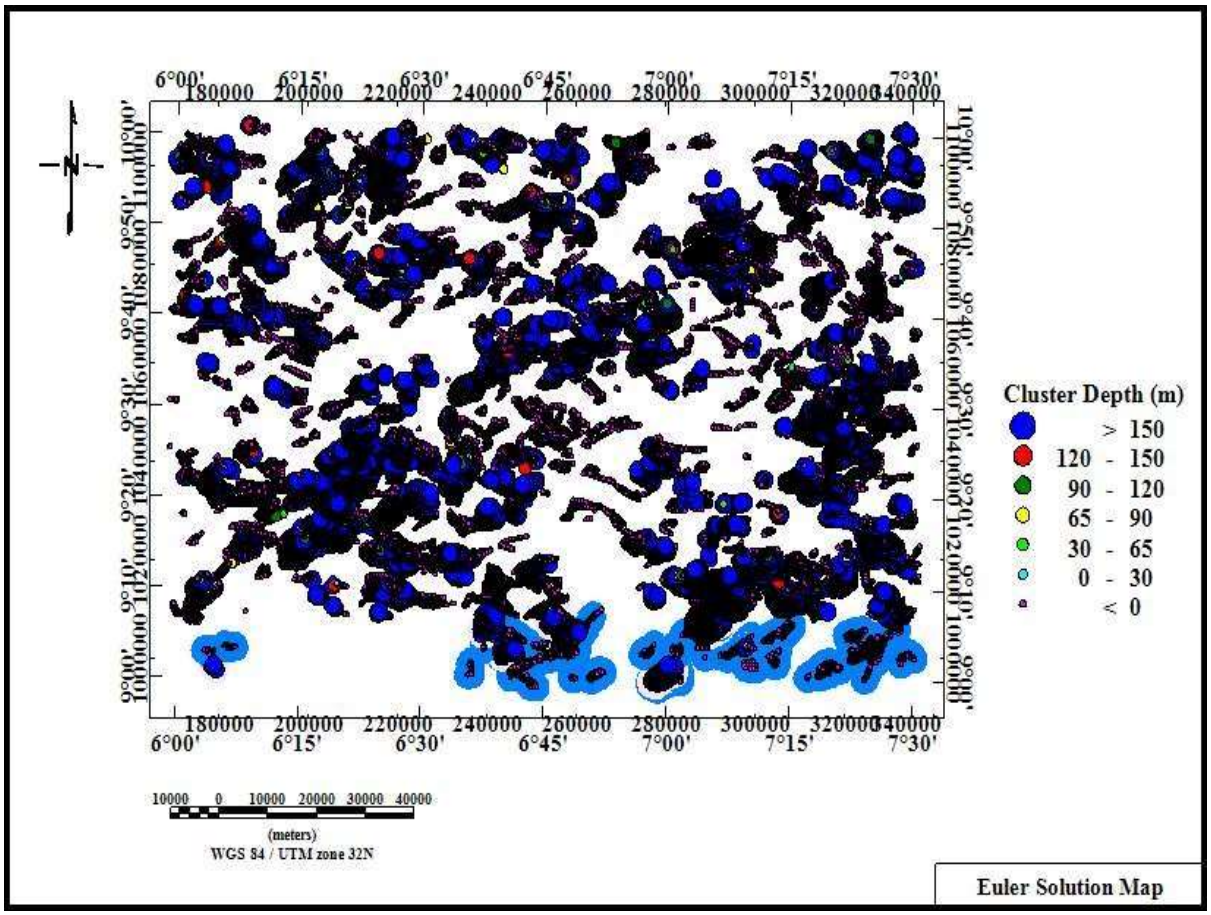

Figure 4.8: Euler Solution Map for a Structural Index (N) of 1 the E-W trending alignments of numerous Euler solutions indicates that the study area is affected by an E-W trending regional fault system, whose history could be due to tectonic effect. Thus, the exhibited Euler solutions prove that most of the lineaments in the study area exist at relatively shallow depths. Linear grouping (clustering) of different depth solutions shows variation in depths along the fault zones. Besides, lots of lineaments whose depths are above 150 m are featured in almost every part of the map. Also, Euler solutions with less than 120 m in depth that trend towards E-W and NE-SW directions are few on the map. A close examination of the geology map of the study area (Figure 2.1b) and Euler solutions map (Figure 4.8) shows that swarm of lineaments with E-W and NE-SW trends are well articulated in the Basement Complex terrain, though, minor lineaments are obviously well articulated in the Sedimentary terrain.

4.2.7 Source parameter imaging (SPI) map

Figure 4.9 (SPI map) exemplified and highlighted magnetic anomalies alleged to be the spatial location of different lineaments (geologic structures) at different depths within the study area. The map (Figure 4.9) reveals the depth estimate of lineaments in connection with ore mineral deposits in the study area. Figure 4.9, reveals that the depth estimates of the structures vary between -734.32 and 9504.26 m. Consequently, the depth effects of several notable anomalies depicted in Figure 4.9 those not correspond to the Euler depth solutions depicted in Figure 4.8.

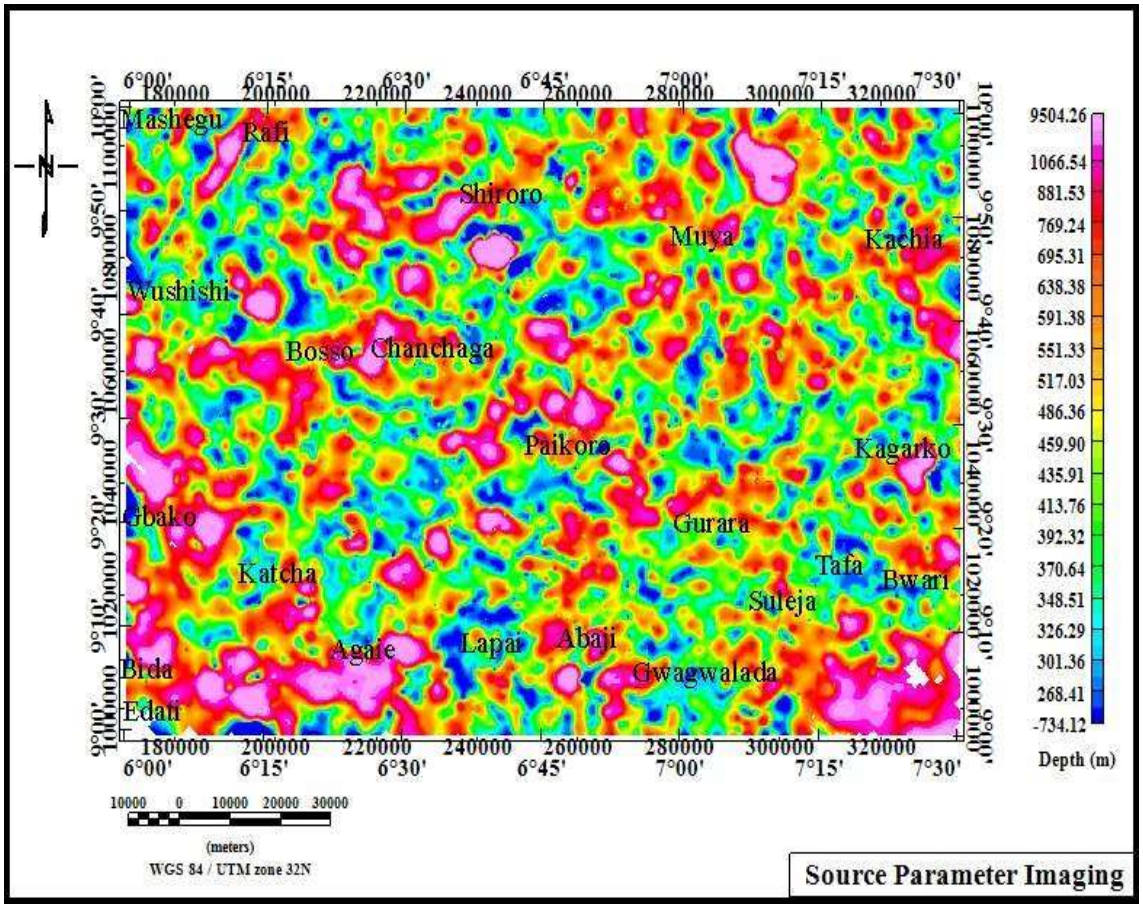

Figure 4.9: Source Parameter Image (SPI) Map of the Study Area. Colour Bar at the Right Side Signifies the Depth Estimate of Structures Measured in Metres (m).

4.2.8 Power spectrum analysis

Figure (4.10) is one of the 14 plots (graphs) of log of spectral energy against frequency (cycle/km). The remaining plots are displayed in Appendix A. On each graph, the two straight line segments displayed and labelled as slopes were used to calculate depth to near surface seated structures and deep seated structures respectively using equation (3.31) in the previous chapter. The slopes of each of the line segments were first evaluated, after which the results of D_2 and D_1 was calculated. The results for each of the 14 spectral blocks were summarized in Table 4. 1.

In Figure 4.10 which is also applicable to the remaining plots, the log of energy reduces with increasing frequency. In order words, the amplitude of the log of the spectral energy decreases with increasing frequency on each plot. Given that the results from all physical sources contribute to any measurement taken in potential field (Adepelumi and Falade, 2017), therefore, the energy spectrum evidently illustrates the ensemble of sources that contributed to the energy from low to high frequency. Thus, the line segment in the higher frequency domain is for the near surface (m_2) structures while the line segment in the lower frequency range is for deep seated structures (m_1). However, the series of points noticed on the straight line segments signifies bodies occurring within a particular depth range. In this research, the higher frequency sources, that is, near seated structures are the main target of interest. In this regard, the average depths estimated from each of the 14 blocks especially for D_2 in Table 4.1 was employed to generate the extrapolated depth map of the study area. Figure 4.11 is the grid map showing depth estimates of near surface seated structures associated with mineralisation targets. It is obvious that the depth estimates of the structures exist between 0.20 and

3.50 Km.

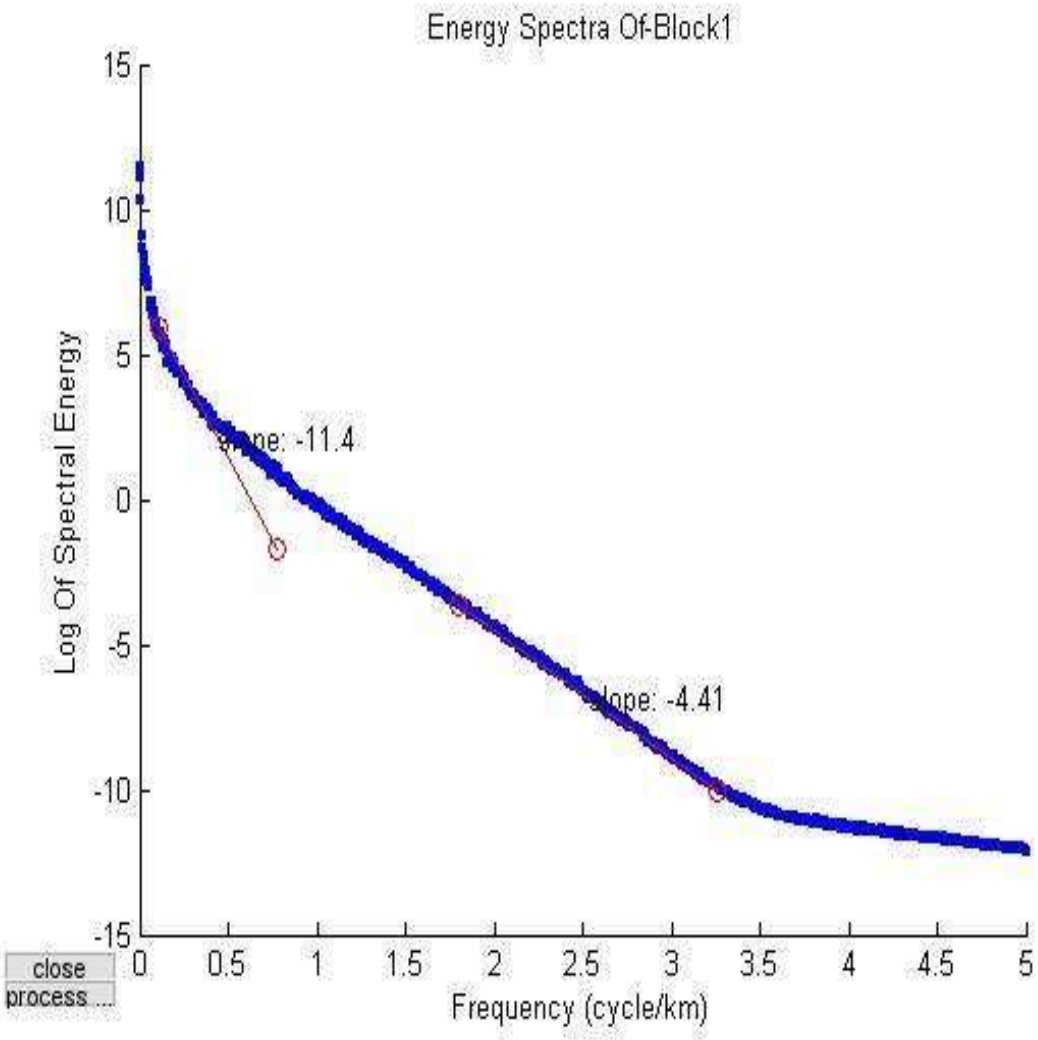

Figure 4.10: Plot of the Log of Spectral Energy against Frequency

Table 4.1: Estimates of Spectral Depths and the Coordinates for the 14 Ensembles of Near Surface Structures (D_2) and Deep Seated Geologic Structures (D_1) In the Study Area

Blocks	Longitude (Degree)	Latitude (Degree)	Shallow Structures Depth (D_2) (Km)	Deep Seated Structures Depth (D_1) (Km)
1	6.25	9.75	0.35	0.91
2	6.75	9.75	0.32	0.63
3	7.25	9.75	0.06	2.38
4	6.25	9.25	0.33	0.75
5	6.75	9.25	0.34	0.68
6	7.25	9.25	0.34	0.77
7	6.5	9.75	0.35	0.69
8	7	9.75	0.34	0.57
9	6.5	9.25	0.33	0.73
10	7	9.25	0.48	0.37
11	6.25	9.5	0.32	0.71
12	6.75	9.5	0.33	0.88
13	7.25	9.5	0.34	0.73
14	6.75	9.5	0.35	0.91

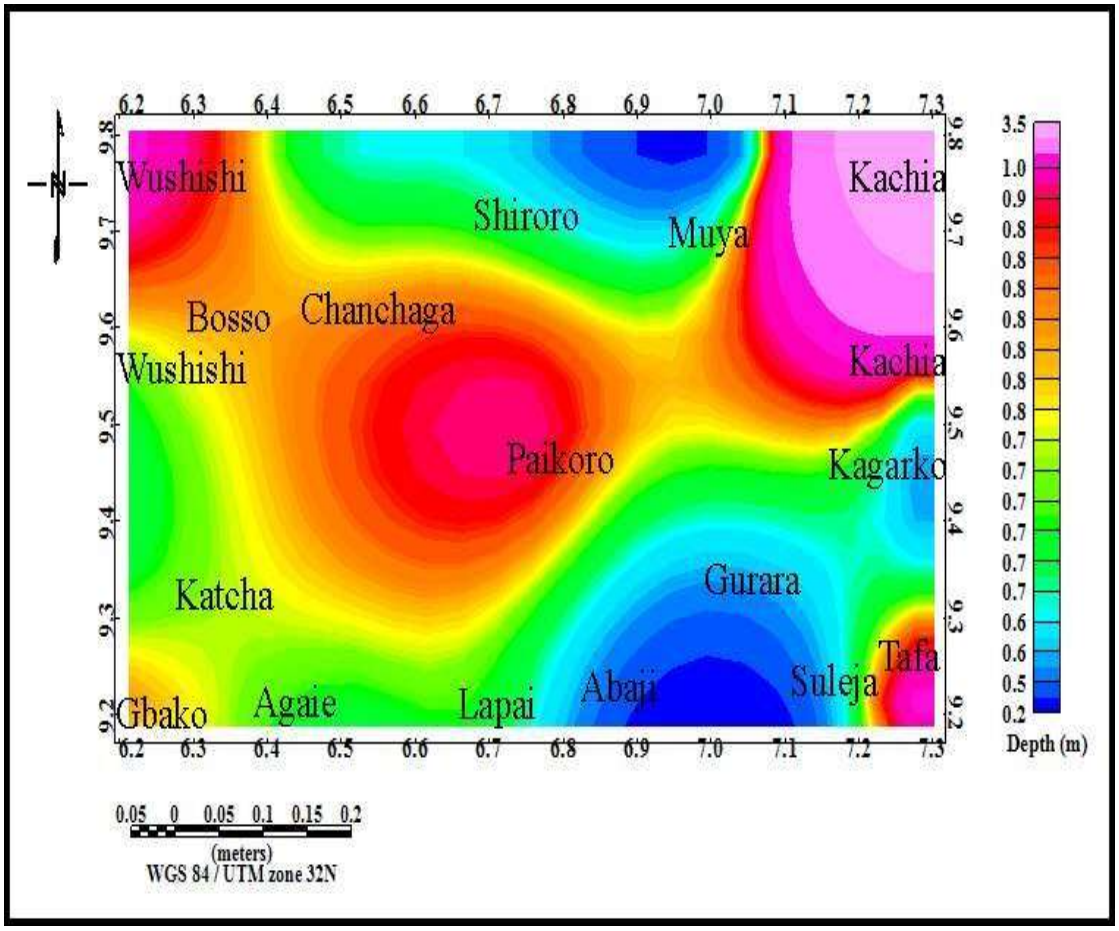

Figure 4.11: Depth Estimation Map of the Study Area Inferred From Power Spectral Analysis. Colour Bar at the Right Indicate Depth Values Measured In Kilometres (Km).

These values corroborate the end results on Euler Solution map (Figure 4.8), and depth estimate values of shallow structures connected to mineralisation zones on SPI map (Figure 4.9). In the map (Figure 4.11), the portions with red and pink colours with depth values greater than 0.8 m are indicative of nearest surface structures. Also, portions with yellow and light green colours with depth estimate values ranging between 0.7 and 0.8 m, are indicative of shallower seated structures while blue/ light blue colours with depth estimate values less than 0.7 m are indicative of the shallowest seated structures in

connection with ore mineral deposits. All the same, the depth estimated values of structures obtained through the three depth estimators resulted in good agreement. Though, the Euler Solution map (Figure 4.8), demonstrates a more localised estimation of depths than the SPI map (Figure 4.9) and Spectral map (Figure 4.11). However, Figure 4.8 reveals a depth map of higher resolution. Also, the difference in depth ranges obtained from the Figure 4.9 and Figure 4.11 is as an effect of the average depths calculated from the spectral windows.

4.3 Radiometric Interpretation

The resulting radiometric maps give a synthetic view of the heterogeneities of the geological formations encountered based on the radiometric signature of the different rock units as well as the structural trends that have an effect on them. Significantly, the radiometric maps aided the development of ratio maps to delineate Potassium enrichment zones which serve as an indicator of hydrothermal alteration zones. These maps demonstrate the apparent surface distribution of each of the radioelements principally Potassium (K), equivalent Thorium (eTh) and equivalent Uranium (eU) maps. Each of the radioelement images give views of the whole patterns of elements and more often than not contain patterns linked to various lithologies.

However, the resulting radiometric maps give a view of the heterogeneities of the geological formations encountered based on the radiometric signature of the different rock units and the structural trends that affect them. Airborne gamma-ray spectrometric dataset were utilised to interpret the spatial distributions of K, eTh and eU and distinctively map lithological units.

4.3.1 Potassium (K) distribution map

Figure 4.12 shows the dominance of K (%) in the study area. The percentage of K (%) contents in the study area range between 0.19 and 11.63%. The map (Figure 4.12) shows three concentration levels of K (%) contents. The highest K (%) is represented by orange to purple, and ranges from 1.1 to 10.8 %. The intermediate of K (%) level ranges from 1.53 to 2.88 %, it is symbolised by light green to yellow colours. The lowest concentration K (%) level symbolised by pale blue to light green colours ranges from 0.19 to 1.53 %. Furthermore, the high percentages of K (%) contents in outlined zones in the Basement terrain (Zone B) labelled as HK are indicative of granitic bodies in the area. The low-to-moderate K (%) within the sedimentary terrain (Zone S) and some parts with traces of sediments within the Basement part of the map (Zone B) labelled as LK are indicative of intrusive formations in the area. Note, feldspars is a name given to a large group of rock-forming silicate minerals containing Calcium (Ca), Sodium (Na) and Potassium (K) that make up the Earth's crust. The rock-forming mineral groups are mainly Orthoclase ($KAlSi_3O_8$), Albite ($NaAlSi_3O_8$) and Anorthite($CaAl_2Si_2O_8$) (John *et al*., 2022). Figure 4.12 demonstrates that the emanation of K (%) content stalks from the
K-feldspar (Orthoclase ($KAlSi_3O_8$)) in the area.

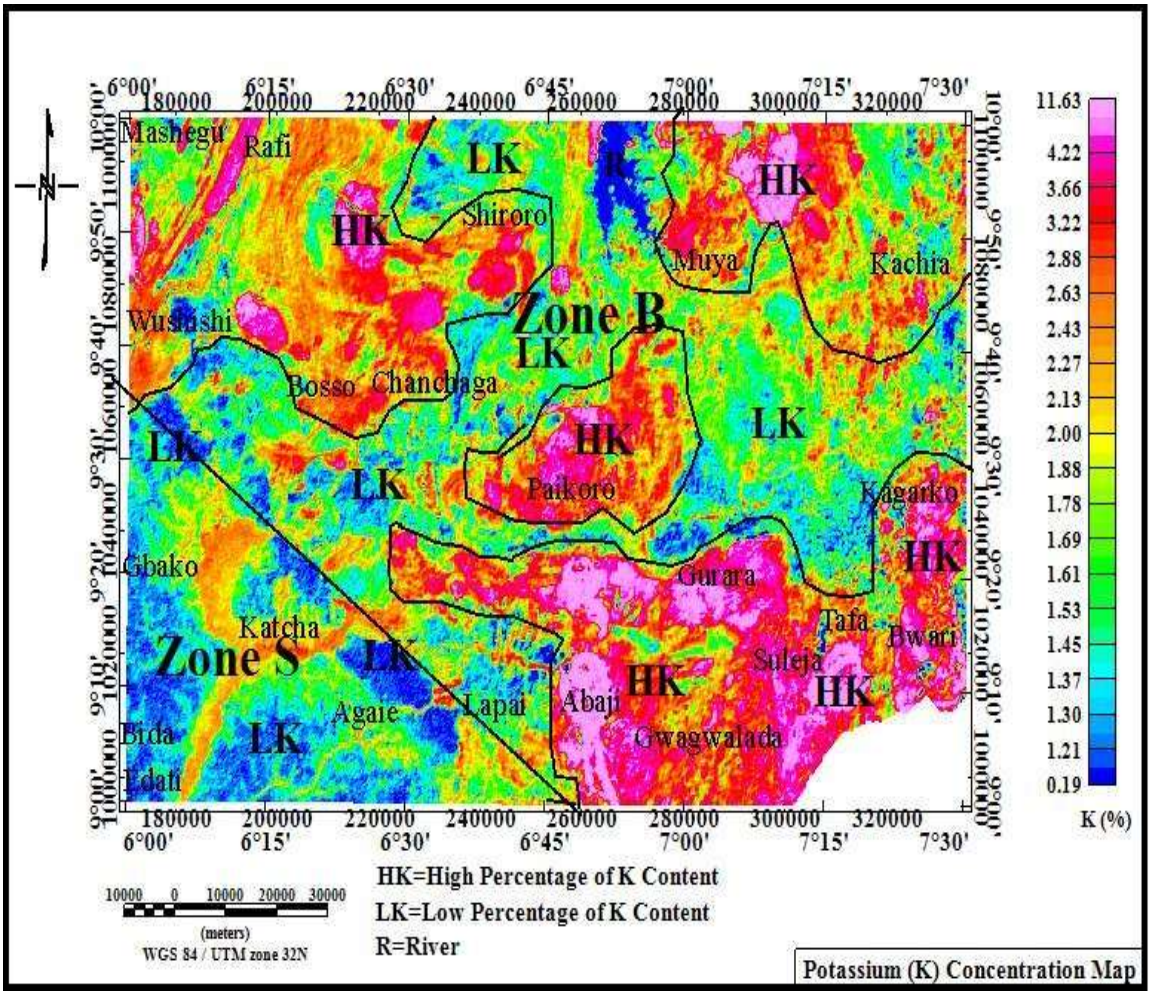

Figure 4.12: Potassium (K) Concentration Map Measured in Percentage (%) These minerals are usually present and high in felsic rocks (granite and rhyolite), low in mafic rocks (basalt and gabbro) and almost not present in ultramafic rocks (peridotite) (Manu, 1993; Telford *et al.*, 1990). Felsic rocks are light in colour and composed of light colour minerals rich in Silica contents but poor in Magnesium. Mafic rocks are dark in colour, composed of dark colour minerals rich Magnesium contents but poor in Silica contents while ultra-mafic rocks are composed of minerals rich in Magnesium contents with little or no Silica contents. However, the obvious K anomalies in the map (Figure 4.12) do not only relate to K-feldspar abundance but also indicate the degree of weathering of rocks in the area (Sanusi and Amigun, 2020a). Further, the high of K (%) content noticed on the outlined zones labelled as HK correlate with Amphibolite schist, Banded Gneiss, Biotite Gneiss, Migmatitic Gniess, Prophyritic Granite and Mylonites of the geological map

(Figure 2.1b) of the study area. On the other hand, the areas labelled LK in the map expressed as low of K (%) contents are due to

prolonged weathering activities.

4.3.2 Equivalent thorium (eTh) concentration map

In interpretation of radiometric data, estimates of Thorium (Th) and Uranium (U) concentration are normally reported as equivalent Thorium (eTh) and equivalent Uranium (eU) for the reason that these estimates are constantly based on the assumption of equilibrium condition (Adepelumi and Falade, 2017). Figure 4.13 shows the distribution of eTh concentrations in Part Per Million (ppm) in the study area. The concentrations of eTh (ppm) contents range between 0.91 and 163.75 ppm. Generally, high concentrations of eTh (ppm) contents are the most constituent of monazites, minerals mixed with rare earth and Thorium phosphates (Telford *et al*., 1990).

Figure 4.13: Equivalent Thorium (eTh) Concentration Map Measured in Part Per

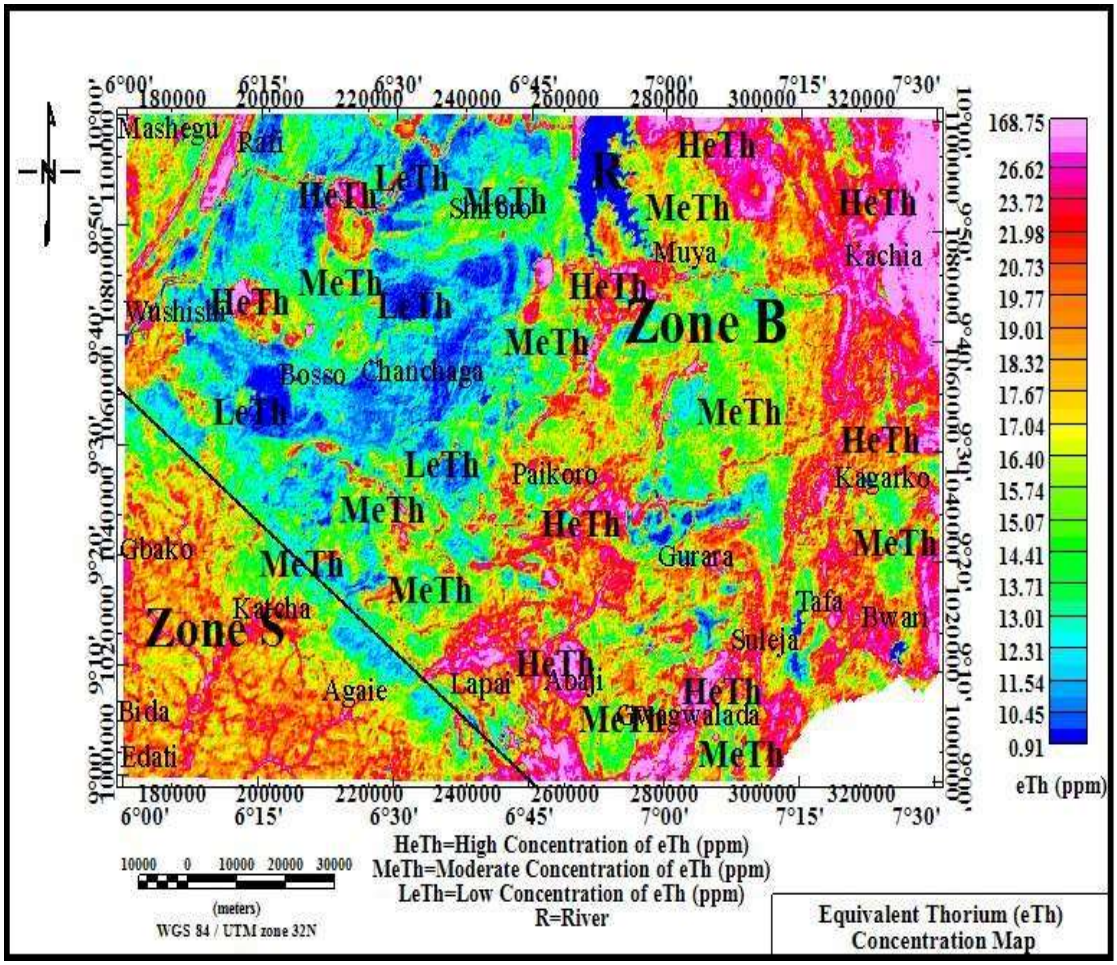

Million (ppm)

On the other hand, low concentrations of eTh (ppm) contents are usually noticed in mafic rocks composed of dark colour minerals (Shives, 2008). Generally, Th is considered an immobile radioactive element (Silva *et al*., 2003). Nevertheless, zones with low concentration of eTh (ppm) cannot be attributed to depletion due to hydrothermally

altered haloes within the area. Principally for interpretation purpose, the concentration of eTh (ppm) in Figure 4.13 was grouped as high concentration (> 19.77 ppm), moderate concentration (13.71–19.77 ppm) and low concentration (< 13.71 ppm). Hence, in Figure 4.13, the sedimentary terrain (Zone S) and parts of the granitic rocks that forms the Basement terrain (Zone B) labelled as 'HeTh' are characterised by moderate-to-high concentration of eTh (ppm) signatures. The obvious displayed moderate-to-high concentration of eTh (ppm) contents is as a result of the presence of Monazite minerals in the rocks present in the study area. The parts in the Basement terrain labelled as 'LeTh' that shows low concentration of eTh (ppm) signatures is due to the presences of mafic minerals in the rocks situated in that area (Telford *et al*., 1990). The anomalous locations of moderate-high concentrations of eTh (ppm) signatures in the map are dominated by Granite Gniess, migmatite, coarse porphyritic granite, Schist and granite. In contrast, areas with relatively low concentrations of eTh (ppm) signatures are dominated by Quartz vein, grained Biotite granite and Amphibolite schist when compared with geological map of the study area (Figure 2.1).

4.3.3 Equivalent uranium (eTh) concentration map

Figure 4.14 shows the distribution of eU (ppm) concentration in the study area. The map (Figure 4.14) shows different anomalous signatures with total concentrations of eU (ppm) varying between 0.44 and 26.29 ppm.

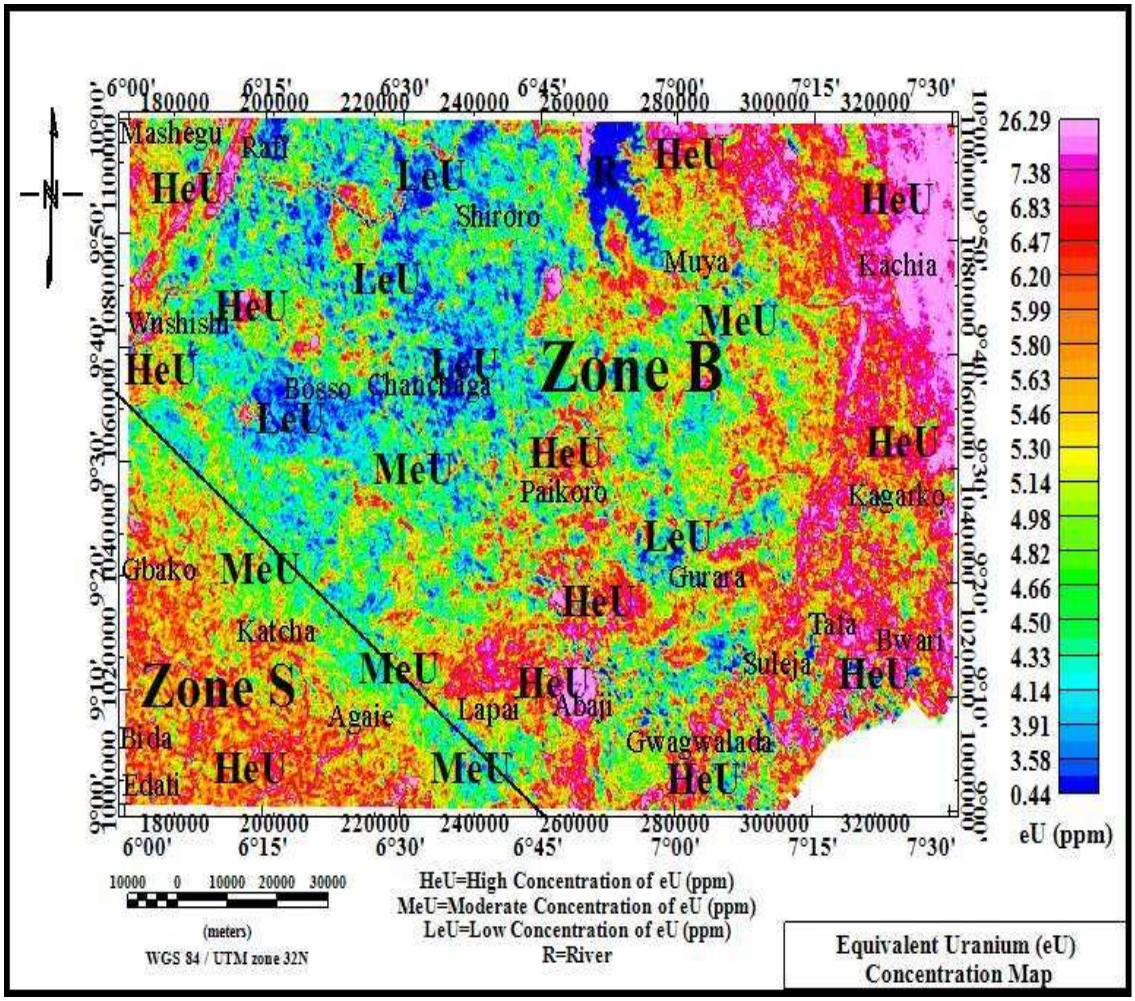

Figure 4.14: Equivalent Uranium (eU) Concentration Map Measured in Part Per Million (ppm)

The map (Figure 4.14) shows high presence of of eU (ppm) contents which is mainly related to Younger Granites. In other words, the eU map (Figure 4.14) shows shortwavelength anomalies compared to the anomalies displayed on K (%) and eTh (ppm)

maps. This is could be due to variations in atmospheric radon concentrations during the survey ensuing in significant streaking in the image (Silva *et al*., 2003). This outcome is a distinctive feature found in eU images in spite of the micro-levelling (Minty *et al*., 1997). For this study, the concentrations of eU (ppm) were relatively grouped as high (> 5.80 ppm), moderate (4.50 -5.80 ppm) and low (< 4.50 ppm). However, It was observed that most of the granitic bodies in the Basement terrain (Zone B) fall within "HeU" and the alluvial deposits in the Sedimentary terrain (Zone S) are associated with moderatehigh concentrations of eU (ppm) signatures, while other significant granitic bodies in 'Zone B' labelled as "LeU" show low concentrations of eU (ppm) signatures.

Comparison of Figure 4.14 with the geological map (Figure 2.1) of the study area shows that moderate-high concentrations of eU (ppm) contents are observed on regions underlain by Granite Gniess, Migmatite, coarse Porphyritic granite, Schist and granite. This is probably due to their mineralogical composition. Whereas, area with low concentrations of eU (ppm) contents are observed in the same regions are underlain by Quartz vein, grained Biotite gneiss, Mylonite interlaid with Amphybolite rocks and Migmatitic gneiss. Thus, the concentrations of eU (ppm) anomalies observed in the entire map (Figure 4.14) demonstrates high degree of weathering and mineralogical composition of rocks in the area as well. Obviously, the connection between the concentration contents of eTh (ppm) is linearly proportional to that of eU (ppm). Thus, this is an indication that both elements (eTh (ppm) and eU (ppm)) go along with each other in most rocks present in the study area. Relatively, high concentration of eTh (ppm) and eU (ppm) can be associated with the presence of Iron (Fe) or another metal element deposits formed by the magmatic activities (Adepelumi and Falade, 2017). Also, the high concentrations of eTh (ppm) and eU (ppm) are characteristic of the prevalent intrusive rocks (mostly granite) in the study area. The relationship between K (%) are

more complex in comparisons with that of eTh (ppm) and eU (ppm). This is because eTh (ppm) and eU (ppm) belong to the actinide elements, both have similar geochemical properties, whereas K (%) belong to alkaline element with different geochemical characteristics (Akinniyi *et al*., 2020).

As observed on the K (%), eTh (ppm) and eU (ppm) maps (Figures 4.12, 4.13 and 4.14), the river channel labelled 'R' in the study area shows low percentages of K(%) and low concentrations of eU (ppm) and eTh (ppm). However, this does not mean that rivers do not contain radioactive material; instead it is an indication that water is a strong absorber of radiation (Darnley 1975).

4.3.4 Total count (TC) concentration map

In addition to the three gamma-ray spectrometric images, (Figures 4.12, 4.13 and 4.14), In the TC rate radiometric map (Figure 4.15), the radiometric signatures were grouped into three major levels of lithological units to represent different rock types in the study area. The grouping was based on the distributed concentrations of K (%), eTh (ppm) and eU (ppm) in the area. in this study, the high level labelled as lithology "A" ranges from 17.1 to 184.9 µR/h, it is symbolised by the orange, red and purple colours. The lowest level ranges from -6.0 to 9.4µR/h, this range is symbolised by pale blue and blue colours. The intermediate level has colour from light green to yellow and it ranges from 10.3 to 17.l µR/h. This range is distributed all over the map. It is labelled as lithology "B". This range is correlated mainly with the Basement terrain (zone "B)" and labelled as lithology "C".

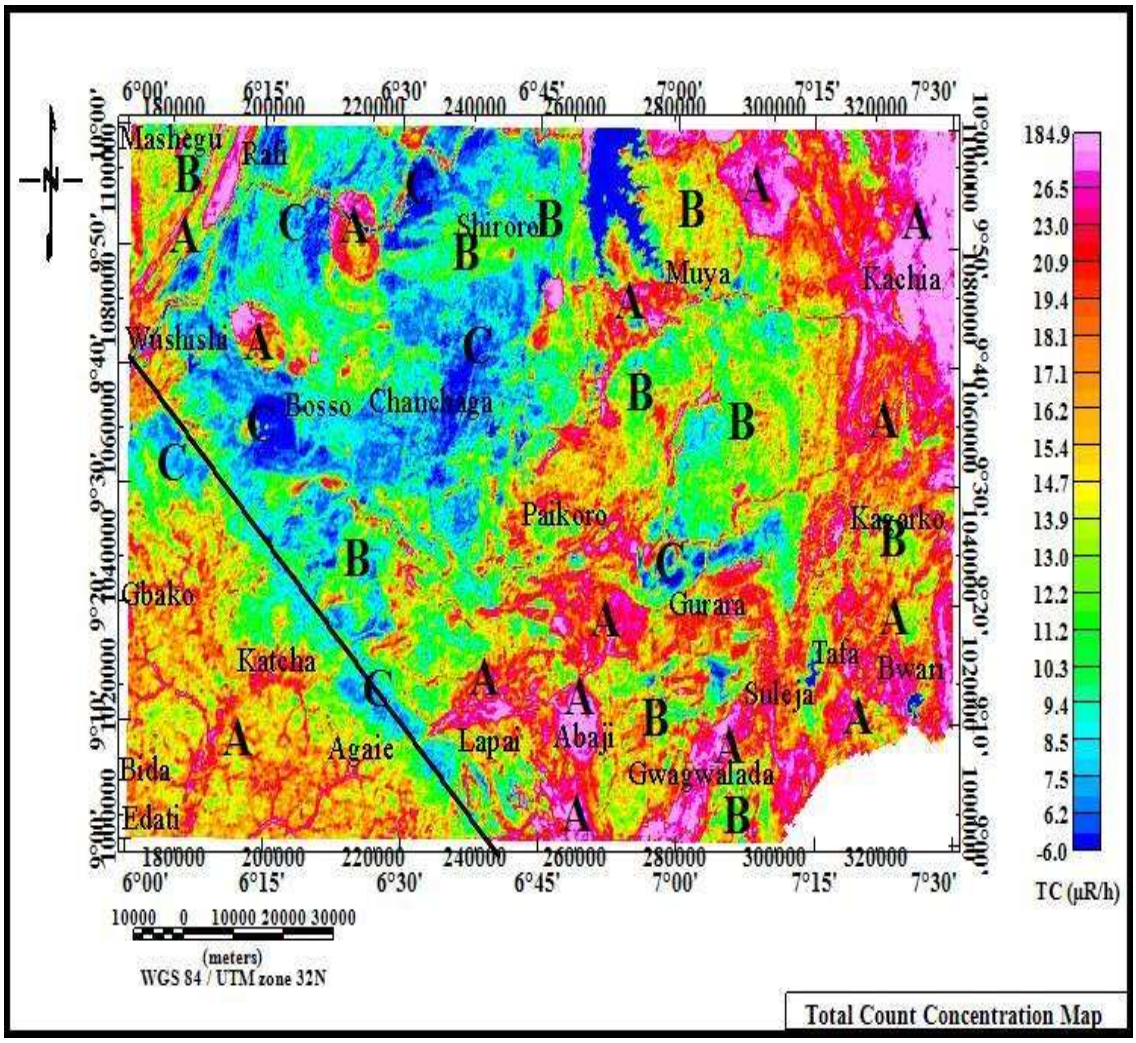

Figure 4.15: Total Count (TC) Rate Concentration Map Measured in µR/h.

In other words, the high radiometric anomalies noticed in the map (Figure 4.15) are as a result of relatively high concentration levels of the three radioelements in the study area. Relatively, high of TC (µR/h) levels are an indication that high radio-activities in more than 60 % of the entire area. These are attributed to the presence of intrusive formations and granitic bodies in area (in both zones). Whereas, the intermediate and relatively low

concentrations of TC (µR/h) levels noticed in the entire map could be due to the presence of sediments in the entire area. The intervals of the variation of the K (%), eTh (ppm) and eU (ppm) for each lithology are summarised in Table 4.2.

Lithology A are composed of either deposits rich in radioactive elements or rocks with the highest concentration of K (%), eTh (ppm) and eU (ppm), suggesting the occurrence of the granitic bodies such as Granite Gneiss, Migmatite, coarse Porphyritic granite, Schist and Granite in the study area. Possibly, these rocks could be igneous or metamorphic rocks. Majorly, the rocks in this lithology are present in Zone B where there are outcrops of the Crystalline Basement Complex. Generally, K (%) contents ranges from a few five percent to up tenth percent, suggesting the absence of potassium salt deposit (Akinniyi *et al*., 2020). Thus, the high percentages K (%) contents together with high concentrations of eTh (ppm) and eU (ppm) indicate the presence of the outcrop of the intrusive formation. Lithology B are composed of rocks characterised by moderate concentration contents of K (%), eTh(ppm) and eU (ppm) in the area, suggesting the occurrence of metamorphic rocks such as grained Biotite Gneiss, Granite Gneiss, Quarttz vein, Banded Gneiss, Amphybolite Schist and Migmatitic Gneiss in the area. Such rocks must have been subjected to metamorphism or were formed through the deposition and solidification of sediments.

Table 4.2: Ranges of Percentages of K (%) and Concentrations of eTh (ppm), eU (ppm) and TC (%, ppm, ppm) in the Rocks of the Different Lithological Units

Lithological Units	K (%)	eTh (ppm)	eU (ppm)	TC (%, ppm ppm)
A (High)	> 2.88	>19.77	> 5.80	>17.1

B (Intermediate)	1.53 to 2.88	13.71 to 19.77	4.5 to 5.80	9.4 to 17.1
C (Low)	< 1.53	< 13.71	< 4.50	< 9.4

Lithology C are characterised by most common rocks like sedimentary rocks composed of low concentration contents of K (%), eTh (ppm) and eU (ppm) in the area. The rocks of this lithology are present majorly in Zone B, where there are outcrops of Crystalline Basement rocks. The radioelement maps including the TC map (Figures 4.12, 4.13, 4.14, and 4.15) show that the study area is covered with rocks of different compositions. Obviously, there is harmony between the indicated concentration levels of radioactivity and the corresponding rock types. The foremost linear trend, which could be interpreted

from the elongation of the radiometric anomalies, is the E-W and NE-SW trend. The trend aligns with the responses of linear magnetic structures interpreted on the basis of the FVD map (Figure 4.3) of the study area. Therefore, the E-W and NE-SW trends appears to be the most recognized trend from both aeromagnetic and aeroradiometric interpretation maps. In addition to this, it corroborates the effective role of these trends on the geological frame of the area under investigation.

4.4 Ratio Maps (R-maps)

The R-maps were developed to delineate hydrothermally altered zones in view of the fact that high concentration level of K (%) and low concentration level of eTh (ppm) and eU (ppm), though not in all cases, are pointer for altered zones in various ore mineral deposits (Ostrovskiy, 1975). Following the *F*-parameter expression developed by (Efimov, 1978), lithology differentiation related to Potassium enrichment zones which serve as an indicator for hydrothermally altered zones associated with mineralisation were delineated on the produced R-maps. The R-maps were generated from meaningful numerical combination of either two or the three radioelement grids. The creation of R-maps helped to enhance subtle features that may not have been apparent in the original individual radioelement grids, and in accentuating the presence of mineral alterations in area under investigation. Four R-maps were adopted in this research.

4.4.1 K/eTh ratio map

In addition to the three (3) radiometric grid maps (Figures 4.12, 4.13 and 4.14), a K/eTh R-map was calculated to highlight locations with high concentration Potassium (K (%)) content. High concentration of K (%) contents is an indicator of probable areas of hydrothermal alterations (Abd El Nabi, 2013). K/eTh R-map (Figure 4.16) shows that the distribution of the K/eTh (%/ppm) signatures is variable. The relatively high of

K/eTh (%/ppm) contents is associated with granitic rocks in the area. However, the K/eTh R-map (Figure 4.16) was attained by dividing K (%) grid (Figure 4.12) by the eTh (ppm) grid map (Figure 4.13) of the study area. In the view of the fact that during alteration processes, K is known to be more mobile than Th in terms of element mobility during chemical alteration processes (Fall *et al*., 2018; Silva *et al*., 2003; Elkhateeb and Abdellatif, 2018), and high percentage of K (%) contents with low concentration of eTh (ppm) are associated with alterations in a lot of ore deposits (Ostrovskiy, 1975), high K/eTh (%/ppm) is often considered the best indicator of

Potassium enrichment zones linked to hydrothermal alteration (Fall *et al*., 2018). Hence, Figure 4.16 shows the level of K/eTh that enhances alteration signatures and a number of lithologic contrasts. Since K is more mobile than Th, Figure 4.16 also shows K/eTh anomalies that distinguish zones of hydrothermal alteration characterised by K (%) enrichment. In addition, the ratio map (Figure 4.16) displays possible locations with a relatively high concentration of K (%) and a low concentration of eTh (ppm).

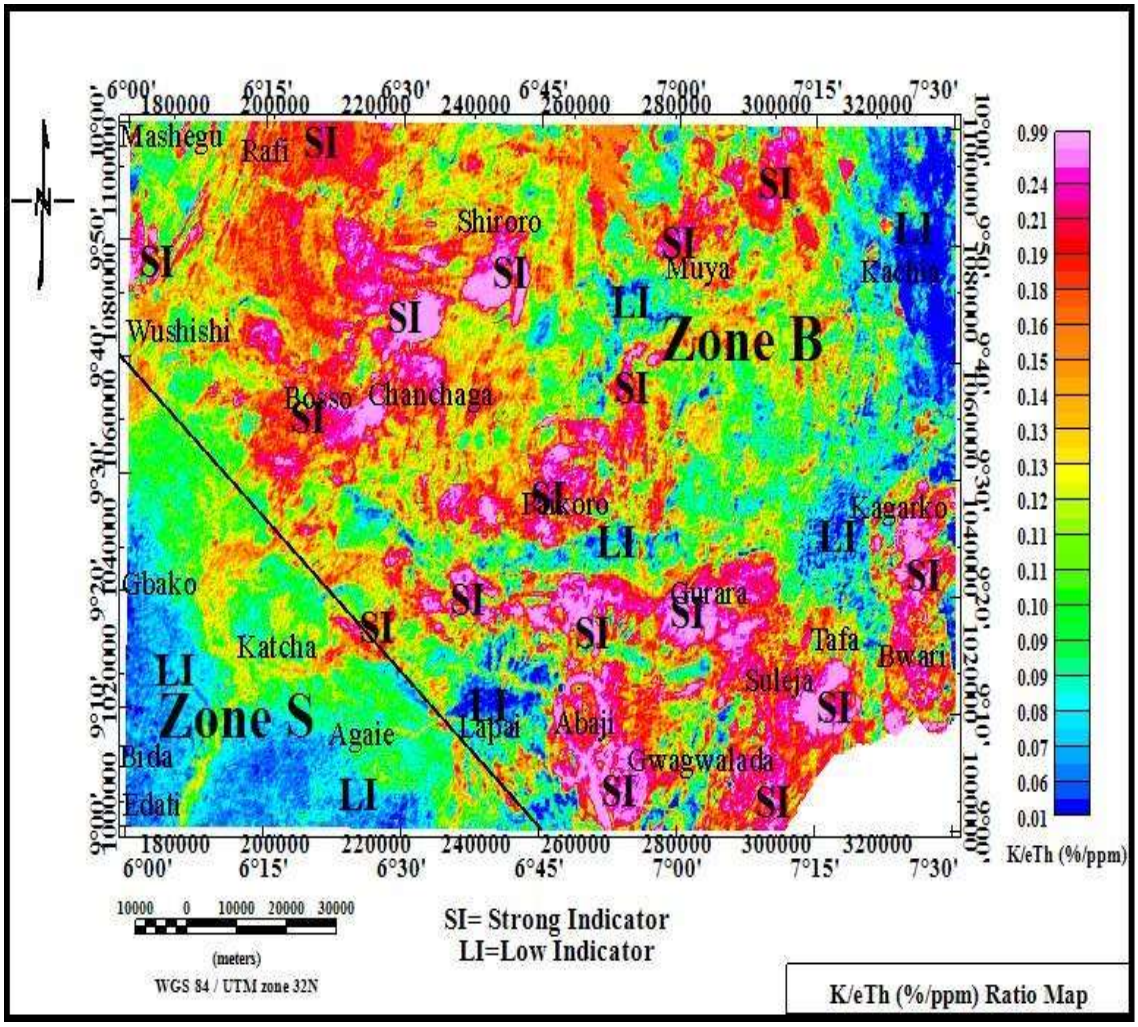

Figure 4.16: Potassium /Equivalent Thorium (K/eTh) Ratio Map. Colour Bar Indicate Ratio Level in Percentage/ Part per Million (%/ppm).

In the map (Figure 4.16), locations affected by the hydrothermal alterations have a high concentration of K/eTh ratio of 0.18 – 0.99 (%/ppm). Thus, an increase in K (%) and decrease in eTh (ppm) is an indication of alteration setting in different ore deposits

(Akinniyi *et al*., 2020). Almost all the anomalous zones shown in K (%) map (Figure 4.12) were noticed in K/eTh ratio map (Figure 4.16). however, some high percentages of K (%) counts in the K (%) map (Figure 4.12) were also enhanced on the K/eTh ratio map (Figure 4.16). In comparison with the geological map (Figure 2.1) of the study area, (Figure 4.16) shows high values of K (%) which are attributes of granitic bodies or alluvial deposits in Zone S (sedimentary terrain). The areas characterised by the high anomalous K/eTh ratio signatures (> 0.18 %/ppm) labelled as "SI" in Figure 4.16 depicts strong indicators of extremely hydrothermally altered zones in the study area areas affected by the hydrothermal alteration processes are featured predominantly in Zone B (Basement Complex terrain). These areas are associated with Quartz vein, grained Biotite granite and Amphybolite schist, Granite Gniess, Migmatite and coarse Porphyritic granite. On the other hand, it is observed that the areas not really affected by the hydrothermal process are featured in Zone S (Sedimentary Terrain) and northeastern flank of Figure 4.16. The areas labelled as "LI" are characterised by the low anomalous K/eTh ratio signatures (< 0.08 %/ppm) associated with alluvial deposits or sediments. Probably, it is an indication of low percentages of K (%) with high concentrations of eTh (ppm) contents. As observed in Figure 4.16, the interpreted hydrothermally altered zones trending towards the E-W and NE-SW directions followed the same pattern with the trends deduced in the TMI-RTE map (Figure 4.2) of the study area.

4.4.2 K/eU ratio map

The K/eU R-map (Figure 4.17) was created by dividing K (%) grid (Figure 4.12) by the eU (ppm) grid map (Figure 4.14). The map (Figure 4.17) shows the presence of different anomalous K/eU ratio signatures with concentration values ranging between -17195.0

and 59877.9 (%/ppm). The concentrations patterns of anomalous K/eU ratio signatures (%/ppm) (Figure 4.17) appear similar to the concentrations patterns of anomalous K/eTh ratio signatures (%/ppm) (Figure 4.16). Thus, the locations labelled as 'SI' characterised by the high K/eU ratio anomalous signatures (> 0.5 %/ppm) are associated with hydrothermal alteration zones related to mineralisation, and are obvious in almost the entire map (Figure 4.16), though more prominent in Zone B. Comparably, high K/eTh and K/eU ratio signatures (Figure 4.16 and 4.17) labelled as 'SI' indicate highly fractured zones and characteristically accentuate K enrichment haloes connected with hydrothermally altered zones related to mineralisation in the study area.

4.4.3 eTh/eU ratio map eTh/eU R-map (Figure 4.18) shows that most of the granitic bodies in the study area contain relatively low concentration contents of eTh (ppm) and eU (ppm). Though, this depends on the mobility of the radioelements. As interpreted previously, the granitic bodies in the area are richer in K (%) contents, as K is more mobile than Th and U (Elkhateeb and Abdellatif, 2018). Figure 4.18 demonstrate intercalations of eTh/eU ratio anomalies ranging from -80137.4 to 76131.3. Figure 4.18 was created by dividing eTh (ppm) grid (Figure 4.13) by the eU (ppm) grid map (Figure 4.14).

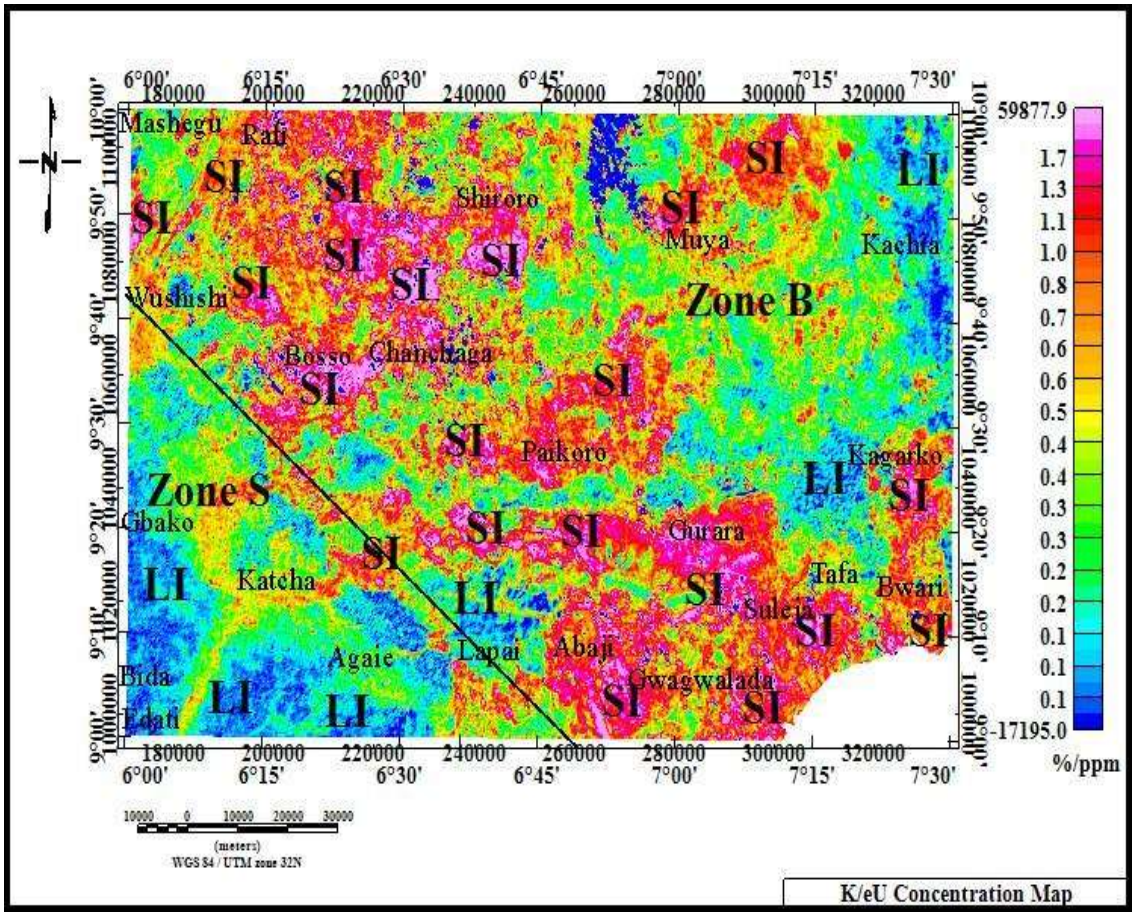

Figure 4.17: Potassium /Equivalent Uranium (K/eU) Ratio Map. Colour Bar Indicate Concentration Level in Percentage/ Part per Million (%/ppm).

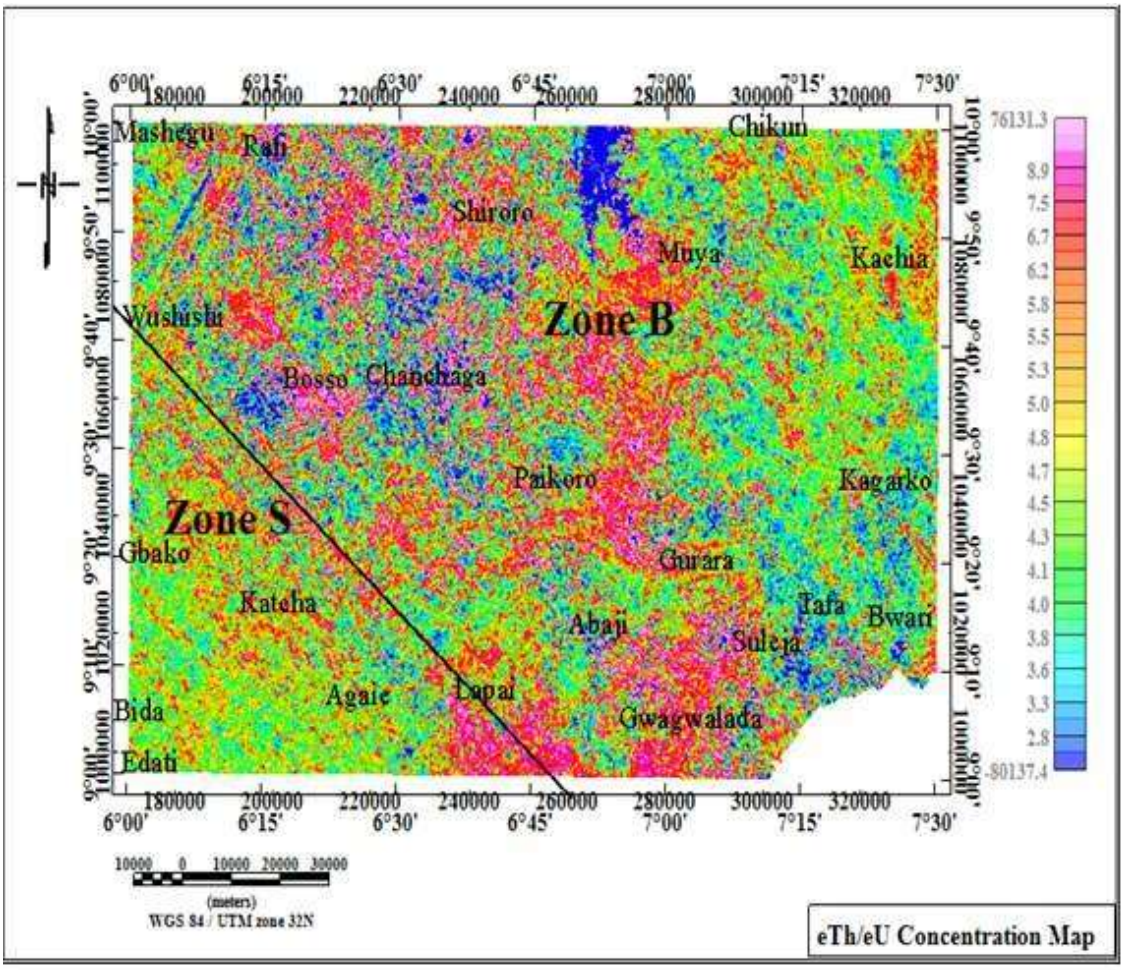

Figure 4.18: Equivalent Thorium /Equivalent Uranium (eTh/eU) Ratio Map. Colour Bar Indicate Concentration Level.

It demonstrates the dominance of relatively low anomalous eTh/eU ratio signatures with the area. Besides, hydrothermally altered zones related to mineralisation were not emphasised on this map.

4.4.4 K*(eTh/eU) ratio map

K*(eTh/eU) R-Map (Figure 4.19) revealed other K enrichment areas that were concealed in the eTh/eU R-map (Figure 4.18) due to weathering effect. In this R-map (Figure 4.19), the relatively high concentration level of K*(eTh/eU) ratio signatures probably depicts granitic bodies with hydrothermally altered zones connected to mineralisation in the area. These zones closely correspond to the relatively high level of

K contents interpreted as hydrothermally altered zones in Figure 4.16 and 4.17. The K*(eTh/eU) R-map (Figure 4.19) was created by multiplying K (%) grid (Figure 4.9) by the eTh/eU grid (Figure 4.18) of the study area. The ratio varies between -107328.4 and 145652.9 %. However, the predominant tectonic trends are E-W and NE-SW directions. Besides, these zones are spatially highly correlated with structures identified in aeromagnetic maps, and are interpreted as conduit for migrating hydrothermal fluids that contemporaneously led to mineralisation zones. Based on the features highlighted in the R-maps (Figures 4.12, 4.13, and 4.15), the extremely high concentration ratio signatures corroborate with high K (%) contents in K distribution map (Figure 4.9) of the study area. Symptomatically, it simply means that K-enrichment zones depict hydrothermal alterations that act as potential zones of mineralisation considered as significant guide for mineral exploration. The high flux of hydrothermally altered zones must have occurred during the interaction of hot aqueous fluids with permeable faulted rocks comprising of quartz vein, granites and migmatite through which they flow, under evolving physiochemical conditions.

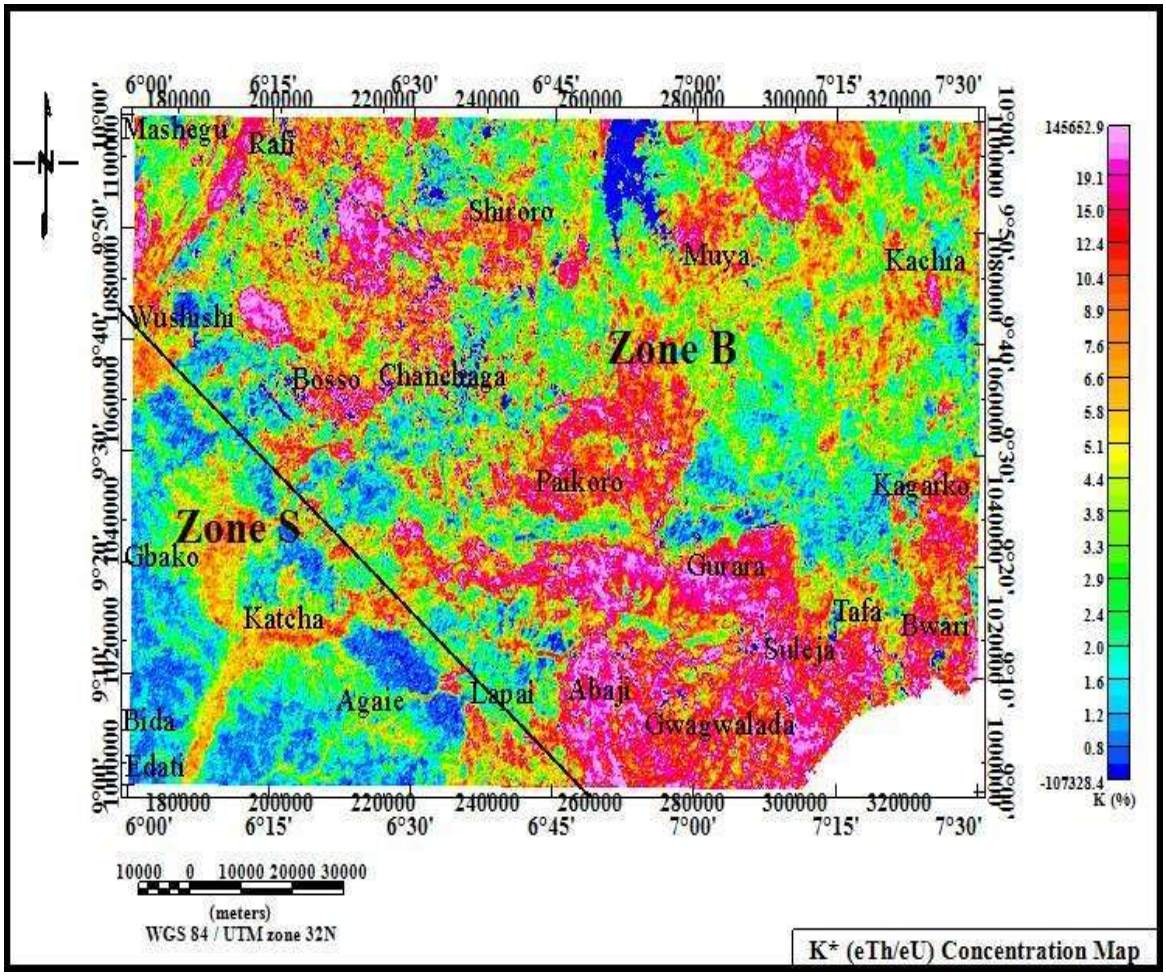

Figure 4.19: Potassium*Equivalent Thorium /Equivalent Uranium (K*eTh/eU) Ratio Map. Colour Bar Indicate Concentration Level in Percentage (%).

As observed on the R-maps (Figures 4.16, 4.17, and 4.19), the hydrothermally altered zones trending towards E-W and NE-SW directions followed almost the same pattern (trend) as the delineated geological structures (lineaments) attained in the derivatives maps. Thus, the E-W and NE-SW trend appears to be the foremost identified trend for both aeromagnetic and gamma-ray spectrometric interpretation. Thus, it is an indication that these trends are very important, and plays an effective role in the geological frame of

the study area. These trends are the most recognised and well-known trend from both derivative and R-maps

Meanwhile, a closer look at the R-maps (Figures 4.16, 4.17, and 4.19) and geology map (Figure 2.1b); it is possible that most rocks in the Basement complex terrain are hydrothermally altered. However, the delineated geological structures figured by tectonic deformation events provide channels through which hydrothermal mineralizing fluids can travel and precipitate minerals.

4.4.5 The ternary map (T-Map)

The T-Map (Figure 4.20) is composed with display of K (%) eTh (ppm) and eU (ppm). Different rock types have dissimilar features of concentration levels of each of the radioelements (K, eTh and eU). Hence, the concentrations analysed from airborne gamma-ray spectrometric data was utilised to recognise zones of consistent hydrothermal alterations and lithological units. The T-Map (Figure 4.20) is a combination of the radioelements grid maps (K (%), eTh (ppm) and eU (ppm) grids) of the study area. The combined composite T-Map (Figure 4.20) of the study area shows the variations occurrence in the concentration of the three radioelements, which mainly reflect lithologic variations (Elkhadragy *et al*., 2016).

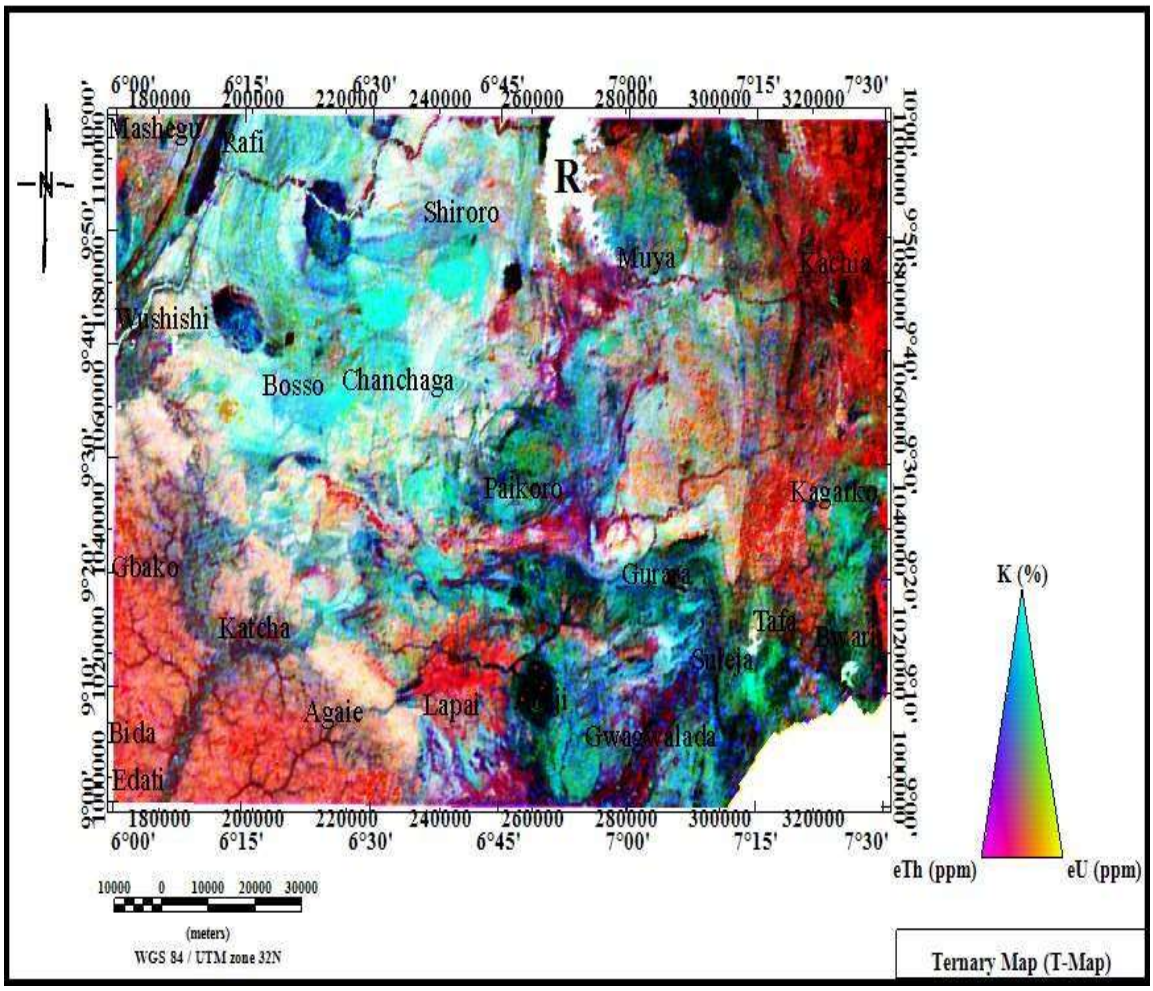

Figure 4.20: Ternary Map (T-Map) of the Study Area.

In other word, the T-Map (Figure 4.20) shows the overall surface distribution by revealing the intensities transpiring in the concentration of the three radioelements, which reflects subtle lithological variations. To some extent, the radiometric responses in the map show a fairly close spatial correlation with the rock units in the geological map (Figure 2.1) of the study area. These responses are an effect of different rock types having different

concentrations of radioelements. The colour index at each angle of the triangular legend as assigned shows K (%) in Cyan, eTh (ppm) in Magenta and eU (ppm) in Yellow indicates total concentration of each of the radioelement. Black regions in the T-Map (Figure 4.20) are attributed to relatively high concentration level of the three radioelement components (K (%), eTh (ppm) and eU (ppm)), can be easily discerned from the weak radioactive rocks (Augustine *et al*., 2022). The apparent Cyan colour in T-Map (Figure 4.20) signifies areas with high concentration level of K (%) but low concentrations level of eTh (ppm) and eU (ppm) contents. the Cyan-coloured zones represent hydrothermal alteration zones characterised by high concentration level of K (%). These features show a close spatial correlation with the areas of relatively high concentration level of K/eTh (%/ppm) and K*eTh/eU (%) ratio signatures (Figures 4.17 and 4.19). These notable areas are associated with different assemblage of stratified rocks that includes Migmatite, Granite gneiss, Biotite granite, Amphibolite schist and Quartz veins when compared with geological map (Figure 2.1) of the study area. In order words, zones that have an effect of hydrothermal alterations have high K (%). Areas coloured with Red signify zones with moderate concentration of eTh (ppm) and eU (ppm), but low K (%) concentration level, while areas coloured with Blue signify zones with moderate concentration levels of eTh (ppm) and K (%) but low eU (ppm) level. In addition, Magenta-coloured zones indicate high concentration of eTh (ppm) with low K (%) and eU (ppm) levels.

The T-Map (Figure 4.20) shows high anomaly of K and Th but low U contents. It is an indication of granitic bodies. Yellow-coloured zones through scanty signify relatively high concentration level of eU (ppm) but low K (%) and eTh (ppm) concentration. The undulating feature labelled “R” reflects a river in the study area. Also, the T-map (Figure 4.20) displays the radiometric signatures connected with identification of hydrothermal alteration zones, lithological units and rocks vital to mineralisation in the area. Amplified K (%) content (Cyan-colour) observed from the T-map map (Figure 4.20) was helpful in

pin-pointing hydrothermal activities within the study area. There is close conformity between the estimated hydrothermally altered zones and specific known locations of mineralisation.

4.4.6 Prospectivity mineral map (PM-Map)

The PM-Map (Figure 4.21) is a direct expression of all the selected numbers, names of criteria and the weights assigned to different thematic maps. The resulting weights of the selected numbers and names of criteria for pair-wise comparisons using Analytic Hierarchy Process is summarised in Table 4.2. Five (5) potential zones of mineralisation were delineated. These are “Very poor”, “Poor”, “Moderate”, “Good” and “Very Good” zones. “Very good” to “good” zones are spatially distributed in almost every part of the study area except in the North-eastern part and to some extent, in the South-western part of the study area. These zones (“Very good” to “good”zones) are deduced as the most favourable zones of probable mineralisation connected with high structural lineaments. Apparently, the areas with high structural complexity (lineament compactness) enhance the movements of the ore minerals during hydrothermal activities (Augustine *et al*., 2022). Structural features and hydrothermally altered areas were delineated in Figure 4.21 as probable.

.

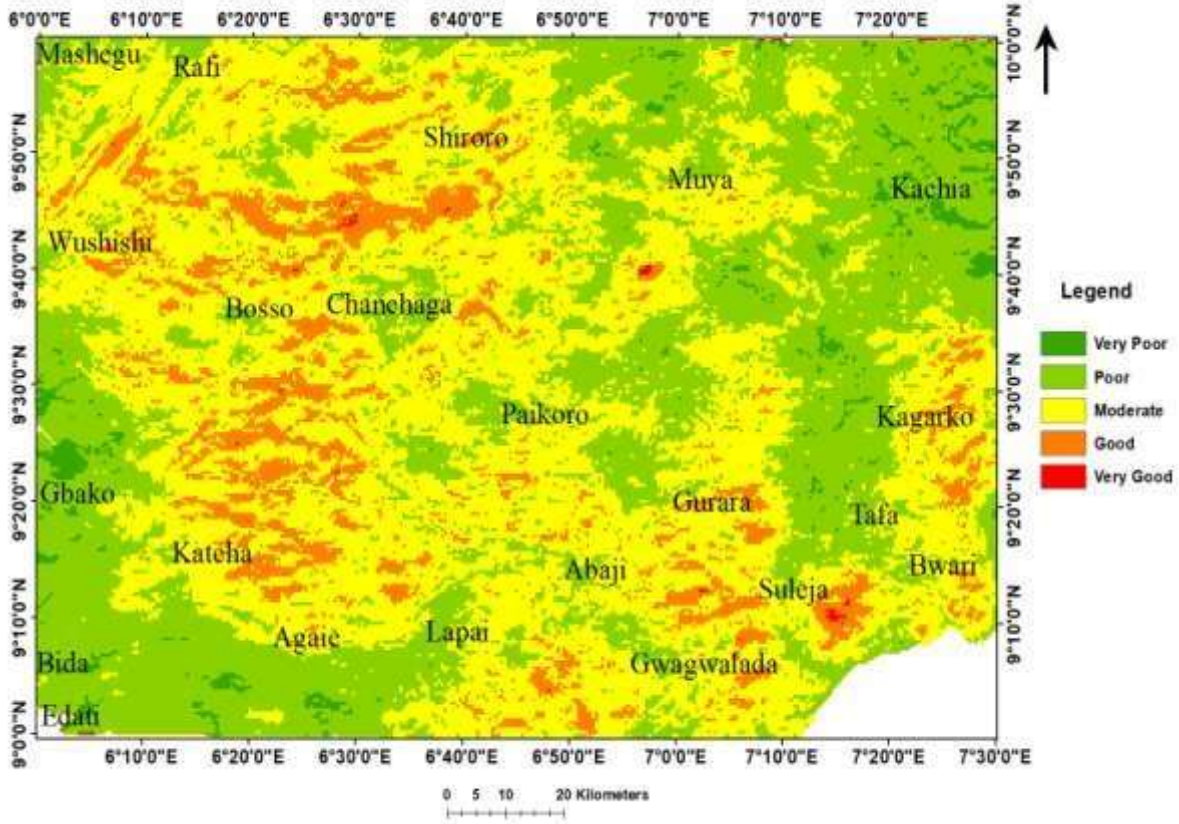

.**Figure 4.21**: Prospectivity Mineral Map (PM-Map) of the Study Area.

Table: 4.3 Pair-wise Comparisons Utilised to Compute Thematic Priorities by the Analytic Hierarchy Process Tool.

	Properties	**Decision Matrix**										
Rank	Criteria	Priority (%)	(+) (%)	(-) (%)		1	2	3	4	5	6	7
1	Geology	40	26.5	26.5	1	1	5.00	4.00	3.00	4.00	5.00	5.00
2	Lineament Density	19.2	8	8	2	0.2	1	1.00	3.00	5.00	5.00	4.00
3	K/eTh	17	4.8	4.8	3	0.25	1.00	1	3.00	4.00	3.00	4.00
4	First Vertical Derivative	7.5	2.8	2.8	4	0.33	0.33	0.33	1	1.00	1.00	3.00
5	Analytic Signal	6.6	2.6	2.6	5	0.25	0.2	0.25	1.00	1	1.00	3.00
6	Tilt Derivative	6	1.3	1.3	6	0.2	0.2	0.33	1.00		1	2.00
7	Source Parameter imaging	3.8	1.8	1.8	7	0.2	0.25	0.25	0.33	0.33	0.5	1
Number of comparisons = 21			Principle eigen value = 7.541									
Consistency Ratio(CR) = 6.7%			Eigenvector solution: 6 iterations, delta = 1.2E-8									

Hence, the coincidence of high structural complexity areas connected with hydrothermal alterations is an indication of high probability of ore deposits. The delineated "Very good" to "good" zones are observed on the Basement Complex terrain which strongly correlated with a range of lithological units made up of different assemblage of stratified rocks that includes Migmatite, Granite gneiss, Biotite granite, Amphibolite schist and Quartz veins in the geological map (Figure 2.1) of the study area. The hydrothermally altered areas connected with these rocks are the most favourable spots for mineralisation. Since, these zones have one or more structural associations, the faulted features serve as channels for migrating hydrothermal fluids that react with rock formation, which were altered afterwards. Thus, these are the potential zones of mineralisation. The output effects correlated with the reports that specific mineralisation in Nigeria is hosted within schist belt with some restricted within quartz veins (Obaje *et al.*, 2011; Garba, 2000).

CHAPTER FIVE

5.0 CONCLUSION AND RECOMMENDATIONS

5.1 Conclusion

The aim of this study was to delineate structural lineaments and hydrothermal alterations linked to mineralisation zones, as well as estimating the depth to source bodies (lineaments) through which mineral deposits are aligned along within the study area. The two airborne geophysical data sets aeromagnetic and aerogamma-ray spectrometric data sets were productively utilised to provide vital information on the structural settings and deduce probable locations of mineralisation within the study area. The aeromagnetic analysis, revealed probable geological structures (lineaments) that are better features to prospect for zones of mineralisation were delineated upon the applications of selected enhancement filtering techniques: FVD, AS, HGM, TD and CET techniques on the produced TMI_RTE map (Figure 4.2) of the study area. Thus, the lineaments extracted depict possible extent of tectonic deformation in the area. These linear features are evidences of near surface geologic structures where numerous ore deposit precipitates are mainly concentrated along or aligned with. These structural features also play vital roles in conveying aqueous minerals in a hydrothermal process. Therefore, it is obvious that the concealed ore deposits in the area are structurally controlled. The orientations of the lineament extracted from the CET map (Figure 4.7a) were displayed in a rosette diagram (Figure 4.7b) to analyse the spatial distribution of the lineaments. Directional analysis utilising the rosette diagram (Figure 4.7b) showed that the area is dominated by East-West (E-W) and East-Northeast and West-Southwest (ENE-NSW) trending structural lineaments. Depth to the geological structures

(lineaments) via which mineral deposits are mainly aligned along or concentrated with were estimated using Euler Deconvolution (ED), Source Parameter Imaging (SPI) and Power Spectral Analysis techniques. All the same, the depth estimated values of the three depth estimators resulted in good agreement. Also application of airborne gammaray

spectrometric data provided a better means for identifying zones of consistent hydrothermal alteration signatures as well as lithological units linked with the rocks vital to mineralisation in the study area. The three (3) radioelements grid maps (Figures 4.12, 4.13 and 4.14) of the study area showed the variations occurring in the three (3) radioelements concentrations, which primarily reflect lithologic variations. Since, different rock types have dissimilar characteristic concentrations of radioelement (K, Th and U), therefore, concentrations considered from aero gamma ray spectrometric data were used to pin-point zones of reliable lithological units. However, an increase in concentration level of K (%) contents noticed in K/eTh (%/ppm) and K*(eTh/eU (%) ratio maps depict hydrothermally altered zones. Characteristically, high anomalous ratio signatures indicate highly fractured zones and accentuate K (%) enrichment haloes connected with hydrothermally altered zones related to mineralisation. In other words, areas affected by the hydrothermal processes have a high concentration level of K (%) content. The composite ternary map (T-Map) displays on one show an overall pattern of the radioelement distribution. This map (Figure 4.20) gives much in term of hydrothermally altered zones based on colour differences. Additionally, it is obvious that the key trends in the radiometric maps are the E-W and NE-SW trends. The outcome effect from lineament analysis, hydrothermal alteration assemblages, geology and depth were integrated to deduce most favourable zones of potential mineralisation. The ArcGIS version 10.8.1 software was used to create composite mineralisation map of the study area. The mineral prospectivity map produced by the modelling allowed the delineation zones of potential mineralisation. Hence, the coincidence of high structural complexity areas and hydrothermally altered zones indicated a high possibility for ore mineralisation. There is close conformity between the delineated mineralisation zones in the study area with the reports that specific mineralisation in Nigeria is hosted within schist belt with some restricted within quartz veins (Obaje *et al*., 2009; Garba, 2000).

5.2 Recommendations

The coincidence of high structural complexity and hydrothermal alteration zones was deduced as potential zones of mineralisation in the study area. The areas are located mostly in the western and the eastern parts of the study area respectively (Figure 4.12). In order to identify and assess the exact location of these probable zones, a detailed geophysical ground survey (ground-truthing) in conjunction with borehole coring and geological survey are recommended to authenticate as well as confirm the tectonic structures that established the potential zones of mineralisation in the study area.

5.3 Contributions to scientific knowledge

The evaluation of the mineral prospectivity map derived from the integration of the two airborne geophysical data shows several anomalous zones that could be the object of future mining prospecting. The depth estimate to the source bodies (lineaments) playing host to mineral deposits is approximately between 0 - 300 m. Potential zones of mineralisation were delineated as “Very poor”, “Poor”, “Moderate”, “Good” and “Very Good” zones. “Very good” to “good” zones are deduced as the most favourable zones of potential mineralisation connected with high structural lineaments. Thus, the information obtained serve as a supportive database for further prospective research and mineral exploration in the region, thereby solving the age-long challenges of data dissemination.

REFERENCES

Abd El Nabi, S. H. (2013). Role of γ-ray spectrometry in detecting potassic alteration associated with Um Ba’anib granitic gneiss and metasediments, G. Meatiq area, Central Eastern Desert, Egypt. *Arabian Journal of Geoscience, 6*, 1249–1261.

Abubakar, Y. I. (2012). An integrated technique in delineating structures: a case study of the Kushaka schist belt Northwestern Nigeria. *International Journal of Applied Science and Technology, 2*(5), 164-173.

Adekoya, J. A., Kehinde, O. O., & Odukoya, A. M. (2003). Geological distribution of mineral resources in Southwestern Nigeria. In: A. A Elueze (Ed), Prospects for

Investment in Mineral Resources of Southwestern. *Nigerian Mining and Geosciences Society (NMGS)*,15-56. Retrieved from https://staff.oouagoiwoye.edu.ng/uploads/453_COURSES_Compositional_features_of_Precambrian_pegmatites_of_Ago

Adepelumi, A. A., & Falade, H. A. (2017). Combined high-resolution aeromagnetic and radiometric mapping of uranium mineralization and tectonic settings in Northeastern Nigeria *Acta Geophysica, 65*, 1043-1068. doi: 10.1007/s11600017-0080-3

Adewumi, T. & Salako, K. A. (2017). Delineation of mineral potential zone using high resolution aeromagnetic data over part of Nasarawa State, North Central, Nigeria. *Egyptian Journal of Petroleum*, 5(2), 276- 298 doi: 10.1016/j.ejpe.2017.11.002

Ahmed, S. B. (2018). Integration of airborne geophysical and satellite imagery data to delineate the radioactive zones at west Safaga Area, Eastern Desert, Egypt. *NRIAG Journal of Astronaut Geophysics*, *7*(2), 297–308.

Airo, M. L. (2002). Aeromagnetic and aeroradiometric response to hydrothermal alteration. *Surveys in Geophysics, 23*, 273-302. Retrieved from: http://dx.doi.org/10.1023/A:1015556614694

Airo, M. L. (2007). Application of aeromagnetic data for gold exploration: Implications for the central lapland greenstone belt. *Geological Survey of Finland, 44*, 187208.

Airo, M. L. (2015). Geophysical signatures of mineral deposit types in Finland. *Geological Survey of Finland, 58*, 1-144

Akinniyi, A., Chau, N. D., Anna, W., & Sylwia, T. (2020). Characterization of lithological zones of the Isanlu sheet 225, North Central Nigeria, using aerogeophysical datasets. *Acta Geophysica, 68*, 651–665. Retrieved from https://doi.org/10.1007/s11600-020-00411-6.

Al-Badani, M. A., & Al-Wathaf, Y. M (2018). Using the aeromagnetic data for mapping the basement depth and contact locations, at southern part of Tihamah region, Western Yemen, Egypt. *Egypt Journal of Petroleum*. Retrieved from: https://doi.org/10.1016/j.ejpe.2017.07.015

Al-Banna, A. S., & Daham, A. N. (2019). Application of Source Parameter Imaging (SPI) Technique to Gravity and Magnetic Data to Estimate the Basement Depth in Diyala Area, Eastern, Central Iraq. *Iraqi Journal of Science, 60*(3), 601-609. doi: 10.24996/ijs.2019.60.3.18

Aliyu, S. B., Adetona, A. A., Rafiu, A. A., Ejepu, J. S., & Adewumi, T. (2021). Delineating and Interpreting the Gold Veins Within Bida and Zungeru Area, Niger State Nigeria, Using Aeromagnetic and Radiometric Data *Pakistan Journal of Geology (PJG), 5*(2). doi: 10.2478/pjg-2021-0006

Al-Kadasi, A. N. (2014). Interpretation of aeromagnetic data in terms of surface and subsurface geologic structures, southwestern Yemen. *Arabian Journal of Geosciences, 8*, 1163–1179. doi: 10.1007/s12517-013-1238-1

Almasi, A., Yousefi, M., & Carranza, E. M (2017). Prospectivity analysis of orogenic gold deposits in Saqez-Sardasht Goldfield, Zagros Orogen, Iran. . *Ore Geology Reviews. 91*, 1-1162. doi:https://doi.org/10.1016/j.oregeorev.2017.11.001

Andrew, J., Alkali, A. Salako, K. A,.& Udensi, E. E (2018). Delineating Mineralisation Zones within the Keffi-Abuja Area Using Aeromagnetic Data *Journal of Geography, Environment and Earth Science International, 15(3),* 1-12. doi: 10.9734/JGEESI/2018/37052

Andrson, H., & Nash, C. (1997). Integrated lithostructural mapping of the rossing area, Namibia, using high-resolution aeromagnetic, aeroradiometric, landsat data and aerial photographs. *Exploration Geophysics, 28,* 185-191. Retrieved from *http://*doi.org/10.1071/EG997185

Anudu, G. K., Stephenson, R. A., & Macdonald, D. M. (2014). Using high resolution aeromagnetic data to recognise and map intra-sedimentary volcanic rocks and geological structures across the Cretaceous middle Benue Trough, Nigeria. *Elsevier Journal African Earth Sciences, 99,* 625-636.

Ardestani, V. E., & Motavalli, H (2007). Constraints of analytic signal to determine the depth of gravity anomalies. *Journal of Earth Space Physics, 33,* 77–83.

Arisoy, M. O., & Dikmen, U. (2013). Edge detection of magnetic sources using enhanced total horizontal derivative of the tilt angle. . *Bulletin of the Earth Sciences Application and Research Centre of Hacettepe University, 34*(1), 73– 82.

Augustine, B. A., Awoyemi, M. O., Ajama, O. D., Falade, S, C., Hammed, O, S., Dasho, O. A., & Adenika, C. A. (2022). Integrated Aeromagnetic and Airborne Radiometric Data for Mapping Potential Areas of Mineralisation Deposits in Parts of Zamfara, North West Nigeria. *Pure and Applied Geophysics*. *13,* 72–83 doi: 10.1007/s00024-021-02913-w

Austin, J. R., & Blenkinsop, T. G. (2008). The Cloncurry Lineament: Geophysical and geological evidence for a deep crustal structure in the Eastern Succession of the Mount Isa Inlier. *Precambrian Res, 163*(1-2), 50-68. doi: 10.1016/j.precamres.2007.08.012

Awoyemi, M. O., Hammed, S., & Falade, M. Y (2017) Geophysical investigation of the possible extension of Ifewara fault zone beyond Ilesa area, southwestern Nigeria. Arabian Journal of Geosciences 10(2):27. Retrieved from: https://doi.org/10. 1007/s12517-016-2813-z

Balogun, O. B. (2019). Tectonic and structural analysis of the Migmatite-Gneiss, Quartzite complex of Ilorin area from aeromagnetic data. *NRIAG Journal of Astronaut Geophysics, 8*(1), 22–33.

Bierlein, F. P., Groves, D. I., Goldfarb, R. .J., & Dube, B. (2006). Lithospheric controls on the formation of provinces hosting giant orogenic gold deposits. *Miner Deposita, 41,* 107–126.

Boadi, B., Wemegah, D. D., & Preko, K. (2013). Geological and structural interpretation of the Konongo area of the Ashanti gold belt of Ghana from aeromagnetic and radiometric data. *International Research Journal of Geology and Mining (IRJGM), 3*(3), 124–135. Retrieved from: http://www.interesjournals.org/IRJGM

Burke, K., & Dewey, J. F (1972). Orogeny in Africa. In T. F. J. Dessauvagie, A. J. Whiteman (Eds.), *African geology. Ibadan University Press, Ibadan*, 583-608.

Charbonneau, B. W. H., Holman, & P. B., Hetu, R. J. (1997). Airborne gamma spectrometer-magnetic-VLF survey of northeastern Alberta Exploring for minerals in Alberta: Geological Survey of Canada geosciences contributions, Canada-Alberta Agreement on Mineral Development (1992-1995); by R. W Macqueen (Eds.), *Geological Survey of Canada*, 500, 107-1131. doi:org/10.4095/209209

Chernicoff, C. J., Richards, J. P., & Zappettini, E. O. (2002). Crustal lineament control on magmatism and mineralization in northwestern Argentina: Geological, geophysical, and remote sensing evidence. *Ore Geology Review, 21*(3-4), 127–155. doi: 10.1016/S0169-1368(02)00087-2.

Chinwuko, A., Onwuemesi, A., Anakwuba, E., Onuba, L. & Nwokeabia, N. (2012). Interpretation of Aeromagnetic anomalies over parts of upper Benue Trough and Southern Chad Basin, Nigeria. *Advances in Applied Science Research, 3(3),* 1757 -1766.

Cordell, L., & Grauch, V. J. S., (1985). Mapping basement magnetization zones from aeromagnetic data in the San Juan Basin, In W. J. Hinze (Eds.), The Utility of Regional Gravity and Magnetic Anomaly Maps (Exploration Geophysics). (pp. 181-197). New Mexico.

Core, D., Buckingham, A., & Belfield, S. (2009). Detailed structural analysis of magnetic data-done quickly and objectively, SGEG Newsletter.

Cunha, L. O., Dutra, A. C., & Costa, A. B (2017). Use of radiogenic heat for demarcation of hydrothermal alteration zones in the Pernambuco-Brazil *Journal Applied Geophysics, 145*, 111-123.

Cyril, C. O. (2019a). Delineation of high-resolution aeromagnetic survey of lower benue trough for lineaments and mineralization: Case Study Of Abakikili Sheet 303. *Malaysian Journal of Geosciences, 3(1),* 51-60. doi: 10.26480/mjg.01.2019.51.60

Cyril, C. O. (2019b). High resolution magnetic field signatures over Akure and its environs, Southwestern, Nigeria. *Earth Sciences Malaysia, 3(1),* 09 17, doi:10.2 6480/esmy.01.2019.09.17

Dada, S. S. (2006). Proterozoic Evolution of Nigeria. In: O. Oshi (Ed.), The Basement Complex of Nigeria and its Mineral Resources (A Tribute to Prof. M. A. O. Rahaman). Akin Jinad & Co. Ibadan. 29-44.

Darnley, A. G. (1975). Geophysics in uranium exploration. Geological Survey of Canada, Uranium Exploration. *Ottawa*, 21–31.

Darnley, A. G., Ford, K. L., & Garland, G. D (1989). Regional airborne gamma-ray surveys: a review. In: Proceedings of Exploration 87, Third Decennial International Conference on Geophysical and Geochemical Exploration for Minerals and Groundwater. *Geological Survey of Canada,* 3, 960. Retrieved fro m https://www.books.google.com.ng/books?id=NW68DgAAQBAJ&pg

Dentith, M. (2011). Magnetic methods, airborne. In H. S. Gupta (Eds), *Encyclopedia of Solid Earth Geophysics*, (761-766). Springer, Dordrecht.

Dentith, M., & Mudge, S. T. (2014). Geophysics for the mineral exploration geoscientist. Cambridge Univesity Press. *Cambridge*. ISBN 978-0-521-80951-1

Dobrin, M. B., Savit, C. H (1988). Introduction to geophysical prospecting, 4th Edition. McGraw-Hill Books, New York, . 633-725.

Efimov, A. V. (1978). Multiplikativiniyj pokazatel dlja vydelenija endogennych rud aerogamma-spectrometriceskim dannym in Metody rudnoj geofiziki. Lenigrad. *Naucnoproizvodstvennoje objedinenie Geofizica Ed*, 59–68.

Ejepu, J. S., Unuevho, C. I., Ako, T. A. & Abdullahi S. (2018). Integrated geosciences prospecting for gold mineralization in Kwakuti, North-Central Nigeria. *Journal of Geology and Mining Research*, 10(7), 81-94, doi: 10.5897/JGMR2018.0296

Eldosouky, A. M., Abdelkareem, M., & Elkhateeb, S. O. (2017). Integration of remote sensing and aeromagnetic data for mapping structural features and hydrothermal alteration zones in Wadi Allaqi area, South Eastern Desert of Egypt. *Journal of African Earth Sciences .Elsevier*, *130*, 28–37. doi: 10.1016/ j.jafrearsci.2017.03.006.

Elkhadragy, A. A., Ismail, A. A., Eltarras, M. M., & Azzazy, A. A. (2016). Utilization of airborne gamma ray spectrometric data for radioactive mineral exploration of G.Abu Had – G.Umm Qaraf area, South Eastern Desert, Egypt. *NRIAG Journal of Astronomy and Geophysics*. Retrieved from: http://dx.doi.org/10.1016/j.nrjag. 2016.12.001

Elkhateeb, S. O., & Abdellatif, M. A. G (2018). Delineation potential gold mineralization zones in a part of Central Eastern Desert, Egypt using Airborne Magnetic and Radiometric data. *NRIAG Journal of Astronaut Geophysics, 7*(2), 361–376.

El-Sadek, M. A. (2009). Radiospectrometric and magnetic signatures of a gold mine in Egypt. *Journal of Applied Geophysics*, *67* (1), 34-43. Retrieved from: https ://doi.org/10.1016/j.jappg eo.2008.08.012

Emmanuel, A. I., John, A. Y., & Immaculate, U. I (2018). Investigation of Mambila Plateau In North Central Part of Nigeria For Potential Minerals Using Aeromagnetic Method *Journal of Applied Geology and Geophysics (IOSRJAGG), 6*, 10-22 doi: 10.9790/0990-0602011022

Eslam, E., Ahmed, A., & Abuelhoda, E (2004). Mapping surface geology using airborne gamma-ray spectrometric survey data - A case study. *Research Gate Conference Paper*. Retrieved from https://www.researchgate.net/publication/259 822736

Eze, M. O., Mamah, L. I., Madu, A. J. C., & Leonard, O (2017). Geological and structural interpretation of possible mineralization zones of part of Anambra

basin and Southern Benue Trough using airborne geophysical data *International Journal of Research in Engineering and Applied Sciences (IJREAS), 7*, 70-80.

Falade, H. A., & Adepelumi, A. A (2017). Combined high-resolution aeromagnetic and radiometric mapping of uranium mineralization and tectonic settings in Northeastern Nigeria. *Acta Geophysica, 65*, 1043-1068. doi 10.1007/s11600017-0080-3

Fall, M., Baratoux, D., Ndiaye, P. M., Jessell, M., & Baratoux, L. (2018). Multi-scale distribution of Potassium. Thorium and Uranium in Paleoproterozoic granites from eastern Senegal. *Journal of African Earth Sciences, 148*, 30–51.

Ferreira, F. F., de Castro, L. G., Bongiolo, A. S., de Souza, J., & Romeiro, M. T (2011). Enhancement of the total horizontal gradient of magnetic anomalies using tilt derivatives: part II—application to real data. *SEG Technical Program Expanded Abstracts*, 887–891. Retrieved from: https://doi.org/10.1190/1.3628216

Ferreira, F. J. F., de Souza, J., Bongiolo, A. B. S., & de Castro, L. G (2013). Enhancement of the total horizontal gradient of magnetic anomalies using the tilt angle. *Geophysics, 78*, J33–J41.

Gaafar, I. (2015). Integration of geophysical and geological data for delimitation of mineralised zones in Um Naggat area, Central Eastern Desert, Egypt. *NRIAG Journal of Astronuat Geophysics, 4*(1), 86-99.

Gaboury, D. (2019). Parameters for the formation of orogenic gold deposits. *Applied Earth Science, 128*(3), 1-10. doi: 10.1080/25726838.2019.1583310

Garba, I. (2000). Origin of Pan-African mesothermal gold mineralization at Bin-Yauri, Nigeria. *Journal of African Earth Sciences, 31*(2), 433-449. Retrieved from: https://doi.org/10.1016/S0899-5362(00)00098-1

Goepel, K. D. (2018). Implementation of an Online Software Tool for the Analytic Hierarchy Process (AHP-OS). *International Journal of the Analytic Hierarchy Process,10*, 20469 2048.Retrieved from:https://doi.org/10.13033/ijahp.v10i3.5900

Graham, D. F. (1993). Airborne radiometric data a tool for reconnaissance geological mapping using a GIS. *Photogrammetric Engineering and Remote Sensing,* 59(8), 1243-1249. Retrieved from https://www.inis.iaea.org/search/search.aspx?orig_q=RN:25036190

Graham, K. M., Preko, K., Wemegah, D. D. & Boamah, D. (2013). Geological and structural interpretation of part of the Buem Formation, Ghana, Using Aerogeophysical Data. *Journal of Environment and Earth Science, 4*, 17-31.

Hahn A, K., Kind, E. G, & Mishra, D. C (1976). Depth estimation of magnetic sources by means of Fourier amplitude spectra. *Geophysics Prospecting, 24*, 287-308.

Herbert, S., Woldai, T., Carranza, E. M., & Van-Ruitenbeek, F. A. (2014). Predictive mapping of prospectivity for orogenic gold in Uganda. *Journal of African Earth Sciences, 99*, 666–693.

Hinze, W. J., Von Frese, R. R. B., & Saad, A. H. (2013). Gravity and Magnetic Exploration: Principles, Practices, and Applications. . *Cambridge University Press, New York.*, 515. Retrieved from https://doi.org/10.1017/CBO9780511843129

Holden, E. J., Dentith, M., & Kovesi, P. (2008). Towards the automatic analysis of regional aeromagnetic data to identify regions prospective for gold deposits. *Computer Geoscience, 34*, 1505-1513.

Holden, E. J., Fu, S. C., Kovesi, P., Dentith, M., Bourne, B., & Hope, M. . (2011). Automatic identification of responses from porphyry intrusive systems within magnetic data using image analysis. *Journal of Applied Geophysics, 74*, 255– 262.

Ibraheem, I. M., Gurk, M., Tougiannidis, N., & Tezkan, B (2018). Subsurface investigation of the Neogene Mygdonian Basin, Greece using magnetic data. *Pure Applied Geophysics, 175*, 2955–2973.

Ibraheem, I. M., Haggag, M, & Tezkan, B. (2019). Edge detectors as structural imaging tools using aeromagnetic data: A case study of Sohag Area, Egypt. Geosciences Multidisciplinary Digital Publishing Institute 9(5), 211. Retrieved from: https://doi.org/10.3390/geosciences9050211

Izquierdo, G., Arellano, V. M., Aragón, A., Portugal, E. & Martínez, I. (2000). Fluid acidity and hydrothermal alteration at the Los Humeros geothermal reservoir, Puebla, Mexico. *In Proceedings of the World Geothermal Congress 2000*, 1301-1306. Retrieved from: https://www.geothermal energy.org/pdf/IGAstandard/WGC/2000/R0151.PDF

Jaques, A. L., Wellman, P., Whitaker, A., & Wyborn, D. (1997). High-resolution geophysics in modern geological mapping. *AGSO Journal of Australian Geology and Geophysics,* 17(2), 159-173. Retrieved from: https://www.inis.iaea. org/search/search.aspx?orig_q=RN:28049085

Jean, A. M., Theophile, N. M., Marcelin, B. B., Jean, D. N., & Olivier, U. O. . (2018). Inferring the Subsurface Basement Depth and the Contact Locations from Aeromagnetic Data over Loum-Minta Area (Centre-East Cameroon) *International Journal of Geosciences, 9*, 435-459 doi: http://www.scirp.org/journal/ijg

John, O. A., Sherif, O. S., & Lateef, A. (2022). Geophysical characterisation of rare earth element and gemstone mineralisation in the Ijero-Aramoko pegmatite field, southwestern Nigeria. *Journal of African Earth Sciences, 188*, 104-494. Retrieved from: https://doi.org/10.1016/j.jafrearsci.2022.104494

Joshua, C., Tiyamike, H.,& Gift, T. (2021). Geologic structures associated with gold mineralization in the Kirk Range area in Southern Malawi. *Research Article, 13*, 1345-1357. doi: https://doi.org/10.1515/geo-2020-0304

Jude, S. E., Muftau, O. J., Suleiman, A. & Marrietta, A. M. (2022). Groundwater Exploration Using Multi Criteria Decision Analysis and Analytic Hierarchy Process in Federal Capital Territory, Abuja, Central Nigeria. *International Journal of Geosciences, 13*, 33-53. Retrieved from: https://www.scirp.org/journal/ijg

Kaufmann, H. (1988). Concepts, processing and results. *International Journal of Remote Sensing, 9 (10-11),* , 1639-1658.

Kearey, P., Brooks, M., & Hill, I. (2013). An introduction to geophysical exploration. John Wiley & Sons

Kogbe, C. A. (1989). Review of the basement geology of southwestern Nigeria. *In: Geology of Nigeria.Elizabethan publishing Company Lagos*, 41-58 (originally written by Rahman, M. A., 1976).

Li, X. (2006). Understanding 3D Analytic Signal Amplitude. *Geophysics, 71*, 13-16. Retrieved from: https://doi.org/10.1190/1.2184367

Lo, B. H., & Pitcher, D. H. (1996). A case history on the use of regional aeromagnetic and radiometric data sets for lode gold exploration in Ghana. Annual Meeting Expanded Abstracts. *Society of Exploration Geophysicists*, 592-595.

Luo, Y., Wang, M., Luo, F. & Tian, S. (2011). Direct Analytic Signal Interpretation Of Potential Field Data Using 2-D Hilbert Transform. Chinese Journal of Geophysics *54*, *4*, 551 – 559

Machiwal, D., Jha, M. K. & Mal, B.C. (2011). Assessment of Groundwater Potential in a Semi-Arid Region of India Using Remote Sensing, GIS and MCDM Techniques. *Water Resources Management*, *25*, 1359-1386. Retrieved from: https://doi.org/10.1007/s11269-010-9749-y

Manu, J. (1993). Gold deposits of Birimian greenstone belts in Ghana: hydrothermal alteration and thermodynamics. Verlag Mainz, Wissenchaftsverlag, Aachen Herstellung:. *Fotodruck Mainz GmbH Susterfeldstr*, *83*, 52-72

Marson, L., & Klingele, E. (1993). Advantages of using the vertical gradient of gravity for 3-D interpretation. *Geophysics*, *58*, 1588-1595.

Miller, H. G., & Singh, V. (1994). Potential field tilt – a new concept for location of potential field sources:. *Journal of Applied Geophysics*, *32*, 213–217. doi: https://doi.org/10.1016/0926-9851(94)90022-1

Minty, B. R. S., Luyendyk, A. P. G., & Brodie, R. C. (1997). Calibration and data processing for airborne geophysical data. *ASGO Journal of Australian Geology & Geophysics*, *17*(2), 51–62.

Muhammed, E., Baher, M. G., Nehal, A. R., & Sara, Z. (2017). Hydrothermal Zones Detection Using Airborne Magnetic and Gamma Ray Spectrometric Data of Mafic/Ultramafic Rocks at Gabal El-Rubshi Area, Central Eastern Desert (CED), Egypt *Advances in Natural and Applied Sciences, 11(9)*, 182-196 doi: http://www.aensiweb.com/ANAS

Mono, J. A., Ndougsa-Mbarga, T., Bi-Alou, M.B., Ngoh, J.D. & Owono, O.U. (2018). Inferring the Subsurface Basement Depth and the Contact Locations from Aeromagnetic Data over Loum-Minta Area (Centre-East Cameroon). . *International Journal of Geosciences*, *9*, 435-459. Retrieved from: https://doi.org/10.4236ijg.2018.97028

Nabighian, M. N. (1972). The Analytic Signal of Two-Dimensional Magnetic Bodies with Polygonal Cross-Section: Its Properties and Use for Automated Anomaly Interpretation. *Geophysics, 37*, 507-517. doi: https://doi.org/10.1190/1.1440276

Nafiz, M., & Enver, A. (2015). Gamma ray spectrometry for recognition of hydrothermal alteration zones related to a low sulfidation epithermal gold mineralization (eastern Pontides, NE Türkiye) *Journal of Applied Geophysics*, *122*, 74-85. doi: http://dx.dio.org/10.1016/j.jappgeo.2015.09.003.

Nigerian Geological Survey Agency (NGSA) (2009). Geological map of Nigeria, Map prepared by Nigerian Geological Survey Agency. 31, Shetima Mangono Crescent Utako District, Garki, Abuja.

Nigerian Meteorological Agency (NiMet). (2021) Seasonal Climate Prediction.

Nwokeabia, N., Uche, I., & Ibe, S, O. (2018). Evaluating the Economic Potential of Part of Ife-Ilesha Schist Belt, Western Nigeria, Using Airborne Magnetic and Radiometric Dataset. *IOSR Journal of Applied Geology and Geophysics*, *6*(4), 54-75. doi: www.iosrjournals.org

Nwosu, O. B. (2014). Determination of magnetic basement depth over parts of middle Benue Trough by Source Parameter Imaging (SPI) technique using HRAM. *International Journal of Scientific and Technology Research*, *3*(1), 262–271.

Nyandigisi, J. & Katana, C. (2016). High Temperature Hydrothermal Alteration In Active Geothermal Systems A Case Study Of Olkaria Domes. Proceedings, 6th African Rift Geothermal Conference Addis Ababa, Ethiopia, 2nd–4th November 2016. Retrieved from http://www.theargeo.org/fullpaper/hightemperaturehydrothermalalteration inactive geothermal systems a case study of olkaria domes.pdf

O'leary, D. W., Freidman, J. D., & Pohn, H. A. (1976). Lineament, linear, lineation: Some proposed new definitions for old terms, . *Geology Society Am. Bulletin, 87,* 1463-1469.

Oasis Montaj™ Tutorial (2004). Two-Dimensional frequency domain processing of potential field data.

Obaje, N. G. (2009a). Geology and Mineral Resources of Nigeria (Lecture Notes in Earth Sciences). *Nasarawa State University Department of Geology & Mining Keffi Nigeria: Springe Berlin*. (120). ISBN 978-3-540-92685-6

Obaje, N. G. (2009b). Geology and Mineral Resources of Nigeria. Springer Verlag, Heidelberg (Germany), 240.

Obaje, N. G., Musa, M. K., A. N. Odoma, A. N., & Hamza, H. (2011). The Bida Basin in north-central Nigeria: sedimentology and petroleum geology. *Journal of Petroleumand Gas Exploration Research, 1(1)* 001-013. Retrieved from https://scholar.google.com/citations?user=gDl2bMgAAAAJ&hl=en#d=gs_md_cita_d&u=%2Fcitations%3Fview_op%3Dview_citation%26hl%3Den%26user%3DgDl2bMgAAAAJ%26citation_for_view%3DgDl2bMgAAAAJ%3AHoB7MX3m0LUC%26tzom%3D-60.

Obaje, N. G., Gokib, N. G., Umarc, U. M., Awedad, A. K., Ozojie, T. M., & Nandomf, A (2019). Mapping and Characterization of Some Industrial Mineral Deposits in North-Central Nigeria as Raw Materials for Industrialization *International Journal of Sciences: Basic and Applied Research (IJSBAR), 48(1)* 160-182. Retrieved from https://www.researchgate.net/publication/335402458

Ogungbemi, O. S., Amigun, J. O., & Olayanju, G. M. (2018). Geophysical Characterization of Mineralization Potential of Eastern Parts of Ife-Ijesha SchistBelt, Southwestern Nigeria. *International Journal of Scientific & Technology Research, 7(3)* doi: www.ijstr.org

Ogungbemi, O. S., Ogunyemi, A. T., & Obaniwa, M. M. (2019). Geophysical Interpretation of Geological Features Constraining Bitumen Deposit In Agbabu, Southwestern Nigeria. *Journal of Applied Geology and Geophysics (IOSRJAGG), 7*, 36-44. doi: 10.9790/0990-0704013644

Ohioma, J. O., Ezomo, F. O., & Akinsunmade, A. (2017). Delineation of Hydrothermally Altered Zones that Favour Gold Mineralization in Isanlu Area,

Nigeria Using Aeroradiometric Data. *International Annals of Science*, *2*(1), 20-27. doi: https://doi.org/10.21467/ias.2.1.20-27

Ohioma, O. J. (2020). Detection of Sulphide Deposit Using Uranium/Potassium Ratio Map *Ghana Journal of Geography, 12*(1), 145-158. Retrieved from: https://doi.org/10.4314/gjg.v12i1.8

Olasehinde, P. I., Pal, P. C. & Annor, A. E. . (1990). Aeromagnetic anomalies and structural Lineaments in the Nigerian Basement Complex. Journal of African Earth Sciences. *1(4), ,* 351-355.

Olasunkanmi, N. K., Sunmonu, L. A., Adabanija, M. A., & Oladejo, P. O (2018). Interpretation of high resolution aeromagnetic data for mineral prospect in Igbeti-Moro area, Southwestern Nigeria 2nd International Conference on Science and Sustainable Development *Earth and Environmental Science*. doi: doi :10.1088/1755-1315/173/1/012033

Olomo, K. O., Olayanju, G. M., Adiat K. A. N., & Akinlalu, A. A (2018). Integrated Approach Involving Aeromagnetic and Landsat for delineating structures and its Implication on Mineralisation *International Journal of Scientific & Technology Research, 7*(2). doi: www.ijstr.org

Oluyide, P. O. (1988). Structural trends in the Nigerian Basement Complex. In: Precambrian Geology of Nigeria. Geological Survey of Nigeria. 93 - 98.

Omar, E. S., & Mahmoud, A. G. A. (2018). Delineation potential gold mineralization zones in a part of Central Eastern Desert, Egypt using Airborne Magnetic and Radiometric data. NRIAG *Journal of Astronomy and Geophysics*. Retrieved from https://doi.org/10.1016/j.nrjag.2018.05.010

Ombiro, S. O., Olatunji, A. S., Mathu, E. M., & Ajayi, T. R (2021). Integration of Geophysics and Remote Sensing Techniques in Mapping Zones Mineralised with Disseminated Gold and Sulphide Minerals in Lolgorien, Narok County, Kenya *Tanzania Journal of Science, 47*(2), 754-768. doi: https://dx.doi.org/10.4314/tjs.v47i2.31

Omkarprasad. S. V., & Sushil, K. (2006). Analytic hierarchy process: An overview of applications. *European Journal of Operational Research, 169*, 1–29.

Oruç, B. (2011). Edge detection and depth estimation using a tilt angle map from gravity gradient data of the Kozaklı-Central Anatolia region, Turkey. *Pure Applied Geophysics, 168*, 1769-1780.

Ostrovskiy, E. A. (1975). Antagonism of Radioactive Elements in Well Rock Alteration Fields and Its Use in Aerogamma Spectrometric Prospecting. *International Geological Review, 17*, 461-468. Retrieved from http://dx.doi.org/10.1080/00206817509471687.2018.08.030

Oyawoye, M. O. (1972). The Basement complex of Nigeria. In: T. F. J. Dessauvagie, & A. J. Whiteman (Eds.), African Geology *University of Ibadan Press, Ibadan*, 6799. Retrieved from https://www.scirp.org/(S(czeh2tfqyw2orz553k1w0r45))/reference/ReferencesPapers.aspx?ReferenceID=1160510 1998.05.010

Oyeniyi, T. O., Salami, A. A., & Ojo, S. B (2016). Magnetic surveying as an aid to geological mapping: A case study from Obafemi Awolowo University campus in Ile-Ife, southwest Nigeria. *Ife Journal of Sciences, 18*(2), 331–343.

Phillips, J. D. (1998). Processing and interpretation of aeromagnetic data for the Santa Cruz Basin - Patahonia Mountains Area, South Central Arizona. *U.S. Geological Survey Open-File Report, Arizona*, 02-98.

Phillips, J. D. (2000). Locating magnetic contacts: a comparison of the horizontal gradient, analytic signal, and local wavenumber methods. In: SEG technical program expanded abstracts 2000. 402-405.

Pirajno, F. (1992). Hydrothermal mineral deposits, Principles and fundamental concepts for the exploration geologists. *Springer, Berlin*.

Quentin, M. A. F., , Anatole, E. D. L., Joseph, P. J. P., & Mary, I. N. F (2019). Mapping Hydrothermal Alteration Targets from Landsat 8 OLI/TIRS and Magnetic Data Using Digital Image Processing Techniques in Garoua, North Cameroon *Journal of Geosciences and Geomatics, 7(1),* 28-41. doi: 10.12691/jgg-7-1-4 http://pubs.sciepub.com/jgg/7/1/4

Rahaman, A. M. (1988). Recent Advances in the Study of the Basement Complex of Nigeria. In: Geological Survey of Nigeria (Ed.), Precambrian Geology of Nigeria, 11-43.

Rajesh, H. M. (2004). Application of remote sensing nd GIS in mineral resource mapping-An overview. *Journal of Mineralogical and Petrological Sciences, 99*, 83-103.

Rani, K., Guha, A,. Mondal, S,. Pal, S. K, Vinod,. Kumar, K (2018). ASTER multispectral bands, ground magnetic data, ground spectroscopy and spacebased EIGEN6C4 gravity data model for identifying potential zones for gold sulphide mineralization in Bhukia, Rajasthan, India. . *Journal of Applied Geophysics., 160*, 28-46. doi: 10.1016/j.jappgeo.2018.10.001.

Ravat., D (1996). Analysis of the Euler method and its applicability in environmental magnetic investigations. *Journal Environmental Engineering Geophysics, 1*, 229–238.

Reeves, C. V., Macnab, R., & Maschenkov, V. U. (1998). Compiling all the world's magnetic anomalies. *American Geophysical Union, 338*.

Reid, A. B., Allsop, J. M., Granser, H., Millett, A. J. & Somerton, I. W (1990). Magnetic Interpretation in Three Dimensions Using Euler Deconvolution. *Geophyscis, 55*, 80-90. Retrieved from: https://doi.org/10.1190/1.1442774
Retrieved from: https://www.nimet.gov.ng/seasonal-climate-prediction/ 2017.02.101

Ribeiro, V. B., & Mantovani, M. S. M. (2016). Gamma spectrometric and magnetic interpretation of Cabaçal copper deposit in Mato Grosso (Brazil): Implications for hydrothermal fluids remobilization. *Journal of Applied Geophysics, 135*, 223-231. doi: 10.1016/j.jappgeo.2016.10.016.

Roest, W. R., & Pilkington, M (1993). Identifying remanent magnetization effects in magnetic data. Geophysics *58*, 653–659. doi: https :// doi.org/10.1190/1.14434 49

Roest, W. R., & Verhoef, J. & Pilkington, M (1992). Magnetic interpretation using the 3-D analytic signal *Geophysics, 57*, 116-125.

Saaty, T. L. (2006). Fundamentals of Decision Making and Priority Theory with the Analytic Hierarchy Process. *RWS Publications, Pennsylvania*.

Saaty, R. W. (1987). The Analytic Hierarchy Process—What It Is and How It Is Used. Mathematical Modelling. *9*, 161-176. Retrieved from: https://doi.org/10.1016/0270-0255(87)90473-8

Sadiya, T. B., Abdulrahman, A., Sadiq, A. A., Vaatyough, H. M., Ibrahim, A. T., Muhammed, S. O., Ihenacho, N. M., Yusuf, M. J., Aliyu, I., & Agu, N. V. (2016). Lineaments Extraction from Remote Sensing Data for Detection of Hydrothermal Alteration zones in Northern Nigeria. . *Journal of Environmental Science, Toxicology and Food Technology (IOSR-JRESTFT), 10* (4), 17-22. doi: 10.9790/2402-1004031722

Salem A., Willians. S., Fairhead, J. D., Smith R. & Ravat D. J. (2007). Interpretation of magnetic data using tilt-angle derivatives. *Geophysics*, 73(1), 1-10. doi: https://doi.org/10.1190/1.2799992

Sanusi, S. O., & Amigun, J. O. (2020a). Structural and hydrothermal alteration mapping related to orogenic gold mineralization in part of Kushaka schist belt, Northcentral Nigeria, using airborne magnetic and gamma-ray spectrometry data. . *SN Applied Sciences, 2*(1591). doi: https://doi.org/10.1007/s42452-020-03435-1

Sanusi, S. O., & Amigun, J. O (2020b). Logistic-based translation of orogenic gold forming processes into mappable exploration criteria for fuzzy logic mineral exploration targeting in the Kushaka schist belt North-central, Nigeria. . *Natation Resource Research.* doi: https ://doi. org/10.1007/s1105 3-020-09689-1

Saunders, D. F., Terry, S. A., & Thompson, C. K. (1987). Test of national uranium resource evaluation gamma-ray spectral data in petroleum reconnaissance. *Geophysics, 52*(11), 1547-1556.

Shives, R. B. K., Charbonneau, B. W., & Ford, K. L. (2000). The detection of potassic alteration by gamma-ray spectrometry-recognition of alteration related to mineralization. *Geophysics, 65*(6), 2001-2011.

Shives, R. K. (2008). Spectrometric data related to Mammaslhti Cu-Zn-Au deposit in Southwestern Nigeria *Environmental and earth sciences research journal, 4(3)* 66-75. doi: 10.18280/eesrj.040303

Silva, A. M., Pires, A. C., McCafferty, A., Moraes, R., & Xia, H. (2003). Application of airborne geophysical data to mineral exploration in the uneven exposed terrains of the Rio Das Velhas greenstone belt. *Revista Brasileira de Geociências, 33*(2), 17-28.

Spector, A., & Grant, F. S. . (1970). Statistical Models for Interpreting Aeromagnetic Data. . *Geophysics, 35*, 293-302.

Talabi, A. O. (2013). Hydrogeochemistry and Stable Isotopes ($\delta^{18}O$ and $\delta^{2}H$) Assessment of Ikogosi Spring Waters. *American Journal of Water Resources, 1(3)*. doi: 10.12691/ajwr-1-3-2

Taofeeq, O. L. (2020). Integrated aeromagnetic and aeroradiometric data for delineating lithologies, structures, and hydrothermal alteration zones in part of southwestern Nigeria. *Arabian Journal of Geosciences, 13:775* Retrieved from: https://doi.org/10.1007/s12517-020-05743-7

Taofeeq, O. L., John, S., Korede, F., Muyideen, S. & Taiwo, A. . (2021). Use of Magnetic anomaly data to delineate subsurface structures and depth characterization of Lafiagi and its environs, Northcentral Nigeria. *NRIAG Journal of Astronomy and Geophysics, 10*(1), 157-169. doi: 10.1080/20909977.2021.1900526.

Taufiq, S., Nneka, O. F., Daniel, O. N., & Sani, T. U (2020). Review of Combined Magnetic and Radiometric Methods of Geophysical Survey in Nigeria. . *International Journal of Earth Science and Geophysics*, 6:032. doi: 10.35840/2631-5033/1832

Tawey, M. D., Alhassan, D. U., Adetona, A. A., Salako, K. A., Rafiu, A. A., & Udensi, E. E. (2020). Application of Aeromagnetic Data to Assess the Structures and Solid Mineral Potentials in Part of North Central Nigeria. *Journal of Geography, Environment and Earth Science International, 24*(5), 11-29. doi: 10.9734/jgeesi/2020/v24i530223

Telford, W. M., Geldart, L. P., & Sheriff, R. E (1990). Applied geophysics, 2nd Edition. Cambridge University Press, Cambridge. 611–636

Thomas., L. S. (1983). Conflict resolution and the Falkland Island invasions, Interfaces. *13* .(6), 68–83.

Thompson, D. T. (1982). A new technique for making computer-assisted depth estimates from magnetic data. . *Geophysics, 47*, 31–37.

Thurston, J. B., & Smith, R. S. (1997). Automatic conversion of magnetic data to depth, dip and susceptibility comntrast using the SPITM method. *Geophysics, 62*, 807813.

Tsepav, M. T. (2018). Comparative Analysis of the Source Parameter Imaging and Spectral Depth Techniques of Determining Depth to Magnetic Sources in a Sedimentary Environment, using Aeromagnetic Data. *International Journal of Scientific & Engineering Research, 9*(3), 2229-5518. Retrieved from: http://www.ijser.org

Verduzco, B., Fairhead, J. D., Green, C. M., & MacKenzie, C. (2004). New insights into magnetic derivatives for structural mapping. *Lead. Edge, 23*, 116-119.

Wemegah, D. D., Preko, K., Noye, R. M., Boadi, B., Menyeh, A., Danuor, S. K. & Amenyoh, T (2015). Geophysical Interpretation of Possible Gold Mineralization Zones in Kyerano, South-Western Ghana Using Aeromagnetic and Radiometric Datasets. *Journal of Geoscience and Environment Protection, 3*(3), 67-82. Retrieved from http://dx.doi.org/10.4236/gep.2015.34008.

Wilford, J. R., Bierwirth, P. N., & Craig, M. A (1997). Application of Airborne Gamma-Ray Spectrometry in Soil/Regolith Mapping and Applied Geomorphology. AGSO. *Journal of Australian Geology and Geophysics, 17*, 201-216.

Woakes, M., Rahaman, M. A., & Ajibade, A. C (1987). Some metallogenetic features of the Nigerian basement. *Journal of African Earth Science, 6(5)*, 655–664. Retrieved from www.gpxsurveys .com. au

Yousefi, M., Kreuzer, O. P., Nykänen, V., & Hronsky, J. M. A. (2019). Exploration information systems-a proposal for the future use of GIS in mineral exploration targeting. *Ore Geology Review, 111*, 111:103005. doi: https://doi.org/10.1016/j.orege orev.2019.10300 5

Yousif, M., Sabet, H. S., Ghoubachi, S. Y., & Aziz, A. (2018). Utilizing the geological data and remote sensing applications for investigation of groundwater occurrences, West El Minia, Western Desert of Egypt. *NRIAG Journal Astronomy and Geophysics 7*(2), 318-333. doi: 10.1016/j.nrjag.2018.07.002.

Youssef, M. A. S., & Elkhodary, S. T. (2013). Utilization of airborne gamma ray spectrometric data for geological mapping, radioactive mineral exploration and environmental monitoring of southeastern Aswan city, South Eastern Desert, Egypt. *Geophysical Journal, 195*(3), 1689-1700. doi: 10.1093/gji/ggt375.

APPENDICES

Appendix A

Plots of the Log of Spectral Energy against Frequency

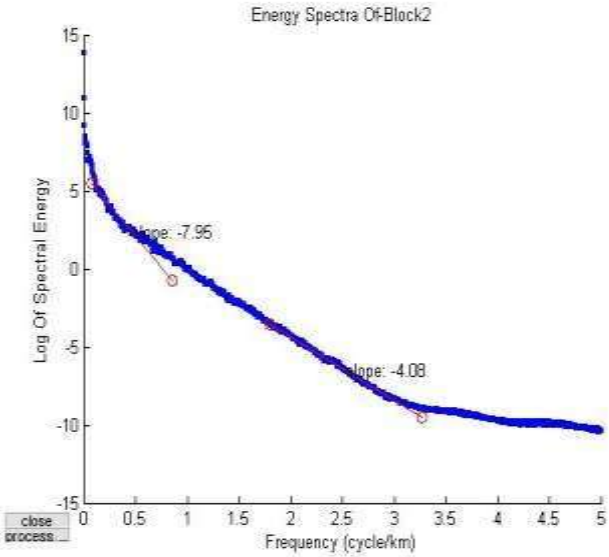
Energy Spectra Of-Block2
Log Of Spectral Energy
Frequency (cycle/km)
Slope: -7.96
Slope: -4.08
close process ...

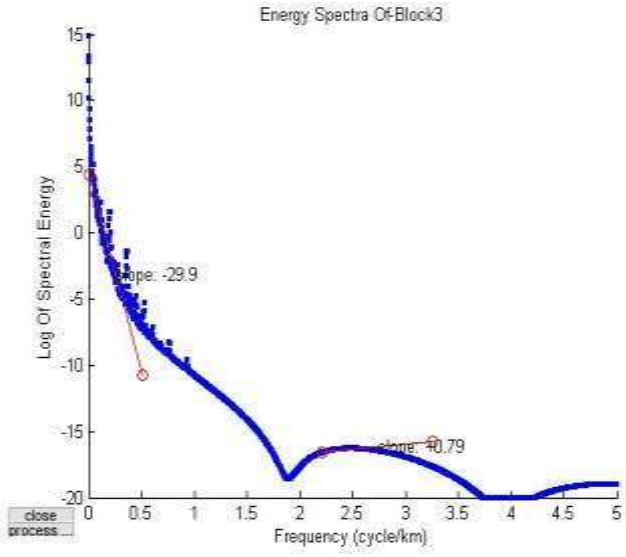
Energy Spectra Of-Block3
Log Of Spectral Energy
Frequency (cycle/km)
Slope: -29.9
Slope: -0.79
close process ...

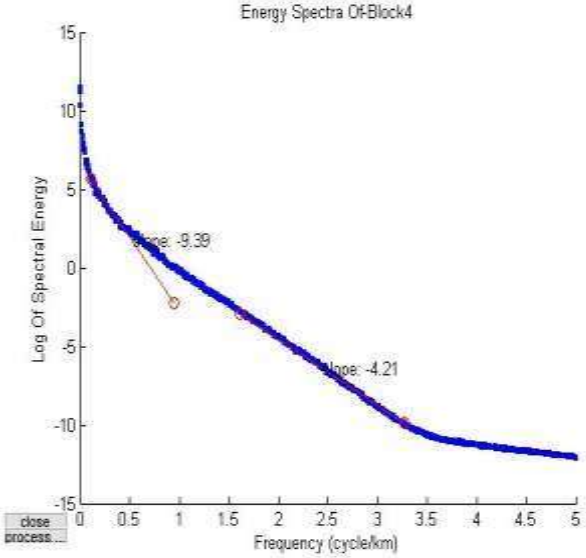
Energy Spectra Of-Block4
Log Of Spectral Energy
Frequency (cycle/km)
Slope: -9.39
Slope: -4.21
close process ...

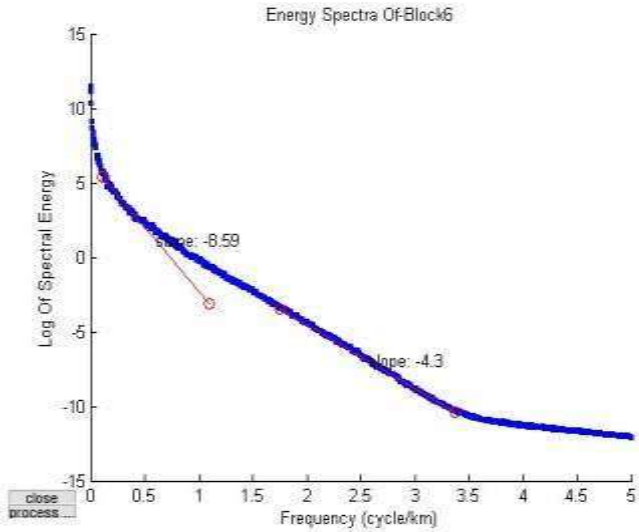
Energy Spectra Of-Block6
Log Of Spectral Energy
Frequency (cycle/km)
Slope: -8.59
Slope: -4.3
close process ...

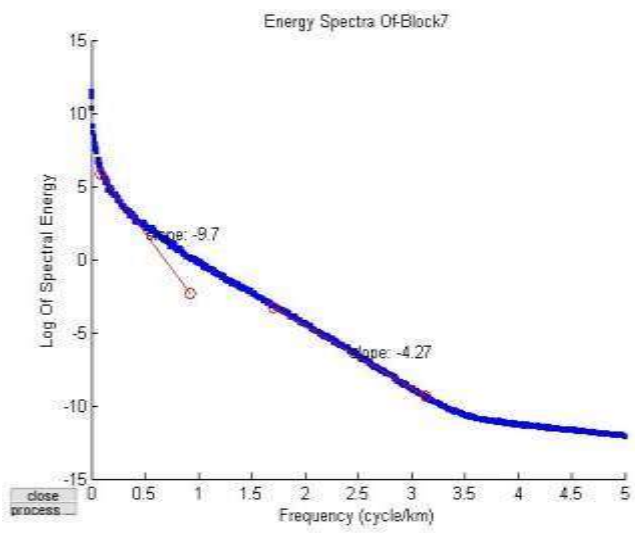
Energy Spectra Of-Block7
Log Of Spectral Energy
Frequency (cycle/km)
slope: -9.7
slope: -4.27
close process

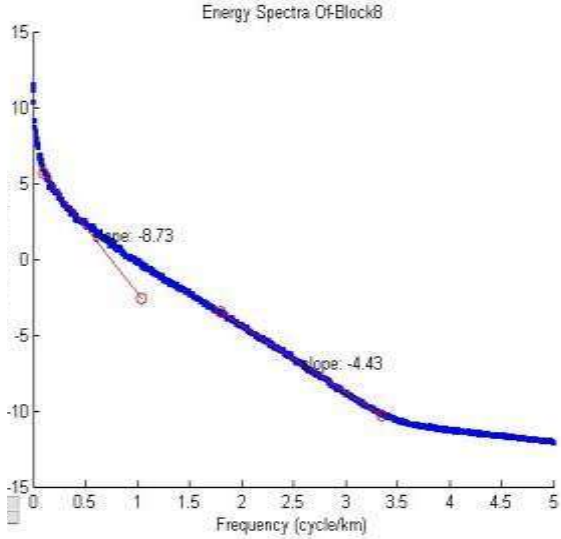
Energy Spectra Of-Block8
Frequency (cycle/km)
slope: -8.73
slope: -4.43

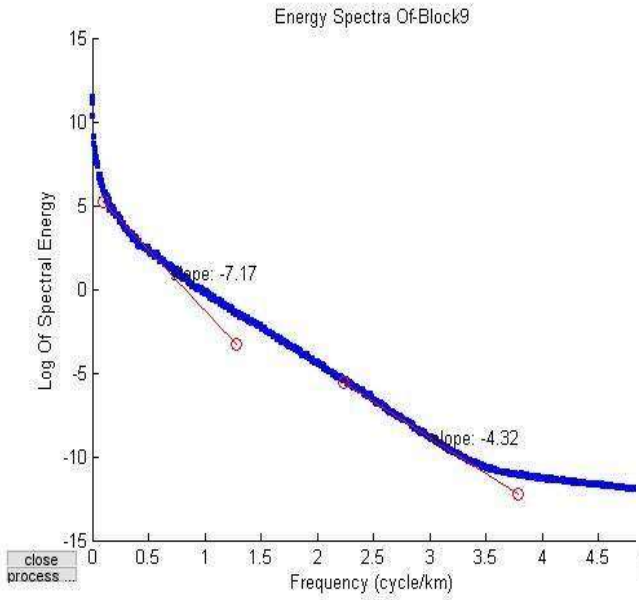
Energy Spectra Of-Block9
Log Of Spectral Energy
Frequency (cycle/km)
slope: -7.17
slope: -4.32
close process

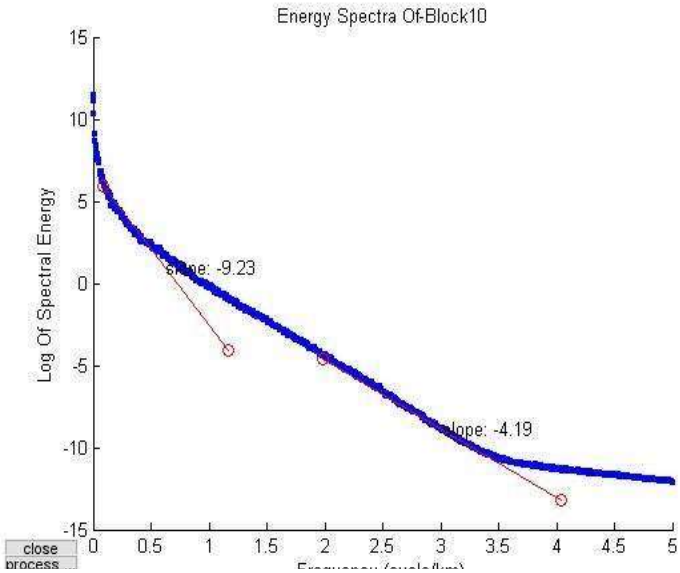
Energy Spectra Of-Block10
Log Of Spectral Energy
slope: -9.23
slope: -4.19
close process

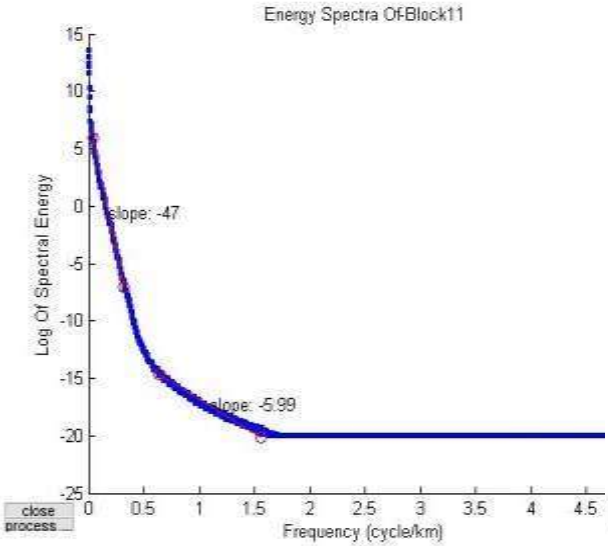
Energy Spectra Of-Block11
Log Of Spectral Energy
Frequency (cycle/km)
slope: -47
slope: -5.99
close process

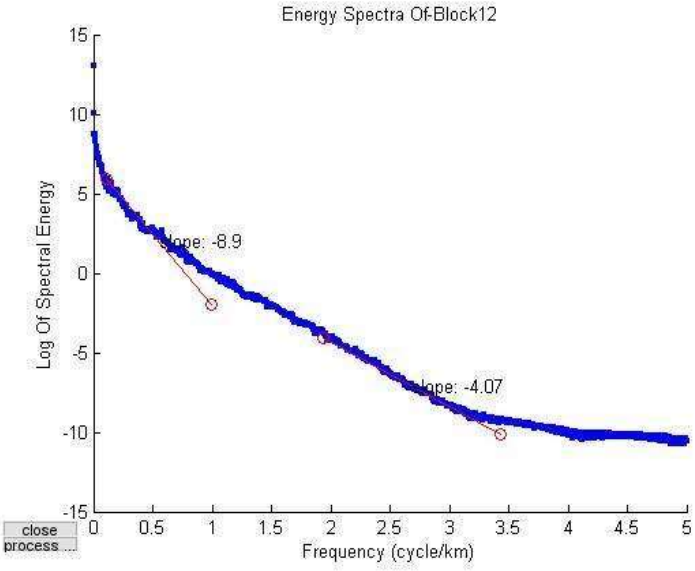
Energy Spectra Of-Block12
Log Of Spectral Energy
Frequency (cycle/km)
slope: -8.9
slope: -4.07
close process